2007, c2006

Synthesis, characterization and photocatalytic application of TiO2 nanosized particles / by Dongliang Liao.

Liao, Dongliang

Synthesis, Characterization and Photocatalytic Application of TiO_2 Nanosized Particles

By
Dongliang Liao

Supervisor
Dr. Baoqiang Liao

Environmental Engineering
Lakehead University
Thunder Bay, Ontario, Canada.
Nov, 2006

Your file Votre référence
ISBN: 978-0-494-31860-7
Our file Notre référence
ISBN: 978-0-494-31860-7

Abstract

In this thesis, effects of surfactant composition and concentration on shape, size, zeta potential, and photocatalytic activity of TiO_2 nanosized particles are reported. Spherical, cubic, rod, ellipse and leaf-like shaped TiO_2 nanosized particles were obtained with the addition of different surfactants in various composition and concentrations during preparation. The results show that the shape and size of the TiO_2 nanosized particles depend on not only surfactant composition but also surfactant concentration.

The pH dependence of zeta potential of TiO_2 nanosized particles was studied. A unique finding is that TiO_2 nanosized particles shaped by sodium dodecyl sulfate (SDS) have two isoelectric points (IEPs), while other shape-controlled TiO_2 nanosized particles have only one IEP. At neutral pH, shape-and size-controlled TiO_2 nanosized particles have a more negative zeta potential than TiO_2 nanosized particles obtained without the addition of surfactants during synthesis and commercial anatase TiO_2 nanosized particles Degussa P-25. Different zeta potential values are observed for TiO_2 nanosized particles obtained with the addition of different surfactants during preparation. The addition of SDS in TiO_2 nanoparticle suspensions causes a shift of the IEPs to lower pH values

Photocatalytic activity of prepared TiO_2 nanosized particles was evaluated in fixed film batch reactors. TiO_2 nanosized particles with different shapes and sizes showed different activities in photocatalytic decomposition of methyl orange (MO) and phenol. Photocatalytic activity of shape- and size-controlled TiO_2 nanosized particles is higher than those without the use of surfactant and P-25. Photocatalytic decomposition of phenol and MO follows the first

order reaction kinetics. The analysis of reaction rate constants and adsorption equilibrium constants shows that the shape is more important than the size in determining the photocatalytic activity of shape- and size-controlled TiO_2 nanosized particles. A comparison of the reaction rates indicated that TiO_2 nanorods have higher photocatalytic activities than spherical and cubic TiO_2 nanosized particles.

All these results indicate that shape, size, zeta potential and photocatalytic activity of TiO_2 nanosized particles can be manipulated with the introduction of surfactants (types and concentrations) during preparation.

Acknowledgments

I would like to express my sincere appreciation and the deepest gratitude to my supervisor, Dr. Baoqiang Liao, for his enthusiastic guidance, endless encouragement and experienced advice through the project of this thesis. He is really quite helpful and patient, when this project experiences any difficulties. At the same time, I would like to show my great appreciation on his help on my study, research and my life in Canada, which improved my English level and my research ability so much.

Financial support arranged by Dr. B. Liao through Natural Sciences and Engineering Research Council of Canada (NSERC) discovery grant is highly appreciated.

In addition, heartfelt thanks are extended to the professors and the graduate students in the Department of Chemical Engineering and Environment Engineering, especially Dr. Lionel J.J. Catalan, Dr. Wa Gao, Dr. Allan F. Gilbert for their helpful comments and their great patience during my graduate study in Lakehead University. I am full of gratitude to the reading committee for their time. Their experience and knowledgeable expertise were of great assistance to this thesis.

Special acknowledgement must be given to the staff of the instrumentation lab, Allan MacKenzie, Ain Raitsakas and Keith Pringnitz, of Lakehead University. Many thanks for their help in the analytical work. Finally, I would like to show my sincere appreciation to all the persons who have offered me help during my study in Lakehead University, they make my life much more wonderful during my academic study.

Table of contents

Abstract II

Acknowledgments IV

List of Tables IX

List of Figures X

List of Nomenclature XII

CHAPTER 1 Introduction 1

1.1 Current problems associated with photocatalytic decomposition on TiO_2 nanoparticles 1

1.2 A rational approach to improving photocatalytic activity of TiO_2 nanoparticles 2

1.3 Motivation of the present study 3

1.4 Objectives 5

CHAPTER 2 Literature Review 7

2.1 Synthesis of TiO_2 nanoparticles 7

2.1.1 Sol-gel methods 7

2.1.2 Solvothermal methods 9

2.1.3 Precipitation and coprecipitation methods 10

2.1.4 Microemulsion 11

2.1.5 Gas phase synthesis of TiO_2 nanoparticles 11

2.2 Methods for shape- and size-controlled TiO_2 nanoparticles 12

2.3 Surfactant assisted shape and size-controlled of nanoparticles 14

2.4 Unique properties of TiO_2 nanoparticles 16

2.4.1 Quantum size effects 16

2.4.2 Photoinduced properties 16

2.4.3 Zeta potential of TiO_2 nanoparticles 17

2.5 Photocatalytic reactions and the applications of TiO_2 nanoparticles 18

2.5.1 Mechanisms of the photocatalysis processes 19

2.5.2 Kinetic model for photocatalysis processes on TiO_2 nanoparticles 21

2.5.3 Applications of photocatalysis processes with TiO_2 nanoparticles 23
2.5.3.1 Photocatalytic synthesis of organic substrates 23
2.5.3.2 Photocatalytic decomposition of organic substrates 23
2.5.3.4 Superhydrophilicity of TiO_2 nanoparticles 28
2.6 Reaction systems of TiO_2 photocatalysis 28
2.6 Summary of literature review 30
2.7 Significance of this study 31
CHAPTER 3 Experimental Materials and Methods 32
3.1 Preparation of TiO_2 nanosized particles 32
3.2 Characterization of TiO_2 nanosized particles 34
3.2.1 Scanning Electron Microscope 34
3.2.2 X-ray diffraction 34
3.2.3 UV-Vis light reflectance 35
3.2.4 FTIR analysis 35
3.2.5 Zeta potential measurement 35
3.3 Photocatalytic activity evaluation 36
3.4 Evaluation of reaction rate constant and adsorption equilibrium constant 37
3.5 Evaluation of the effect of light intensity on the decomposition reaction rates 38
CHAPTER 4 Shape and Size Evolution of TiO_2 Nanosized Particles with Different Surfactants 39
4.1 Morphologies of shape- and size-controlled TiO_2 nanosized particles 39
4.1.1 Effect of surfactants on the morphology of TiO_2 nanosized particles 39
4.1.2 Shape and size evolution of TiO_2 nanosized particles synthesized from $Ti(OBu)_4$ 43
4.1.3 Shape and size evolution of TiO_2 nanosized particles synthesized from $TiCl_4$ 49
4.1.4 Influence of calcination temperature on the morphologies 53
4.1.5 Hypothesized mechanism of the isotropic growth of TiO_2 nanosized particles 54
4.2 X-ray diffraction characterization of TiO_2 nanosized particles. 58

4.2.1 XRD patterns of the nanosized particles synthesized from $Ti(OBu)_4$ 58
4.2.2 XRD patterns of the nanosized particles synthesized from $TiCl_4$ 59
4.2.3 XRD patterns of TiO_2 nanosized particles synthesized with different surfactant/$Ti(OBu)_4$ molar ratios 61
4.3 FTIR spectrum analysis 62
4.4 UV-Vis spectrum analysis 65
4.4.1 UV-Vis reflectance of shape-controlled TiO_2 nanosized particles 66
4.4.2 Effect of calcination temperature on the UV-Vis reflectance. 67
CHAPTER 5 Zeta Potential of TiO_2 Nanosized Particles 70
5.1 Zeta potential of TiO_2 nanosized particles synthesized from $Ti(OBu)_4$ 70
5.2 Zeta potential of TiO_2 nanosized particles synthesized from $TiCl_4$ 72
5.3 Zeta potential of TiO_2 nanosized particles in SDS solution 74
CHAPTER 6 Photocatalytic Activity Studies 77
6.1 Preliminary studies of the photocatalytic reactions 77
6.1.1 Determination of the loading mass of TiO_2 films 77
6.1.2 Effect of calcination temperature on the photocatalytic activities 78
6.2 Photocatalytic activity of the shape- and size-controlled TiO_2 nanosized particles 80
6.3 Kinetic studies of photocatalytic decomposition reactions 83
6.4 Influence of light intensity on the photocatalytic decomposition rates 93
CHAPTER 7 Conclusions and Recommendations 95
7.1 Conclusions 95
7.2 Recommendations 96
References 98
Appendix I Evaluation of methodology 105
Effect of loading mass on the reaction decomposition efficiency 105
Concentration change of phenol (mg/L) and MO (μg/L) in blank experiments 105

Photocatalysts loss by the shear force 106

Effect of calcination temperature on the decomposition efficiency 107

Appendix II Zeta potential of shape- and size-controlled TiO_2 nanosized particles 109

Zeta potential of shape-controlled TiO_2 nanosized particles synthesized from $Ti(OBu)_4$ 109

Zeta potential of SDS shaped TiO_2 nanosized particles synthesized from $Ti(OBu)_4$ in water and SDS solution 109

Zeta Potential of the shape controlled TiO_2 nanosized particles synthesized from $TiCl_4$. 110

Zeta potential of SDS shape controlled TiO_2 nanosized particles synthesized from $TiCl_4$110

Zeta potential of shape-controlled TiO_2 nanosized particles synthesized from $Ti(OBu)_4$ in water and SDS solution 111

Zeta potential of TiO_2 nanosized particles synthesized from $Ti(OBu)_4$ in SDS solutions111

Appendix III Evaluation of photocatalytic activity of the shape-controlled TiO_2 nanosized particles.....112

Phenol concentration change on the TiO_2 nanosized particles synthesized from $Ti(OBu)_4$112

Phenol concentration change on the TiO_2 nanosized particles synthesized from $TiCl_4$ ... 113

MO concentration change on shape-controlled TiO_2 nanosized particles 114

Appendix V Effect of light intensity on the photocatalytic reactions 121

List of Tables

Table 6-1, Calculations of anatase composition in the shape-controlled nanosized particles 80
Table 6-2, Reaction rate constants (k_c) and constants of adsorption equilibrium (K_C) for the photocatalytic decomposition of phenol and MO on different TiO_2 photocatalysts 93

List of Figures

Figure 1-1, Schematic diagram of the research hypothesis 5
Figure 2-1, Possible mechanism of phenol photocatalytic decomposition on illuminated TiO_2 .. 25
Figure 2-2, Applications of photoinduced processes of TiO_2 27
Figure 3-1, Schematic diagram of the the preparation of TiO_2 nanosized particles 33
Figure 4-1, TiO_2 nanosized particles synthesized from $Ti(OBu)_4$ and $TiCl_4$ without using surfactants 39
Figure 4-2, Nanosized particles shape controlled by DBS from $Ti(OBu)_4$ 41
Figure 4-3, Nanosized particles shape controlled by cellulose from $Ti(OBu)_4$ 41
Figure 4-4, Nanosized particles shape controlled by SDS from $Ti(OBu)_4$ 42
Figure 4-5, Nanosized particles shape controlled by DBS synthesized from $TiCl_4$ 42
Figure 4-6, Nanosized particles shape controlled by cellulose synthesized from $TiCl_4$ 42
Figure 4-7, Nanosized particles shape controlled by SDS synthesized from $TiCl_4$ 43
Figure 4-8, Size evolution of TiO_2 nanosized particles with increasing DBS/$Ti(OBu)_4$ molar ratio 44
Figure 4-9, Shape evolution of TiO_2 nanosized particles by increasing cellulose/ $Ti(OBu)_4$ molar ratio 46
Figure 4-10, TiO_2 particles synthesized with cellulose/$Ti(OBu)_4$ molar ratio 5:1 47
Figure 4-11, Shape evolution of TiO_2 nanosized particles by increasing SDS/$Ti(OBu)_4$ molar ratio 48
Figure 4-12, Magnified image of TiO_2 nanorod 49
Figure 4-13, Size evolution of TiO_2 nanosized particles with increasing DBS/$TiCl_4$ molar ratio 50
Figure 4-14, Size evolution of TiO_2 nanosized particles with increasing Cellulose/ $TiCl_4$ molar ratio 51
Figure 4-15, TiO_2 particles synthesized with a cellulose/$TiCl_4$ molar ratio of 5:1. 51
Figure 4-16, Size evolution of TiO_2 nanorods synthesized with different SDS/$TiCl_4$ molar ratio52
Figure 4-17, Shape evolution of TiO_2 nanosized particles with increasing calcination temperature 54
Figure 4-18, Hypothesis of shape evolution of TiO_2 nanosized particles 57
Figure 4-19, XRD patterns of the TiO_2 nanosized particles synthesized from $Ti(OBu)_4$ 58
Figure 4-20, XRD patterns of nanosized particles synthesized from $Ti(OBu)_4$ calcined at different temperatures 59
Figure 4-21, XRD patterns of the TiO_2 nanosized particles synthesized from $TiCl_4$ 60
Figure 4-22, XRD patterns of the TiO_2 nanosized particles synthesized from $TiCl_4$ calcined at different temperatures. 61
Figure 4-23, XRD patterns of TiO_2 nanosized particles synthesized with different cellulose/$Ti(OBu)_4$ molar ratios 62
Figure 4-24, XRD patterns of TiO_2 nanosized particles synthesized with different SDS/$Ti(OBu)_4$ molar ratios 62
Figure 4-25, FTIR spectrum of the TiO_2 nanosized particles synthesized from $Ti(OBu)_4$ 64
Figure 4-26, FTIR spectrum of TiO_2 nanosized particles calcined at different temperatures. 64
Figure 4-27, FTIR spectrum of shape-controlled TiO_2 nanosized particles synthesized from $TiCl_4$ 65
Figure 4-28, UV-Vis reflectance spectra of the TiO_2 nanosized particles calcined at 500^0C 66
Figure 4-29, UV-Vis light reflectance spectrum of the nanosized particles synthesized form $Ti(OBu)_4$ calcined at different temperatures 69

Figure 4-30, UV-Vis light reflectance spectrum of the nanosized particles synthesized form $TiCl_4$ calcined at different temperatures 69
Figure 5-1, Zeta potential of shape-controlled TiO_2 nanosized particles synthesized from $Ti(OBu)_4$ 71
Figure 5-2, Zeta potential of SDS shape controlled TiO_2 nanosized particles synthesized from $Ti(OBu)_4$ 72
Figure 5-3, Zeta Potential of the shape controlled TiO_2 nanosized particles synthesized from $TiCl_4$ 73
Figure 5-4, Zeta potential of SDS shape controlled TiO_2 nanosized particles synthesized from $TiCl_4$ 74
Figure 5-5, Zeta potential of DBS shaped TiO_2 nanosized particles synthesized from $Ti(OBu)_4$ in water and SDS solution 75
Figure 5-6, Zeta potential of cellulose shaped TiO_2 nanosized particles synthesized from $Ti(OBu)_4$ in water and SDS solution 76
Figure 5-7, Zeta potential of SDS shaped TiO_2 nanosized particles synthesized from $Ti(OBu)_4$ in water and SDS solution 76
Figure 5-8, Zeta potential of TiO_2 nanosized particles synthesized from $Ti(OBu)_4$ in SDS solutions 76
Figure 6-1, Effect of loading mass on photocatalytic reaction of TiO_2 nanosized particles 77
Figure 6-2, Comparison of photocatalytic activities of TiO_2 nanosized particles with DBS 79
Figure 6-3, Comparison of photocatalytic activities of TiO_2 nanosized particles with cellulose. 79
Figure 6-4, Comparison of photocatalytic activities of TiO_2 nanosized particles with SDS. 79
Figure 6-5, Relationship between the initial reacrion rate and crystal phase composition 80
Figure 6-6, Comparison of the photocatalytic activities of the shape-controlled TiO_2 nanosized particles 82
Figure 6-7, Comparison of the photocatalytic activities of the shape-controlled TiO_2 nanosized particles 82
Figure 6-8, Relationship between initial reaction rate r_0 and initial concentration C_0 of phenol.. 86
Figure 6-9, Relationship between initial reaction rate r_0 and initial concentration C_0 of MO 87
Figure 6-10, Relationship of $-\ln(C/C_0)$ and time of phenol on TiO_2 nanosized particles synthesized with DBS 88
Figure 6-11, Relationship of $-\ln(C/C_0)$ and time of phenol on TiO_2 nanosized particles synthesized with cellulose 88
Figure 6-12, Relationship of $-\ln(C/C_0)$ and time of phenol on TiO_2 nanosized particles synthesized with SDS 89
Figure 6-13, Relationship of $-\ln(C/C_0)$ and time of MO on TiO_2 nanosized particles synthesized with DBS 89
Figure 6-14, Relationship of $-\ln(C/C_0)$ and time of MO on TiO_2 nanosized particles synthesized with cellulose 90
Figure 6-15, Relationship of $-\ln(C/C_0)$ and time of MO on TiO_2 nanosized particles synthesized with SDS 90
Figure 6-16, Correlation between $1/k_{app}$ and initial concentration of phenol 91
Figure 6-17, Correlation between $1/k_{app}$ and initial concentration of MO 92
Figure 6-18, Relationship between initial reaction rate r_0 and light intensity 94

List of Nomenclature

C_0	Initial concentration of the substrate, mol/L
C	Concentration of the substrate at time t, mol/L
I	Light intensity, mW cm^{-2}
I_a	Anatase phase percentage, %
I_R	Rutile phase percentage, %
k_{app}	Apparent reaction rate constant, t^{-1}
k_c	Langmuir reaction rate constant, mol L^{-1} hr^{-1}
K_C	Adsorption equilibrium constant, L mol^{-1}
r_0	Reaction rate at the first hour of reaction, mol L^{-1} min^{-1}
t	Reaction time, hour
2θ	XRD diffraction degree

CHAPTER 1 Introduction

Nanoparticles are the materials with discrete dimension between 10^{-10}m to 10^{-8}m [1, 2]. Nanoscale materials technology is the intersection of coordination chemistry, reaction kinetic theory, surface chemistry and interface reaction [3]. There has been a wide-range of studies to understand the unique properties and applications of nanoparticle systems and nanoparticle films which are different from their corresponding bulk materials [4, 5]. TiO_2 nanoparticles have been studied extensively because of their potential applications as photocatalysts [6].

1.1 Current problems associated with photocatalytic decomposition on TiO_2 nanoparticles

TiO_2 nanoparticles have been proved to be an important photocatalyst in removal of environmental contaminants [7]. A number of contaminated compounds can be effectively decomposed on the UV illuminated TiO_2 nanoparticles [6]. However, there are still a lot of problems needed to be solved in the practical applications of photocatalysis using TiO_2 nanoparticles. For most of the photocatalytic decomposition processes, photonic efficiency is less than 10% [8]. TiO_2 is close to be an ideal photocatalyst because it is chemically and biologically inert, photocatalytically stable, nontoxic, of a high photocatalytic activity and low cost and easy to get. However, photocatalytic reactions on TiO_2 nanoparticles cannot be induced only by visible light, which limits the application of TiO_2 as a photocatalyst. In addition, the electronic excitation of TiO_2 nanoparticles needs a higher input energy when the particle size decreases because of the quantum size effect [9-11]. Studies have been done to improve the photocatalytic efficiency on TiO_2 nanoparticles. However most of these studies focous on the operational parameters such as the catalyst dosage [12], UV light intensity [13], oxygen concentration [14], temperature [15] and the character and initial concentration of the target

organic compounds [16, 17]. Not much work has been done to improve the photocatalytic efficiency of the photocatalysis processes on TiO_2 nanoparticles by manipulating the structure, such as shape and size, of the nanoparticles. In the studies on the photocatalysis of TiO_2, lots of decomposition processes have been done in the suspensions of TiO_2 nanoparticles because the photocatalysts can contact with the target compound better in aqueous suspension. It is highly desirable to prepare TiO_2 nanoparticles with desirable surface properties, such as surface charge or zeta potential, to form stable particle suspension. One challenge of using the particle suspension system rather than the film system is the recovery of nanoparticle photocatalysts from the treated effluent. The loss and recovery of photocatalyst are problems that limit the scaling up and applications of these systems.

At present, there is a lack of fundamental understanding on the relationship between the structure of TiO_2 nanoparticles and their photocatalytic activity. The fundamental knowledge about the correlation between morphologies of TiO_2 nanoparticles and their photocatalytic activity is essential for higher efficient photocatalytic processes.

1.2 A rational approach to improving photocatalytic activity of TiO_2 nanoparticles

Inorganic nanostructure materials are of theoretical and industrial interest because they show a wide range of novel electrical and optical properties [1]. A number of studies have shown that physical and chemical properties of nanoparticles depends on not only their sizes but also their shapes [18-20]. The shape and size of TiO_2 nanoparticles are key factors for the determination of their photocatalytic activity because their surface adsorptive properties and light sensitive properties are correlated to the shape and size of TiO_2 nanoparticles [21-22]. Zhang et

al. [23] showed that an increase in photocatalytic activity of TiO_2 was observed as particle size decreased to a lower limit of approximately 10nm. In other words, if the shape and size control of TiO_2 nanoparticles is possible, their physical, chemical properties and catalytic activities can be manipulated as desired.

Many studies have described the control of shape and size of inorganic nanoparticles through different methods such as the sol-gel, hydrothermal and chemical vapor deposition methods [24, 25]. One new approach being used is controlling the shape and size of nanocrystals with the presence of surfactants, known as "oriented attachment" [26]. Various shapes of TiO_2 nanocrystals, including short and long nanorods, bullet- and diamond-shaped nanoparticles, nanotubes, cuboids and fractals have been prepared through different processes [7]. Studies suggested that there is a possible correlation between the shape and size of the nanoparticles and the concentrations of surfactants [27].

In this study, we intended to manipulate and improve the photocatalytic activity of TiO_2 nanoparticles by using a relatively new approach by introducing surfactant during preparation. Of particular interest is the effect of surfactant concentration on the shape, size, zeta potential and thus photocatalytic activity of TiO_2 nanoparticles.

1.3 Motivation of the present study

In the studies of TiO_2 photocatalysis, different TiO_2 nanoparticles have been synthesized and the morphologies, structure, physical and chemical properties have been extensively investigated [6]. Others have focused on the photocatalytic processes including elucidation of the

reaction mechanisms and the design of reactors [28-31]. Studies on the shape evolution of TiO_2 nanoparticles have mostly been focused on different types of surfactants [32]. The potential correlations between the shape and size of TiO_2 nanoparticles and their photocatalytic activity have not been reported yet. Shape and size control by using surfactants have explored a new way to improve the photocatalytic activity of TiO_2 nanoparticles. However, not much work has been done to improve the photocatalytic activity through the investigation of the shape and size evolution of the TiO_2 nanoparticles. The potential impact of surfactant concentration on shape and size of TiO_2 nanoparticles has not been well understood yet. Studies on the control of nanocrystal shape and size have been focused on specific materials and crystal shapes. Types of the surfactants being studied are still very limited.

Figure 1-1 shows the hypothesis of this study. In this study, two hypotheses were tested. First, the shape, size, and surface properties (such as zeta potential) of TiO_2 nanoparticles can be manipulated by the composition and concentration of surfactants. Second, through the shape, size, and surface properties control of TiO_2 nanoparticles, their photocatalytic activity can be manipulated and improved.

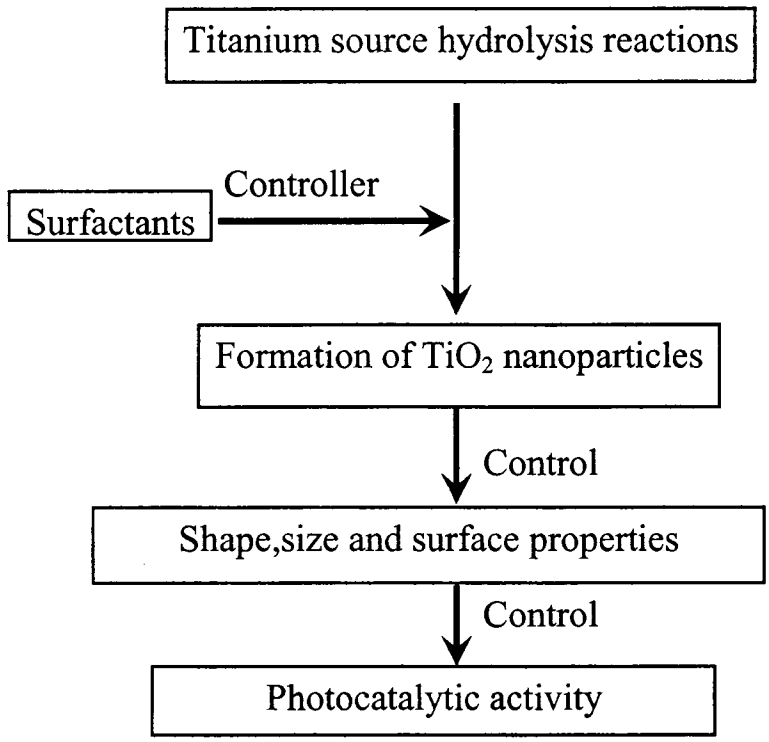

Figure 1-1, Schematic diagram of the research hypothesis

1.4 Objectives

The ultimate goal of this study was to improve the photocatalytic activity of TiO_2 nanoparticles through manipulation of the particle shape, size and surface properties. To reach this goal, we controlled the shape, size and surface properties of TiO_2 nanoparticles by a relatively new approach by introducing surfactants during the synthesis process. The specific objectives of this study are:

1. To study the effects of composition and concentrations of surfactant on the shape and size of TiO_2 nanoparticles.
2. To investigate the effect of the types of titanium precursor on the shape and size of TiO_2 nanoparticles.

3. To study the effect of preparation conditions on the surface properties (e.g. zeta potential) of the TiO_2 nanoparticles.
4. To study the kinetics of photocatalytic reactions and the potential correlation between the photocatalytic activity and the structure of TiO_2 nanoparticles.

CHAPTER 2 Literature Review

2.1 Synthesis of TiO_2 nanoparticles

TiO_2 nanoparticles can be synthesized in the form of powders or films. Solution and gas phase methods have been developed to synthesize TiO_2 photocatalysts, respectively. Both powders and films of TiO_2 nanoparticles can be synthesized from the growth of nanocrystallites with sizes ranging from several nanometers to several micrometers. The general methods used for preparation of TiO_2 nanoparticles are briefly described in the following paragraphes.

2.1.1 Sol-gel methods

Sol-gel methods have been widely used in the synthesis of TiO_2 nanoparticles by many studies because sol-gel methods have many advantages over other synthesis techniques [33-36]:

(a) Superior homogeneity and purity of the final products;

(b) Better microstructural control of the nanoparticles;

(c) Higher BET surface areas of the nanoparticles;

(d) Flexibility in introducing dopants in large concentrations;

(e) Easy control of the stoichiometry; and

(f) The ability to coat large and complex surfaces.

In the synthesis of TiO_2 nanoparticles with sol-gel methods, titanium alkoxide or non-alkoxide can be used as titanium precursors. $Ti(i\text{-}OP)_4$ [33], $Ti(OBu)_4$ [34] and $TiCl_4$ [35] are the most commonly used precursors. In sol-gel processes, TiO_2 is usually prepared by the reactions of hydrolysis and polycondensation of titanium alkoxides. Titanium alkoxides, $Ti(OR)_n$,form

oxopolymers in aqueous phase, and then these oxopolymers are transformed into an oxide network. The reaction scheme is usually discribed as follows [36]:

The non-ionized titanium precursor molecules $Ti(OR)_n$ reacts with water,

$$Ti(OR)_n + xH_2O \rightarrow Ti(OH)_x(OR)_{n-x} + xROH$$

The reactions continue to proceed until the titainum hydroxide ($Ti(OH)_n$) is formed. Then the polymerization reactions take place.

Condensation dehydration:

$$Ti(OR)_n + Ti(OR)_{n-1}(OH) \rightarrow Ti_2O(OR)_{2n-2} + ROH$$

Dealcoholation:

$$2Ti(OR)_{n-1}(OH) \rightarrow Ti_2O(OR)_{2n-2} + H_2O$$

The overall reaction can be expressed as:

$$Ti(OR)_n + \frac{n}{2}H_2O \rightarrow TiO_{\frac{n}{2}} + nROH$$

When titanium butoxide is used as precursor, the reactions can be written as follows:

$$[Ti(OC_4H_9)]_n + 4nH_2O \rightarrow [Ti(OH)_4]_n + 4nC_4H_9OH$$

$$nTi(OH)_4 \rightarrow (TiO_2)_n + 2nH_2O$$

Condensation reactions pull the constitute particles together into a compact mass and thus build up the metal oxide crystal [37]. Gelation of the solute occurs and forms a three-dimensional reticulation gel. Calcination temperature is especially important for removing the organic molecules from the final products and completing the crystallization.

Some factors can affect the morphology of TiO_2 nanoparticles in the synthesis with the sol-gel method such as type of the titanium precursors [38-40], chemical complexation in the sol-

gel system [41-44], pH and stochiometry of the reactants [45], drying processes and calcination temperature [46, 47]. Inorganic precursorss may be more economical than alkoxides. An important reason for the limitation of inorganic precursors is the severely fast hydrolysis of inorganic precursors which is very hard to control. In order to control the size of TiO_2 nanoparticles, some studies have been done to slow down the rate of hydrolysis of alkoxides including alkoxides modification by complexation with coordination agents [48, 49]. It has been proved that acetic acid can act as a stabilizer in the sol to reduce or prevent the condensation and the precipitation of titania [50]. Calcination at high temperatures leads to a decrease in surface area, loss of hydroxyl groups and growth of crystal size. All of theses will lead to a decrease in photocatalytic activity of the synthesized TiO_2 nanoparticles. Recently, some reports showed that crystallized TiO_2 could be synthesized at low temperatures [51, 50].

2.1.2 Solvothermal methods

These methods employ chemical reactions in aqueous (hydrothermal method) or organic media (solvothermal method) under autogenerated pressures at low temperatures. The precipitates obtained by sol-gel are normally amorphous, so a subsequent thermal treatment is needed to crystallize the final products [52]. This calcination process will inevitably cause the crystal growth and reduction in specific surface areas of the particles and even induce phase transformation. Solvothermal synthesis can solve those problems encountered in sol-gel process, because crystallization of the nanoparticles can occur under autogenerated pressure during the hydrolysis process. In addition, the solvothermal method with an aqueous solvent as a reaction medium is environmentally friendly since the reactions are carried out in a closed system and the contents can be recovered and reused after cooling down to room temperature [53].

The solvothermal methods are useful to control the size, morphology, crystalline phase and surface chemistry by regulating the sol composition, reaction temperature, pressure, property of solvent and aging time [53]. Most of the solvothermal synthesis processes require a precise control of low temperature and pressure of the systems [54]. The temperature during the precipitation in the solvothermal method was usually controlled below 250^0C. The self-produced pressure was within 2.0-6.0atm. Complete hydrolysis of titanium precursor could be obtained in the autoclave without adding excessive water [55].

2.1.3 Precipitation and coprecipitation methods

The precipitation methods involve precipitation of hydroxides by addition of a basic solution to a raw material followed by calcination to crystallize the oxide. Under particular conditions, crystallized rutile TiO_2 may be obtained at room temperature. The disadvantage of these methods is the difficulty of controlling particle size and size distribution. Uncontrolled precipitation often causes formation of larger particles instead of nanoparticles [6, 56].

The products of precipitation reactions are generally sparingly soluble species formed under conditions of high supersaturation [56, 57]. Such conditions indicate that nucleation will be a key step of the precipitation process and that a large number of small particles will be formed. Secondary processes, such as Ostwald ripening and aggregation, will dramatically affect the size, morphology and properties of the products. $TiCl_3$ [58] and $TiCl_4$ [59] are commonly used precursors in the formation of TiO_2 nanoparticles through precipitation methods. Shuttle-like, sphere with needles and uniform rutile TiO_2 nanoparticles have been synthesized by hydrolysis of $TiCl_4$ [59].

2.1.4 Microemulsion

Microemulsions can be defined as thermodynamically stable, optical isotopic solutions of two immiscible liquids consisting of microdomains of one or both stabilized by an interfacial film of surfactant. Nanoparticles can be obtained from microemulsions by mixing two microemulsions (one containing the precursor and the other the precipitating agent) or by adding the precipitating agent to the precursor containing microemulsion [60]. In the synthesis of TiO_2 nanoparticles, the reactions in microemulsion methods are very similar to the reactions used in the sol-gel methods. Both anatase and rutile TiO_2 phases could be obtained through microemulsion methods.

Other synthesis methods for TiO_2 nanoparticles in liquid phases have been investigated including templated synthesis, biomimetic synthesis, surface derivatized [56], combustion method [61] and electrochemical synthesis [62].

2.1.5 Gas phase synthesis of TiO_2 nanoparticles

Vapor phase synthesis is another important route for the synthesis of TiO_2 nanoparticles. In the studies of the formation of TiO_2 nanoparticles films, vapor phase synthesis is commonly used. The most common vapor phase synthesis method is chemical vapor deposition (CVD) because it can coat large surface in a short time [63-65]. Experimental and theoretical parameters that affect the CVD processes of the formation of TiO_2 nanoparticles have been investigated. Physical vapor deposition (PVD) is another typical vapor phase synthesis method for TiO_2 thin films [62, 66]. In physical vapor deposition, the substrates are placed straight on the source. Collision of gas molecules and pollution of the films can be deduced because evaporation takes

place under reduced pressure. The commonly used PVD technique is thermal evaporation, in which a material is evaporated from a crucible and deposited onto a substrate [67].

The techniques for TiO_2 nanoparticles synthesis in vapor phase can also be divided by the form of precursors. When solid precursors were used, inert gas condensation, pulsed laser ablation, spark discharge generation and ion sputtering method were developed. When liquid and vapor precursors were used, spray pyrolysis, laser pyrolysis/photothermal synthesis, thermal plasma synthesis, flame and flame spray pyrolysis were developed [68]. The high cost for the synthesis equipments and process control limits the application of vapor phase synthesis of TiO_2 nanoparticles. Another limitation of these vapor phase synthesis methods is that the productivity of powder nanoparticles is very low.

2.2 Methods for shape- and size-controlled TiO_2 nanoparticles

Studies have described the control of shape and size of inorganic nanoparticles through different methods such as the sol-gel, hydrothermal and chemical vapor deposition methods [28, 68, 69]. Recently, synthesis of shape-controlled nanocrystals with the use of some surfactants was studied [28, 32, 70].

Various shapes of TiO_2 nanocrystals have been synthesized by different researchers, using different processes or procedures [71, 72]. Chemseddine et al. [73] demonstrated elongated TiO_2 nanocrystals can be synthesized from the hydrolysis reaction of titanium alkoxide. Short and long nanorods, bullet- and diamond-shaped nanocrystals, platelets, nanotubes and fractals have been prepared [29, 74-76]. Alivisatos et al. [77] reported the shape evolution of anatase

TiO_2 nanocrystals from bullet- and diamond-shape to rods structures by the modulation of surface energies of different crystal facets with the use of surfactants. The long axes of the nanocrystals were parallel to the c-axis of the anatase structure. The hexagonal nanorods truncated with two (001) and four (101) facets were observed. The branched shape was believed to be the product of growth along (101) directions starting from the hexagonal shape [31]. Zhu et al. [78] synthesized TiO_2 cuboids of dimension about 50nm by the sol-gel method. Rabatic et al. [79] correlated the TiO_2 nanoparticle synthesis with the selective activity of organic compounds. Large scale production of organic-capped TiO_2 nanorods were synthesized by hydrolysis of titanium tetraisopropoxide in oleic acid. The TiO_2 nanorods synthesized at low temperatures had a high aspect ratio of anatase [81].

Recently, TiO_2 nanotubes have attracted a wide attention owing to their potential application in high efficiency photocatalysts and photovoltaic cells. A one-step templating synthesis of TiO_2 nanoarrays in solutions was developed by Leu et al [80]. Well-aligned TiO_2 nanotubes were synthesized by the sol-gel method in some studies [82]. Wang et al. [83] proposed a model for the formation mechanism of TiO_2 nanotubes. This model suggested that the TiO_2 nanotubes were formed following a three-dimension, two-dimension to one-dimension process. They found the two-dimensional lamellar TiO_2 is essential for the formation of the TiO_2 nanotubes. Li et al. [82] synthesized the TiO_2 nanotubes with anodic aluminum oxide as template. It was found that nanotubes or nanofibres could be obtained by controlling the immersion time of template membrane in precursor sol. TiO_2 nanotubes were synthesized from layered titanate particles by a soft chemical process by Wei et al [84]. They also proposed an exfoliating-rolling

model for the formation of nanotube structure. Composite TiO_2 nanotubes including WO_3/TiO_2, Ni/ TiO_2 nanotubes Zn-doped and carbon nanotube base TiO_2 nanotubes have been synthesized.

TiO_2 nanofibres have been synthesized by a templating process [85] and a wet chemical reaction [86]. In order to avoid the agglomeration and excessive growth of TiO_2 nanoparticles, crystallized anatase and rutile TiO_2 nanoparticles have been synthesized successfully at low temperatures (75^0C and 110^0C, respectively) [87, 88].

2.3 Surfactant assisted shape and size-controlled of nanoparticles

Vidal-Iglesias et al [89] synthesized preferentially oriented nanoparticles of Pt(100) with a hydrogen adsorption/desorption process. Tetrahedral and octahedral nanoparticles were formed when hydrogen and methanol were used as reductive materials, respectively. It has been reported that the ratio of (100) and (111) facets of the gold nanoparticles could be manipulated when iodide was used as surfactant [90]. Teranishi et al. [90] controlled the shape of Pt nanoparticles precisely with the presence of sodium polyacrylate (PAA) and poly (N-vinyl-2-pyrrolidone) (PVP). They reported that the dominant shape of Pt nanoparticles was controlled by changing the reduction rate of Pt^{4+} ions.

Margeat et al. [91] reported that the shape-controlled iron nanoparticles synthesized with the introduction of organic polymer matrix or mixtures of long chain acid ligands were spherical nanoparticles and magnetically independent. The nanocubes with edges of 7.2 or 8.4nm were magnetic. Qian et al. [92] used the anion surfactant sodium dodecyl benzene sulfonate to synthesize the desired Ni nanobelts through the hydrothermal method. Ultra-thin Ni nanobelts of

~500 to 1000nm in width, up to 50μm in length, and ~15nm in thickness were obtained. These Ni noanbelts showed ferromagnetic properties.

Over the past several years, semiconductor nanoparticles of various shapes have been synthesized successfully, such as nanosphere [64], nanodots [65], nanorods [77] and nanowires [30]. A wide class of semiconductor nanoparticles have been synthesized in different structural forms. Various shapes of CdSe nanorods were synthesized successfully [22]. In the synthesis of these CdSe nanoparticles, a popular method, the so-called TOPO/TOP (trioctylphosphine oxide/trioctylphosphine) method was proposed. This synthesis method for the formation of nanoparticles was to inject the precursors that underwent pyrolysis into the surfactant solutions at high temperatures [69]. Cheon et al. [93] reported a simple synthesis method for one-dimensional zinc telluride nanorods with a single precursor. They developed ZnTe nanorods in a hot amine surfactant mixture with a single precursor. They also synthesized various shapes of MnS one-dimensional nanocrystals from the thermal decomposition of a single molecular precursor in a monosurfactant system [32].

Different kinds of oxides including ZnO, CuO, Co_3O_4, Fe_3O_4, MnO and CdO nanoparticles with different morphologies have been synthesized through different processes such as the pyrolysis of metal fatty acid salts and hydrothermal method [94, 95]. Binary oxide nanoparticles have also been studied. O'Brien et al. [96] reported the self-assembly of PbSe quantum dots and Fe_2O_3 magnetic nanoparticles into precisely ordered three-dimensional super lattices.

2.4 Unique properties of TiO_2 nanoparticles

Shape and size of nanoparticles are key factors for the determination of their chemical and physical properties. Some properties of nanocrystals are quite different from conventional materials [97]. As an important semiconductor, the unique properties of TiO_2 nanoparticles have been studied by a number of researchers and summarized below.

2.4.1 Quantum size effects

Quantum size effect of TiO_2 nanoparticles is the dominant size effect and has been well studied [97]. As the size of a particle decreases to a nanometer regime, the electronic structure has altered from the continuous electronic bands to the discrete or quantized electronic levels. The continuous optical transitions between the electronic bands become discrete and the properties of the nanoparticles become shape- and size-dependent [98].

2.4.2 Photoinduced properties

Photocatalysis on illuminated TiO_2 nanoparticle surface is an important property of TiO_2 nanoparticles. When photons have a higher energy than the band gap of TiO_2 nanoparticles, they can be absorbed and an electron of TiO_2 nanoparticles is promoted to the CB (conduction band), leaving a hole in the VB (valence band). This excited electron can be used directly to drive a chemical reaction, which is called photocatalysis [6]. The surface atoms of TiO_2 nanoparticles are more active than the bulk atoms because of less adjacent coordinate atoms and unsaturated sites. Due to the small size of the nanoparticles, more surface defects exist. The surface defects can act as hole trapping centers in the photocatalysis process. With the size decrease, the surface

to volume ratio increases and the surface effect becomes more apparent [99]. In TiO_2 nanoparticles, a high surface-to-volume ratio can be obtained.

Superhydrophilicity is a newly studied photoinduced property of TiO_2 nanoparticle films. With the illumination of UV light on TiO_2 films, smaller water contact angle will be obtained with longer illumination time. Finally, a contact angle close to zero will be obtained. This means that water spreads perfectly across the surfaces [100, 101].

2.4.3 Zeta potential of TiO_2 nanoparticles

The stability of dispersions of inorganic particles in the aqueous phase plays an important role in particle processing and application. The relationship between surface charge or zeta potential and stability of nanoparticles in water has been widely studied in a variety of systems [102-104]. However, the role of specifically adsorbed ions resulting in the zeta potential of the nanoparticles is not clearly understood [102, 103]. Studies have shown that many organic substrates can be mineralized into carbon dioxide and water on UV irradiated TiO_2 nanoparticle suspensions. Though there are many factors that affect photocatalytic reactions, one of the key factors is the preparation of particle suspensions with a high degree of homogeneousness and stability in the aqueous phase. The viability of the organic substrate removals can be enhanced by increasing the stability of nanoparticles in the suspension and the adsorption of various organic molecules onto TiO_2 nanoparticle surfaces [104].

In an aqueous system, nanoparticles always carry charges because of ionization, the adsorption of ions or the preferential substitution of ions from the particle surfaces [105, 106].

Physical properties of TiO_2 nanoparticles suspensions are mostly dependent on the behavior of aqueous suspensions, which are especially reactive to the electrical and ionic structure of the particle-liquid interface. Zeta potential is an important index which represents the intensity of repulsive forces among particles and the stability of dispersion. Zeta potential is crucial on the stability control of TiO_2 nanoparticles in suspensions and the adsorption properties of TiO_2 nanoparticle surfaces [105, 106].

Studies showed that the isoelectric points (IEP) could be correlated with the photocatalytic activity of TiO_2 particles and that the surface charge of TiO_2 particles affected the inactivation kinetics of bacteria significantly [107, 108]. Zeta potential of each sample with different chemical composition had different dependence on pH values. The addition of alcohol strongly affected the zeta potential values of particles [108-111].

2.5 Photocatalytic reactions and the applications of TiO_2 nanoparticles

Recent studies of TiO_2 photocatalyst have covered the photoelectrochemical conversion of solar energy, environmental photocatalytic reactions, self-cleaning surfaces, and photoinduced superhydrophilicity [8]. The most active field of TiO_2 photocatalysis is photocatalytic decomposition of organic substrates. A large variety of organic substrates, viruses, bacteria, fungi, algae and even cancer cells can be completely degraded and mineralized to CO_2 and H_2O [7]. Some recent reviews [112, 113] have provided fundamental knowledge about heterogeneous photocatalysis of TiO_2.

2.5.1 Mechanisms of the photocatalysis processes

In general, the photocatalyzed reaction can be summarized into the following equation:

$$(Ox_1)_{ads} + (\mathrm{Re}\, d_2)_{ads} \xrightarrow{h\nu > Eg} \mathrm{Re}\, d_1 + Ox_2$$

Where $(Ox)_{ads}$ is the adsorbed oxidant and $(Red)_{ads}$ is the adsorbed reducer.

Depending on the sign of Gibbs free energy, positive or negative, the reaction can be photocatalysis or photosynthesis. Hoffmann et al. [112] proposed a general mechanism for hetergeneous photocatalytsis on TiO_2. Various steps involved in the mechanism are listed as follows:

a) The electron transfer on the TiO_2 surface during the photocatalysis process:

Generation of charge-carrier

$$TiO_2 + h\nu \rightarrow h_{vb}^+ + e_{cb}^- \qquad \text{(fs)}$$

Charge-carrier trapping

$$h_{vb}^+ + > Ti^{IV}OH \rightarrow \{> Ti^{IV}OH\cdot\}^+ \qquad \text{Fast (10ns)}$$

$$e_{cb}^- + > Ti^{IV}OH \leftrightarrow \{Ti^{III}OH\} \qquad \text{Shallow trap (100ns)}$$

Dynamic equilibrium

$$e_{cb}^- + > Ti^{IV} \rightarrow > Ti^{III} \qquad \text{Deep trap (10ns)}$$

Irreversible

Charge-carrier recombination

$$e_{cb}^- + \{> Ti^{IV}OH\cdot\}^+ \rightarrow > Ti^{IV}OH \qquad \text{Slow (100ns)}$$

$$h_{vb}^+ + \{> Ti^{III}OH\} \rightarrow > Ti^{IV}OH \qquad \text{Fast (10ns)}$$

Interfacial charge transfer

1 $\{>Ti^{IV}OH\cdot\}^{+} + \mathrm{Re}d \rightarrow> Ti^{IV}OH + \mathrm{Re}d^{\cdot +}$ Slow (100ns)

2 $e_{cb}^{-} + Ox \rightarrow> Ti^{IV}OH + Ox^{\cdot -}$ Very slow (ms)

3 b) Adsorption of organic substrates:

4 $Organic \Leftrightarrow Organic(ads)$

5 Here use RX_{ad} to represent the adsorbed organic substrates.

6 $O_2(g) \Leftrightarrow O_2(ads)$

7 c) Electron transfer from either the adsorbed substrate (RX_{ad}) or the adsorbed hydroxyl radicals

8 ($\cdot OH_{ad}$) to the holes h^{+}:

9 $h^{+} + RX_{ad} \rightarrow RX_{ad}^{+}$

10 $h^{+} + H_2O_{ad} \rightarrow \cdot OH_{ad} + H^{+}$

11 $h^{+} + OH_{ad}^{-} \rightarrow \cdot OH_{ad}$

12 The second and third steps appear to be of great importance, because the major oxidant, adsorbed

13 hydroxyl radicals ($\cdot OH_{ad}$), is generated in these steps.

14 d) Molecular oxygen is presented in oxidative decomposition processes, because it is an electron

15 acceptor in the electron-transfer reaction:

16 $O_{2ad} \rightarrow 2O_{ad}$

17 $O_{ad} + e^{-} \rightarrow O_{ad}^{-}$

18 $e^{-} + O_2 \rightarrow O_2^{-}$

19 e) The superoxide anion can subsequently be involved in the following reactions and give more

20 ($\cdot OH_{ad}$) groups:

21 $H^{+} + O_2^{-} + HO_2 \rightarrow H_2O_2 + O_2$

22 $H_2O_2 + h\nu \rightarrow 2\cdot OH$

g) Finally the active free radicals ($\cdot OH_{ad}$) oxidize organic substrate (RX_{ad}) adsorb onto the surface of the semiconductor particles.

$$\cdot OH_{ad} + RX_{ad} \rightarrow Intermediate \rightarrow Alcohol, Ketone, Acid, CO_2, H_2O$$

Though some models and ideas have been proposed, our knowledge of photocatalysis mechanism on TiO_2 surfaces is not complete yet. The initial steps involving the reactive oxygen species and organic molecules are of particular interest. In most processes, oxygen acts as primary electron acceptor and the electron transfer process is the rate-determining process. According to the mechanism, the hydroxyl radical is the principal reactive oxidant in photocatalytic reactions of TiO_2 [114, 115]. H_2O_2 can act as an electron acceptor or as a direct source of hydroxyl radicals. Depending on the reaction conditions, hydroxyl radicals, superoxide H_2O_2 and O_2 can play important roles in photocatalytic reactions.

2.5.2 Kinetic model for photocatalysis processes on TiO_2 nanoparticles

Kinetics of the photocatalytic decomposition of organic substrates on TiO_2 surfaces have been well described using the Langmuir-Hinshelwood model [116, 117]. A first order kinetic versus initial substrate concentration has been well established by many studies [118-121]. The reaction rate after the adsorption equilibrium can be expressed as:

$$R = -\frac{d[C]}{dt} = \frac{k_c K_C [C]}{1 + K_C [C]} \qquad (2\text{-}1)$$

Where $[C]$ is the concentration of the substrate at time t, t is the reaction time, k_c is the Langmuir reaction rate constant, and K_C is the adsorption equilibrium constant.

Photocatalytic decomposition reactions of substrate follow the pseudo-first-order kinetics with respect to the concentration of the substrate in the bulk solution [C]:

$$-\frac{d[C]}{dt} = \frac{k_c K_C [C]}{1 + K_C [C]} = k_{app}[C] \qquad (2\text{-}2)$$

Where k_{app} is the apparent reaction rate constant.

After integration of Equation (2-2), the correlation of concentration and time can be expressed as:

$$-\ln(\frac{[C]}{[C]_0}) = k_{app} t \qquad (2\text{-}3)$$

Where C_0 is the initial concentration of the substrate.

From the definition of k_{app} in Equation (2-2), the relationship among k_{app}, k_c and K_C can be expressed as a linear equation:

$$\frac{1}{k_{app}} = \frac{1}{k_c K_C} + \frac{[C]_0}{k_c} \qquad (2\text{-}4)$$

A plot of $-\ln([C]/[C]_0)$ vs. t yields a slope of k_{app}, which represents the apparent reaction rate constant. Similarly, a plot of $1/k_{app}$ vs. $[C]_0$ yields a slope of $1/k_c$ and an intercept of $1/(k_c K_C)$. Therefore, parameters k_{app}, k_c and K_C can be found from these plots.

Operational parameters affecting the reaction rate have been well studied [12-15]. In general, higher catalyst loading mass leads to a higher decomposition rate due to the increase in surface areas and active reaction sites. An increase in oxygen concentration dose not always lead to a higher decomposition rate, because the contact of substrates with the photocatalyst surface

may be inhibited by the hydroxyl products [14]. Minor changes of temperature do not change the decomposition rate much [15].

2.5.3 Applications of photocatalysis processes with TiO_2 nanoparticles

2.5.3.1 Photocatalytic synthesis of organic substrates

Photocatalytic synthesis of organic substrates includes oxidation, reduction, isomerization, substitution and polymerization. Recently, aromatic compounds [122], acetonitrile and butyronitrile [123], saturated and unsaturated alicyclic hydrocarbons [124], alcohols [125] and amines [126] have been synthesized through the TiO_2 photocatalytic synthesis processes. Choi et al. [122] studied the effects of various parameters on the direct synthesis of phenol from benzene. In the UV-illuminated TiO_2 suspension, the phenol yield and selectivity were both enhanced. Amine could be obtained through the TiO_2 photocatalytic processes [126].

2.5.3.2 Photocatalytic decomposition of organic substrates

The most important environmental application of TiO_2 photocatalysis is the photocatalytic decomposition of organic substrates. Photocatalytic decomposition of organic substrates on TiO_2 has the following advantages over other purification methods:

a) It gives nonselective decomposition of organic and inorganic compounds under ambient temperature and pressure.

b) TiO_2 photocatalysis can work with very low concentration of contaminants (ppb level of concentration of contaminants).

c) There is no need for additional oxidants.

d) It is known to be effective for inactive substrates such as surfactants and dyes.

In the studies of the photocatalysis of TiO_2, lots of work has been done using TiO_2 nanoparticle suspension systems [20, 21]. Since it is difficult to separate and recover nanoparticles in the suspension after the reaction, various studies began to work on immobilized TiO_2 films [127- 129]. Some studies have been focused on supported TiO_2 photocatalyst films [130].

Over the past several years, a large number of applications of photocatalytic technology have been examined. Mills et al. [18, 19] studied the photocatalytic decomposition of 4-chlorophenol in a TiO_2 suspension using the commercial photocatalyst P-25 with photocatalyst loading of 0.5mg/mL. Photocatalytic decomposition of other compounds including methyl blue [131] and stearic acid [132] were also studied. They also studied the functions of different electron acceptors for the oxidation of water photocatalyzed by TiO_2 [133].

Photocatalytic decomposition of phenol and its derivates were also studied, because they are important compounds of environmental concerns in industrial effluents [134-136]. The decomposition of phenol showed different behaviors depending on the initial phenol concentration. Rodriguez et al. [134] observed two possible pathways of the decomposition of phenol. The insertion of hydroxyl radicals is favoured at low phenol concentrations (0.1g/L). The insertion of hydroxyl radicals did not affect the decomposition reaction much at high phenol concentrations (1g/L), because the decomposition took place on the TiO_2 surface by means of peroxocompound formation. It was also found that types of substrates, electronic nature of the substrates, and the position of the aromatic rings can affect the photocatalytic reactivity [137].

Sobczynski et al. [138] studied the mechanism of photocatalytic decomposition of phenol in a three phase fluidized bed reactor with a loading mass of catalyst at 0.02g/165mL. Intermediates including six hydroxylated aromatic compounds, p-benzoquinone and four aliphatic compounds were found in the decomposition of phenol. A possible mechanism of phenol photocatalytic decomposition was presented in Figure 2-1.

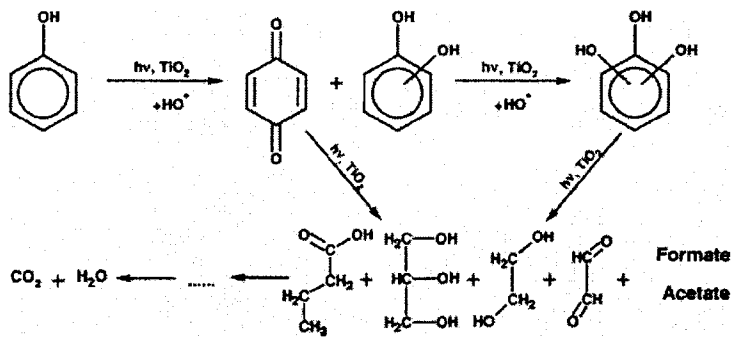

Figure 2-1, Possible mechanism of phenol photocatalytic decomposition on illuminated TiO_2 [138]

Photocatalytic decomposition of other organic substrates such as methyl orange [118], methylene blue [131], dyes [139, 140], herbicides [141, 142] and surfactants [143, 144] have also been studied. When considering the volume and chemical composition of the industrial effluents, textile dyes are one of the major pollutants in industrial effluents. Photocatalytic decomposition rate of different dyes were significantly different [139]. Depending on the nature of the substrate and pH of the solution, three possible mechanisms can contribute to dye decomposition: hydroxyl radical attack, direct oxidation by holes and direct reduction with conduction band electrons. Surfactants are increasingly used in domestic and industrial fields, although most of them are principlly biodegradable. Photocatalytic decomposition of EDTA [143], dodecyl benzene sulfonates (DBS) and sodium dodecyl sulfate (SDS) [144] showed photocatalysis is an effective alternative to remove surfactants in wastewater.

As for the inorganic contaminants, photocatalytic purification leads to deposition of environmentally harmful toxic metals on the surface of the semiconductor. Studies on the photocatalytic purification of metal ion have been reported concerning Cu^{2+}, Hg^{2+}, Cr^{6+}, and Pb^{2+} [100, 101]. Mechanism analysis of photocatalytic decomposition of nitrate on TiO_2 surfaces suggested that the major product of the photooxidation was nitrite [145]. It has been confirmed that the photocatalytic decomposition of hydrogen sulfide could occur on the TiO_2 [146].

To kill or to remove biological hosts pathogenic organisms, including bacteria, viruses, fungi, protozoa and algae from water, photocatalytic disinfection is a good alternative process [147]. It has been confirmed that the TiO_2 photocatalytic decomposition of bacteria can be described with the first-order kinetics [148]. Sakai et al. reported that it was possible to selectively kill a single cancer cell using an illuminated TiO_2 microelectrode [149]. Major applications of the TiO_2 photocatalysis process are shown in Figure 2-2.

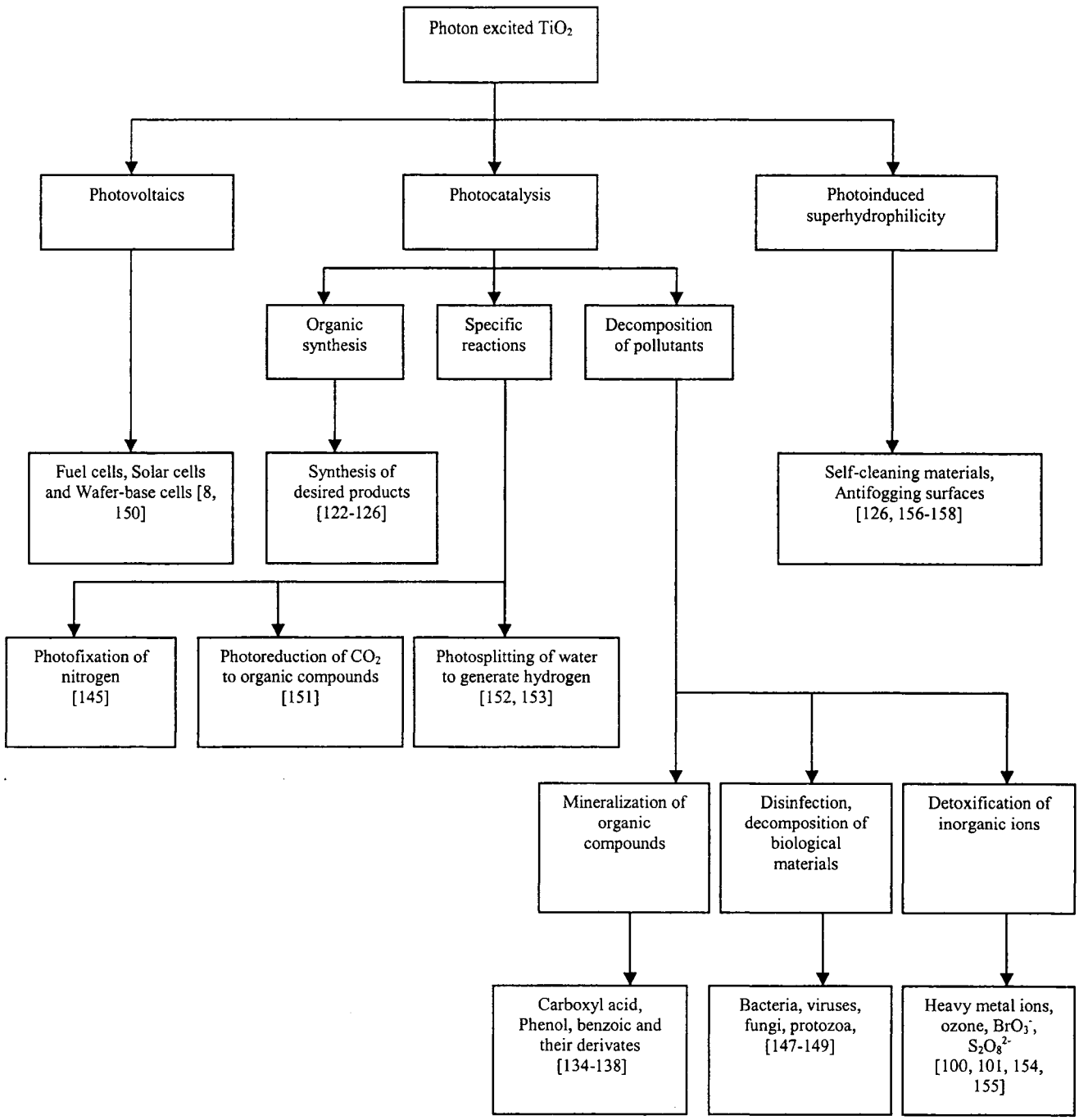

Figure 2-2, Applications of photoinduced processes of TiO_2 [6, 7]

2.5.3.4 Superhydrophilicity of TiO_2 nanoparticles

Superhydrophilicity is a newly studied photoinduced property of TiO_2 films. Water uniformly spreads on the UV light illuminated TiO_2 surface can be explained by the oxygen vacancy generated on the photoexcited TiO_2 surface. The subsequent adsorption of water after the generation of oxygen vacancies leads to the increase of Van de Waals forces and hydrogen bonding interactions between H_2O and -OH [156, 157]. Self-cleaning and anti-fogging surfaces can be synthesized according to the superhydrophilic effect. This unique property shows promising applications to the preparation of anti-stain architectural materials, anti-fogging glass and accelerated drying materials [6, 158].

2.6 Reaction systems of TiO_2 photocatalysis

Design of TiO_2 photocatalytic reaction systems has mainly focused on using either suspensions or immobilized TiO_2 films as batch or continuous flow systems. Each system has its own advantages and disadvantages.

Lots of work has been done using the TiO_2 suspensions [20, 21]. When compared with the immobilized TiO_2 systems, mass transfer and adsorption of the organic substrates on the TiO_2 surface are better in the suspension systems. When the reactions were carried out under stirring, the photocatalysts moved with the reaction solutions, the light was hard to concentrate on the TiO_2 photocatalysts. So a light concentrating reflector is commonly required in the suspension system. The major concern for the applications of TiO_2 suspensions is the separation and recovery of the suspended TiO_2 nanoparticles after reactions. Because of the tiny size of the nanoparticles, it is difficult to separate and recover the TiO_2 catalysts from the suspension

through conventional separation methods such as sedimentation, filtration or centrifugation. In addition, the suspended nanoparticles tend to aggregate at high concentrations which leads to a decrease in the surface area of the photocatalysts. The challenge in the recovery of the TiO_2 photocatalysts limits the application of the TiO_2 suspension systems.

The problem of photocatalysts recovery could be avoided by using the TiO_2 films on different substrates. Various studies were conducted on immobilized TiO_2 films [153-155]. Some studies have been focused on supported TiO_2 photocatalyst films [156]. In immobilized TiO_2 film, the TiO_2 nanoparticles were commonly immobilized on inert stationary supports such as glass, fiberglass, sand, silica gel, activated carbon, stainless steel, anodized iron, woven fibers and ceramic membranes. Immobilized TiO_2 systems are generally favored in scaling up because these designs can exclude the expensive secondary recovery of catalyst and are more suitable for the continuous flow reaction systems One of the main concern when developing immobilized TiO_2 system is the photocatalytic reaction rates may be limited by the mass transfer rates in the solutions. The light scattering phenomenon is another major concern for an immobilized TiO_2 system. When the TiO_2 photocatalyst is coated on some supports, detachment of some nanoparticles from the supports may occur in the liquid phase. To solve these problems, some studies have been done to improve the performance of immobilized TiO_2 systems, such as reducing the limitation of mass transfer through backflow and turbulence [157]. According to some reports [158], it was observed that the films exhibit higher photocatalytic activity than the powders.

2.6 Summary of literature review

1. TiO_2 nanoparticles are novel materials with unique properties. The size and shape of TiO_2 nanoparticles are key factors to determine the chemical and physical properties of TiO_2 nanoparticles. If precise control of shape and size of nanoparticles is possible, TiO_2 nanoparticles with desired photocatalytic activity can be obtained.

2. Lots of studies have been done on the synthesis of shape- and size-controlled nanoparticles with different processes. Sol-gel methods, solvothermal methods, TOPO/TOP (trioctylphosphine oxide/trioctylphosphine) method and chemical vapor deposition methods are the major methods that have been used to synthesize shape- and size-controlled nanoparticles. It was found that surfactants can control not only the size but also the shape of nanoparticles. It was suggested that the selective adsorption of surfactant molecules is the key factor in the shape controlling process of nanoparticles in solution.

3. TiO_2 nanoparticle is an important semiconductor nanomaterial and has been extensively studied because of its photocatalysis properties. The most attractive application of TiO_2 nanoparticle is the photocatalytic decomposition of environmental contaminants. The feasibility of photocatalytic decomposition of various organic and inorganic contaminants has been confirmed.

4. In order to use TiO_2 nanoparticles more effectively, synthesis of TiO_2 nanoparticles with tunable photocatalytic activity is very important. As presented previously, synthesis of TiO_2 nanoparticles with surfactants is an effective way to synthesize desired shape- and size-

controlled TiO_2 nanoparticles. Studies showed that the TiO_2 nanoparticles with different morphologies had different physical and chemical peoperties.

2.7 Significance of this study

In this study, the shape and size of TiO_2 nanosized particles were controlled by a new approach of introducing surfactants during the synthesis process. This study can provide some fundamental understanding about the correlation between the shape and size of TiO_2 nanosized particles and their photocatalytic activity. This study also gives some understanding of how to manipulate surface properties of TiO_2 nanosized particles through shape and size control. Kinetic studies of photocatalytic decomposition of phenol and methyl orange were conducted to study the potential correlation between TiO_2 nanosized particle shape and size and their photocatalytic activity. For the first time, we found that the shape, size, zeta potential and photocatalytic activity of TiO_2 nanosized particles depend on not only surfactant composition but also surfactant concentration. These results can be used to guide the preparation of TiO_2 with desired morphologies and photocatalytic activity for specific catalytic applications.

CHAPTER 3 Experimental Materials and Methods

3.1 Preparation of TiO_2 nanosized particles

TiO_2 nanosized particles were prepared through the sol-gel method with the introduction of surfactants. Titanium butoxide ($Ti(OC_4H_9)_4$ or $Ti(OBu)_4$, 97%), titanium chloride ($TiCl_4$, 99%), ethanol, sodium dodecyl benzene sulfonate (DBS), sodium dodecyl sulfate (SDS), hydroxypropyl methyl cellulose, methyl orange and phenol were purchased from Sigma-Aldrich Ltd. and used without further purification. Double distilled and deionized water was used throughout this research. Commerical TiO_2 nnoparticles, Degussa P-25, obtained from Degussa Co. Ltd., was used as the reference for photocatalystic reactions. It contains approximately 80% anatase and the rest is rutile with an average size of 50nm.

Figure 3-1 shows the process of preparation of TiO_2 nanosized particles. TiO_2 nanosized particles were obtained through the hydrolysis of $Ti(OBu)_4$. $Ti(OBu)_4$ was dissolved in ethanol with a $Ti(OBu)_4$/ethanol molar ratio of 1:10. The pH of the solution was adjusted to 2.0 with HCl. Surfactants were dissolved in ethanol according to a setting molar ratio and fed into the titanium precursor solution slowly (0.5mL/min). Then the $Ti(OBu)_4$/surfactant mixture was fed into a mixture of deionized water/ethanol ($Ti(OBu)_4$:water:ethanol molar ratio=1:4:10, 0.5mL/min). Hydrolysis reaction and polymerization took place in this mixture and TiO_2 sol was formed. After gelation for 24 hours, the gel was dried at 70^0C in an oven until yellow crystal was obtained (about 48hours). After being treated at a high temperature (500-800°C) in a muffle furnace, white TiO_2 nanosized particles were obtained.

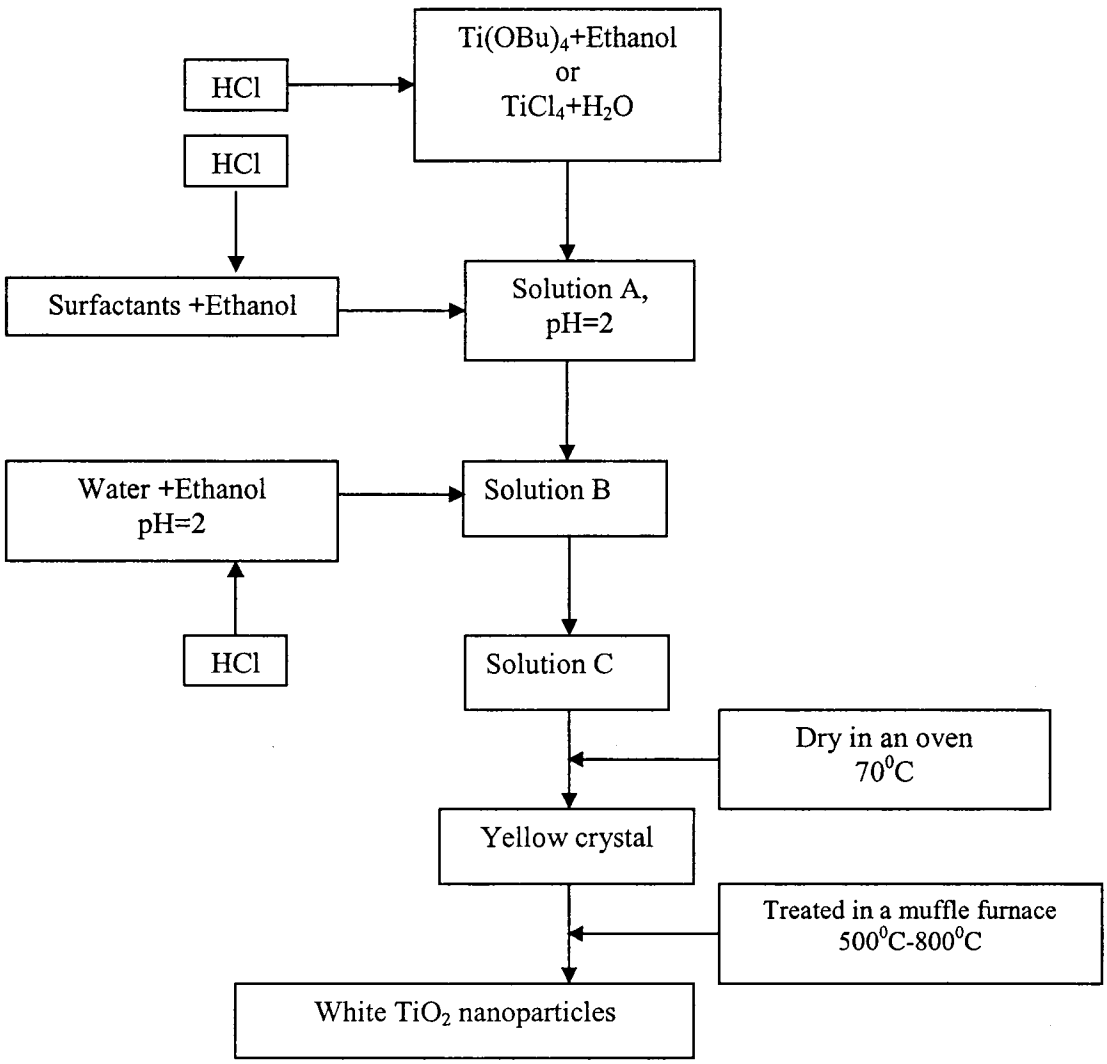

Figure 3-1, Schematic diagram of the the preparation of TiO_2 nanosized particles

3.2 Characterization of TiO_2 nanosized particles

3.2.1 Scanning Electron Microscope

The microstructure and morphology of the TiO_2 nanosized particles were observed using a Scanning Electron Microscope, JEOL5900/OXFORD SEM/EDS. Particle sizes and size distribution were studied with Image-pro Plus V4.50, Media Cybernetics, Inc. The white TiO_2 nanosized particles (0.05g) were dispersed in test tubes with 10mL deionized water. The dispersions were treated in an ultrasonic bath (Cole-Parmer Ultrasonic Cleaner, model 08895-16, 100W) for one hour. 0.02mL of the TiO_2 dispersion were droped on a piece of glass ($0.25cm^2$) and then dried in an oven at 105^0C for 24 hours. Then the nanosized particles were studied with the Scanning Electron Microscope.

3.2.2 X-ray diffraction

An XRD scan of the nanosized particles was performed using a D/Max III x-ray diffractometer using Cu-Kα radiation (Philips). In the XRD patterns of TiO_2 nanosized particles, rutile and anatase characteristic peaks can be used to identify the crystal composition of the TiO_2 nanosized particles.

The characteristic peaks of anatase locate at [7]:

$2\theta = 25.28^0$ (101 facet) and $2\theta = 48.0^0$.

Whereas the characteristic peaks locate at:

$2\theta = 27.42^0$ (110 facet) and $2\theta = 54.5^0$.

Using the characteristic diffraction peak strengths, the compositions of the crystals can be evaluated.

$$X_A(\%) = \frac{100}{(1+1.265\frac{I_R}{I_A})} \qquad (3\text{-}1)$$

Where X_A is the anatase percentage, I_A is the diffraction peak strength at $2\theta=25.28^0$, I_R is the diffraction peak strength at $2\theta=27.4^0$.

3.2.3 UV-Vis light reflectance

The light reflectance property was studied with Cary50 UV-VIS-NIR spectrophotometer (Varian Australia PYT Ltd).

3.2.4 FTIR analysis

Fourier transform infrared spectrums (FTIR) of the synthesized nanosized particles were studied with Bruker Ten 37 FTIR Spectrometer (Bruker Co, Ltd).

3.2.5 Zeta potential measurement

The TiO_2 nanosized particles were dispersed in deionized water and sonificated in an ultrasonic bath for one hour. The pH of this suspension was adjusted to setting points with HCl or NaOH. Zeta potential of dispersed TiO_2 nanosized particles in aqueous phase was measured using a Zetacompact Z8000 model (CAD Instrumentation). The Smoluchowski equation was chosen in the software to calculate the zeta potential of TiO_2 nanosized particles. The electric field added on the suspension was controlled by the cell voltage of Zetacompact Z8000 model and was fixed at 80v. The zeta potential of TiO_2 nanosized particles was measured at different pH values.

3.3 Photocatalytic activity evaluation

The photocatalytic activity of prepared TiO_2 nanosized particles was evaluated in fixed film batch reactors using phenol and methyl orange (MO) as model compounds. TiO_2 nanosized particles were dispersed in deionized water in a test tube and then treated in an ultrasonic bath for 30 minutes. Then the suspension was evenly poured onto a 10cm diameter petri dish. The dishes were dried in an oven and flushed with deionized water until the pH value of the flushing water became neutral and the weight of the dishes was constant after drying at 105^0C. The loading weight of TiO_2 nanosized particles in each petri dish was controlled at 0.50 mg/cm^2. 80mL of model compound solution was added into the TiO_2 coated dishes. The solution was mixed by using a magnetic stirrer (1.5cm in length) at a stirring speed of 60rpm. The reaction was illuminated by a 6w UV lamp (Blak. Ray UVL 56, wavelength = 365nm) in a black box. The light intensity was measured by a light intensity meter (Photon Technology International) and controlled at 2.5mW/cm^2 during this study (except for the study of light intensity). The change in the concentration of methyl orange or phenol solution with time was determined by using a Cary50 UV-VIS-NIR spectrophotometer (Varian Australia PYT Ltd) with 1 mL sample withdrawn each time for analysis. The samples were poured back to the reactor rightaway after analyses were done.The wavelength used for the measurement of phenol and MO concentration was 270 and 465nm, respectively.

The results of blank experiments under similar conditions but without the addition of catalysts indicated that there was a loss of 1-2% (wt%) solution volume due to the UV irradiation and reactor open to the air but the loss of substrate was negligible. A comparison of the TiO_2 catalyst loading weight before and after experiment suggested that 3-6% (wt%) of fixed TiO_2 films were sheared out from the Petri dish surface into the solution as suspended particles. For a comparative study of catalyst activity, effect due to this change should not be significant.

3.4 Evaluation of reaction rate constant and adsorption equilibrium constant

Kinetic studies of MO and phenol were done on different nanosized particles synthesized with different surfactants and molar ratios. The photocatalytic decomposition of MO was studied on four concentrations: 1500, 2500, 3000 and 3500μg/L.

It was reported that the reaction rate of phenol decomposition on the UV illuminated TiO_2 was strongly retarded at 100mg/L and 150mg/L [138]. The decomposition rate of phenol increased with an increase in the phenol concentration ranging from 10mg/L to 120mg/L [159]. In addition, according to our preliminary study, the concentration of phenol has good linear correlation with the absorbance at a wavelength of 270nm when the concentration is lower than 150mg/L. The photocatalytic decomposition of phenol was studied on four concentrations: 100mg/L, 50mg/L, 25mg/L and 5mg/L, respectively.

The reaction rate constants and adsorption equilibrium constants were calculated according to Equations (2-1) to (2-4). A plot of $-\ln([C]/[C]_o)$ vs. t yields a slope of k_{app}, which represents the apparent reaction rate constant (k_{app}). Similarly, a plot of $1/k_{app}$ vs. $[C]_o$ yields a

slope of $1/k_c$ and an intercept of $1/(k_cK_C)$. Therefore, parameters k_{app}, k_c and K_C can be found from these plots.

3.5 Evaluation of the effect of light intensity on the decomposition reaction rates

Illuminating light intensity is a determining factor of the decomposition rates of organic substrates. In this study, the nanosized particles synthesized at a DBS/$Ti(OBu)_4$ molar ratio of 5:1, a cellulose/$Ti(OBu)_4$ molar ratio of 1×10^{-3}:1 and a SDS/$Ti(OBu)_4$ molar ratio of 0.02:1, had the highest photocatalytic activity in each surfacetant at different concentrations and were thus used for the evaluation of the effect of light intensity.

Light intensity was adjusted by changing the distance between the solutions and light source and measured by a light intensity meter obtained from Photon Technology International. The photocatalytic decomposition of phenol and MO were carried out under the following light intensities: 1.4, 2.0, 2.5, 3 and 3.4mW/cm^2. The initial concentration of phenol and MO was 0.001mol/L and 0.004mol/L, respectively.

CHAPTER 4 Shape and Size Evolution of TiO_2 Nanosized particles with Different Surfactants

4.1 Morphologies of shape- and size-controlled TiO_2 nanosized particles

4.1.1 Effect of surfactants on the morphology of TiO_2 nanosized particles

In order to learn about the effect of surfactants on the shape and size of nanosized particles, it is necessary to know the morphology of TiO_2 nanosized particles synthesized through sol-gel method without surfactants. The morphology of TiO_2 nanosized particles synthesized from $Ti(OBu)_4$ and $TiCl_4$ without surfactants is shown in Figure 4-1.

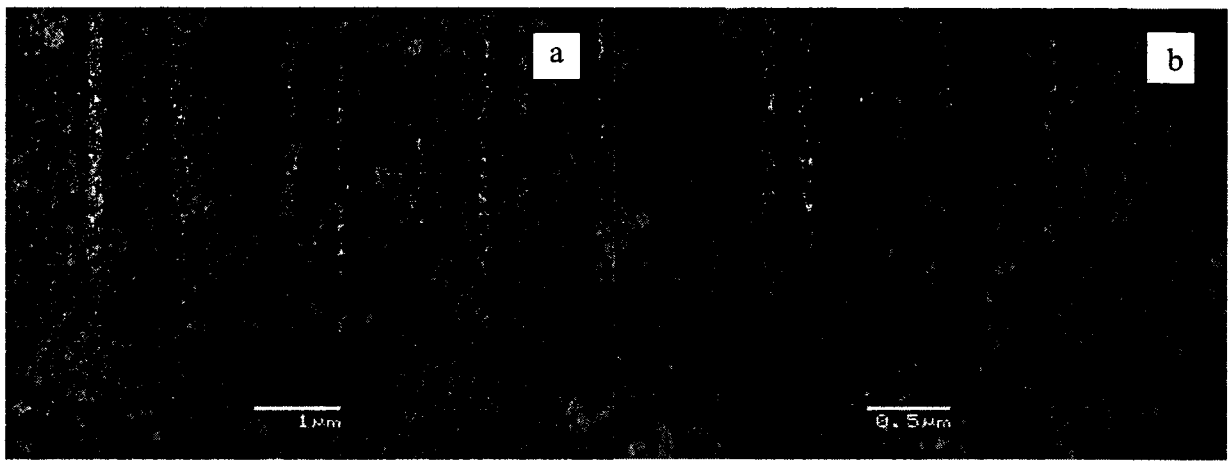

Figure 4-1, TiO_2 nanosized particles synthesized from $Ti(OBu)_4$ and $TiCl_4$ without using surfactants (a) $Ti(OBu)_4$, (b) $TiCl_4$.

As shown in Figure 4-1, the average sizes of the TiO_2 nanosized particles ranged from ~100nm to ~200nm and were irregularly shaped. In addition, the nanosized particles aggregated and formed large blocks. Effects of surfactants on the shapes of TiO_2 nanosized particles are shown in Figures 4-2 to 4-7. The TiO_2 nanosized particles were all synthesized with a surfactant/$Ti(OBu)_4$ molar ratio of 1:1. Run 1 and Run 2 in Figures 4-2 to 4-4 represent two TiO_2

nanosized particles synthesized under the same conditions. They show the reproduciability of the experiments.

Figures 4-2 to 4-4 show the morphologies of the TiO_2 nanosized particles synthesized from $Ti(OBu)_4$ whereas Figures 4-5 to 4-7 show the morphologies of the TiO_2 nanosized particles synthesized from $TiCl_4$. Uniform spherical TiO_2 nanosized particles with an average diameter of ~250nm were obtained when DBS was used (Figure 4-2). Uniform cubic shape nanosized particles were obtained when cellulose and SDS were used respectively (Figures 4-3 and 4-4). TiO_2 nanosized particles shaped by SDS contain an average dimension of ~150nm. TiO_2 nanosized particles shaped by cellulose contain a slightly larger dimension of ~300nm, as compared to the TiO_2 nanosized particles shaped by SDS. A relatively larger particle size with the use of cellulose would be due to the higher viscosity of the sol. Cellulose contains larger molecular sizes and links than that of the DBS and SDS, which lead to a high viscosity of the TiO_2 sol. The high viscosity of the sol results in a larger sol particle size, and this affects its final size. Through the comparison of Figure 4-1 and Figures 4-2 to 4-4, the shape- and size-controlled TiO_2 nanosized particles show much better uniformity in shape and size distribution than those prepared without surfactants.

A striking difference in the shape of TiO_2 nanosized particles were found when $TiCl_4$ was used as a titanium precursor (Figures 4-5 to 4-7). Uniform ellipse-shape particles with a diameter in width of about 500nm were formed when DBS was used, as shown in Figure 4-5.

As shown in Figure 4-6, short TiO_2 nanorods were observed when cellulose was used. The nanorods had an average dimension of 300nm in diameter and 1000nm in length. Similar to

the use of $Ti(OBu)_4$ precursor, cubic nanosized particles, as shown in Figure 4-7, were obtained when $TiCl_4$ was used as the titanium precursor with the introduction of SDS. In the cases of using $TiCl_4$ precursor, the average dimension of TiO_2 nanosized particles was 250nm which was slightly larger than the cubic nanosized particles prepared from $Ti(OBu)_4$. As compared to the TiO_2 nanosized particles prepared without using surfactants, shape-controlled nanosized particles had slightly larger sizes but had fewer aggregates, much better shape uniformity, and narrower size distribution.

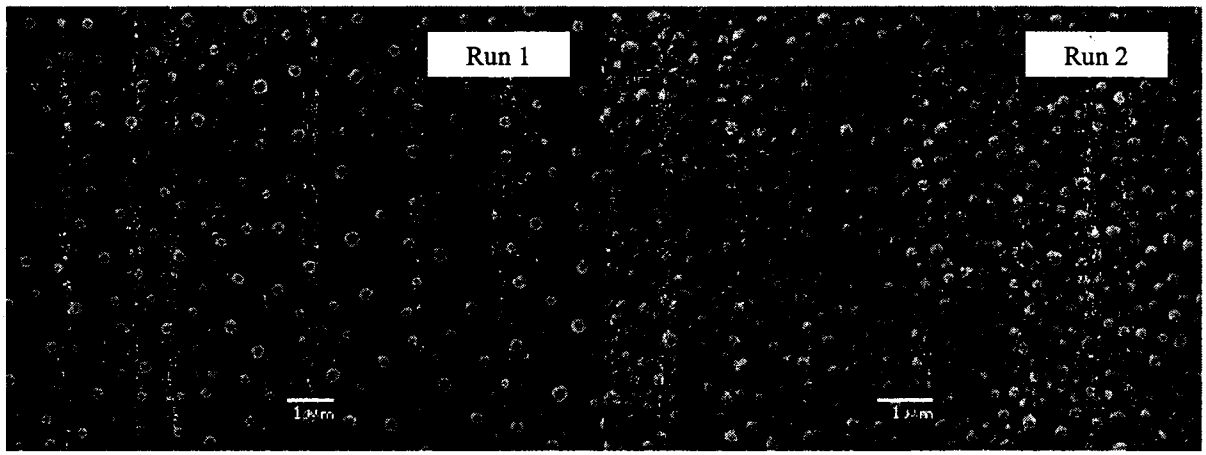

Figure 4-2, Nanosized particles shape controlled by DBS from $Ti(OBu)_4$

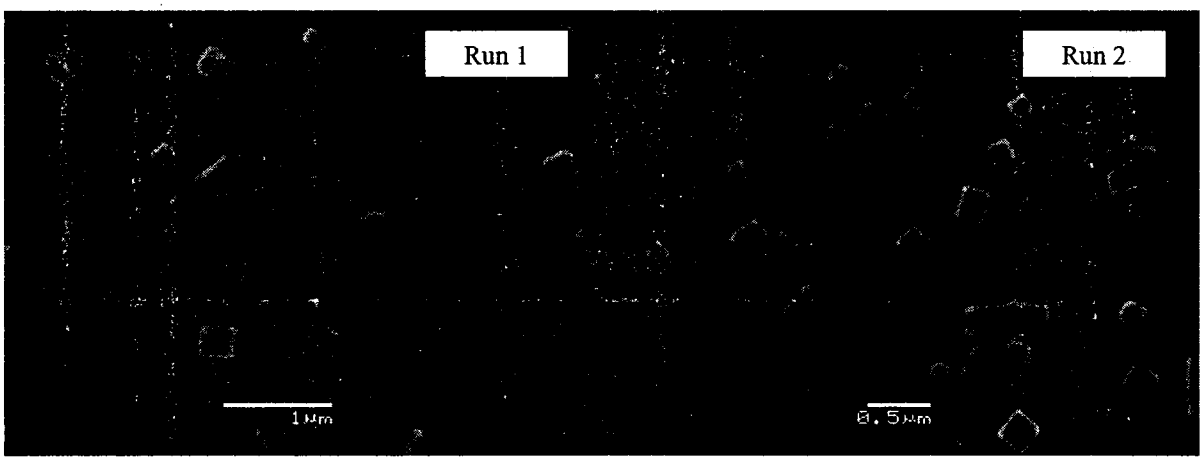

Figure 4-3, Nanosized particles shape controlled by cellulose from $Ti(OBu)_4$

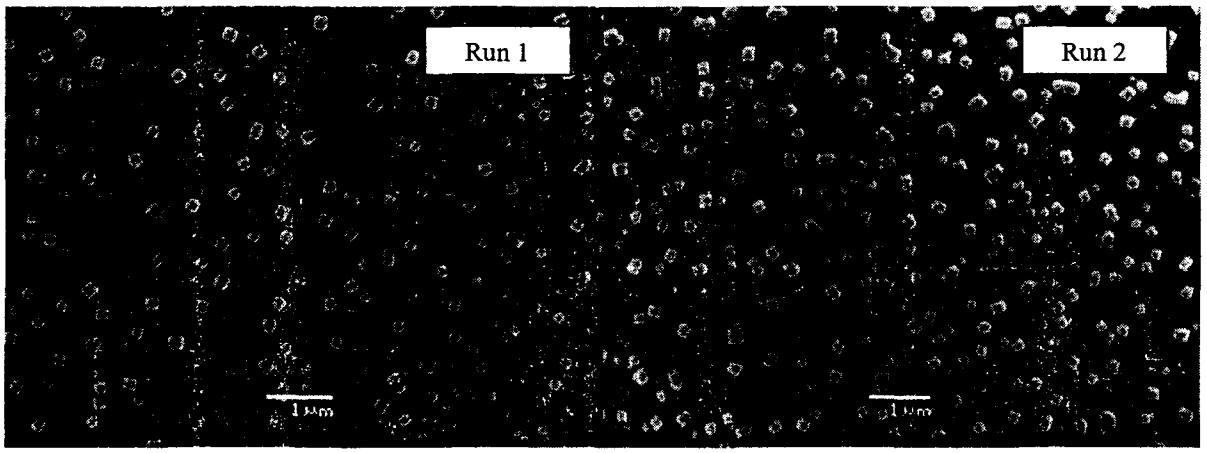

Figure 4-4, Nanosized particles shape controlled by SDS from $Ti(OBu)_4$

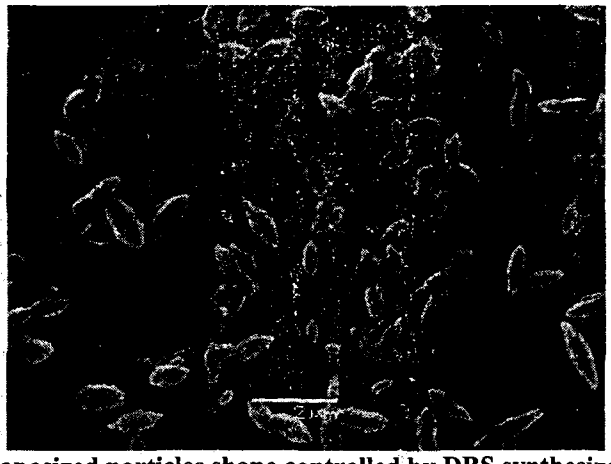

Figure 4-5, Nanosized particles shape controlled by DBS synthesized from $TiCl_4$

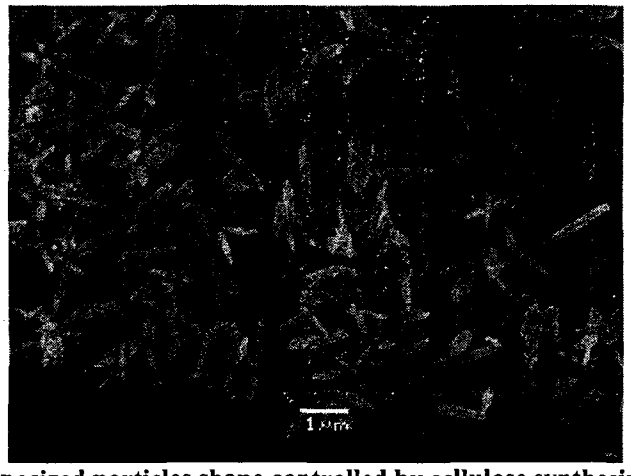

Figure 4-6, Nanosized particles shape controlled by cellulose synthesized from $TiCl_4$

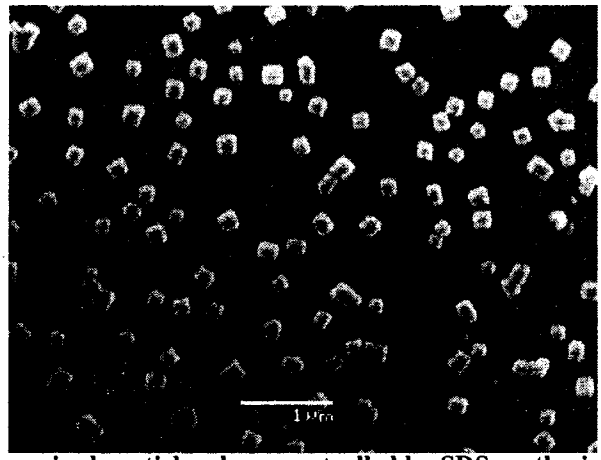

Figure 4-7, Nanosized particles shape controlled by SDS synthesized from $TiCl_4$

4.1.2 Shape and size evolution of TiO_2 nanosized particles synthesized from $Ti(OBu)_4$

The effect of sodium dodecyl benzene sulfonate (DBS)/$Ti(OBu)_4$ molar ratio on the shape and size evolution of TiO_2 nanosized particles is shown in Figure 4-8 (a-f). Spherical TiO_2 nanosized particles were obtained when DBS was used. Shape uniformity of TiO_2 nanosized particles was improved with the use of DBS when compared with the nanosized particles in Figure 4-1. The size of the nanosized particles decreased from 1μm (Figure 4-8 (a)) to 50nm (Figure 4-8 (f)) when the molar ratio of DBS/$Ti(OBu)_4$ was increased from 0.25:1 to 5:1. Narrower size distribution of the nanosized particles can be obtained with higher DBS/$Ti(OBu)_4$ molar ratios. As proposed by Pileni et al. [31], lower concentrations of precursor monomer favour the formation of spherical nanosized particles. With an increase in the DBS/$Ti(OBu)_4$ molar ratio, TiO_2 nanosized particles were formed with smaller sizes and narrower size distributions.

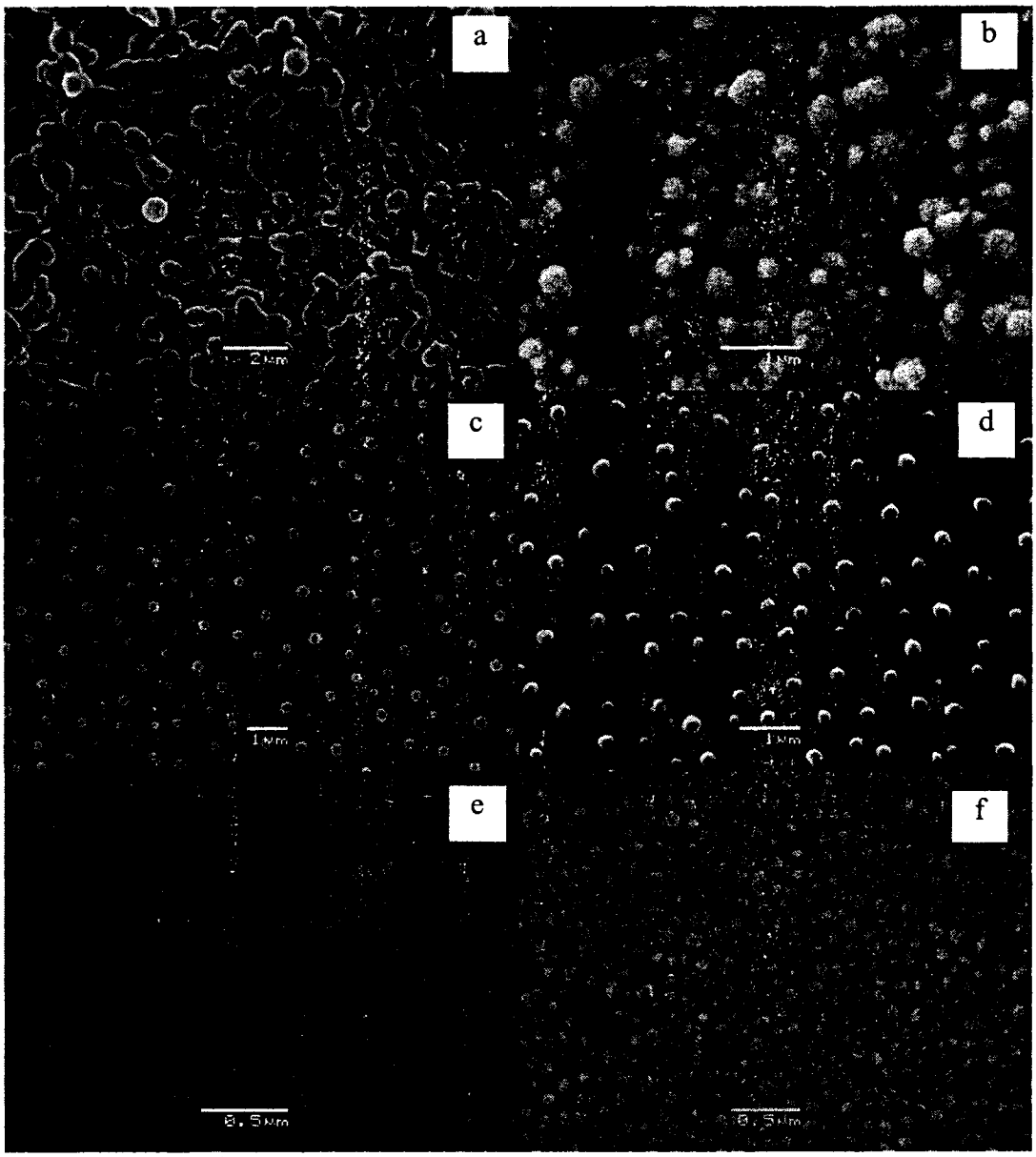

Figure 4-8, Size evolution of TiO_2 nanosized particles with increasing DBS/Ti(OBu)$_4$ molar ratio (calcined at 600^{0}C):
(a) 0.25:1, (b) 0.5:1, (c) 1:1, (d) 2:1, (e) 4:1, (f) 5:1.

Figure 4-9 (a-h) show the size evolution of TiO_2 nanosized particles obtained by increasing the molar ratio of cellulose/$Ti(OBu)_4$ from $5x10^{-4}$:1 to $1x10^{-1}$:1 and keeping the $Ti(OBu)_4/H_2O$ molar ratio constant (1:4). Figure 4-9 (a-d) shows that TiO_2 nanorods could be obtained with a lower cellulose/$Ti(OBu)_4$ molar ratio ($\leq 2x10^{-3}$:1). The dimensions of the nanorods were decreased from 500nm in diameter and 5000nm in length to 100nm in diameter and 500nm in length with an increase in the cellulose/$Ti(OBu)_4$ molar ratio. When a higher cellulose/$Ti(OBu)_4$ molar ratio ($1x10^{-2}$:1 to $1x10^{-1}$:1) was used, cubic nanosized particles were formed (Figure 4-9 (e-h)). The dimensions of the cubic TiO_2 nanosized particles were decreased from ~200nm to ~50nm when the cellulose/$Ti(OBu)_4$ molar ratio was increased from $1x10^{-2}$:1 to $8x10^{-2}$:1. Uniformity of the nanosized particles was also improved when the cellulose/$Ti(OBu)_4$ molar ratio was increased.

Figure 4-10 shows the morphology of the particles synthesized with a cellulose/$Ti(OBu)_4$ molar ratio of 5:1. When the cellulose/$Ti(OBu)_4$ molar ratio was increased to 5:1, the viscosity of the TiO_2 sol increased dramatically. Gelation took place at the early stage of the hydrolysis of $Ti(OBu)_4$. There was not enough time and space for the TiO_2 nanocrystal nucleus to grow and form good crystallinity. As shown in Figure 4-10, large TiO_2 particle blocks were formed and no uniformly shaped TiO_2 nanosized particles were obtained.

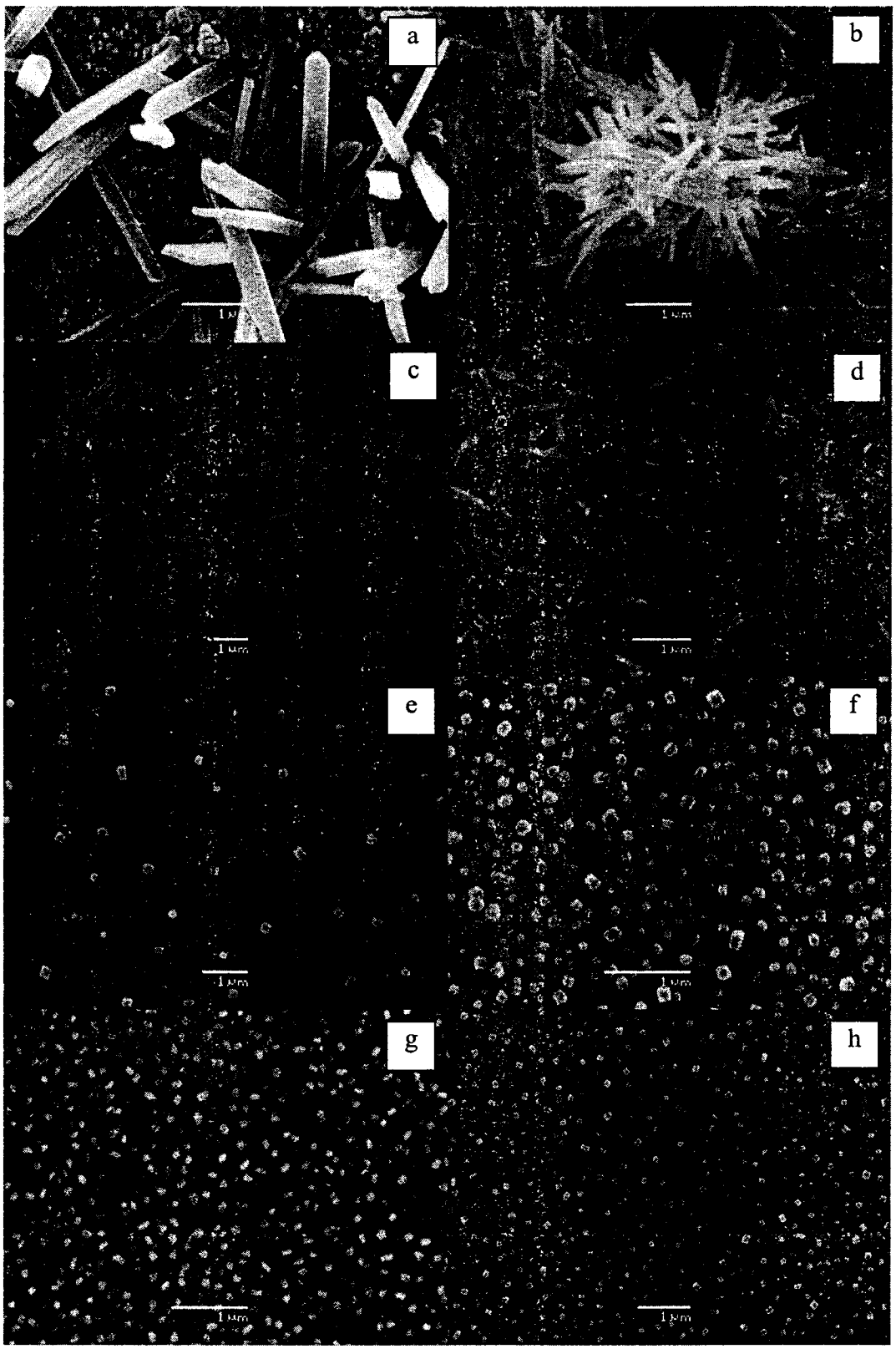

Figure 4-9, Shape evolution of TiO_2 nanosized particles by increasing cellulose/ $Ti(OBu)_4$ molar ratio (calcined at 600^0C):
(a) $5x10^{-4}$:1, (b) $7x10^{-4}$:1, (c) $1x10^{-3}$:1, (d) $2x10^{-3}$:1, (e) $1x10^{-2}$:1, (f) $4x10^{-2}$:1, (g) $8x10^{-2}$:1, (h) $1x10^{-1}$:1.

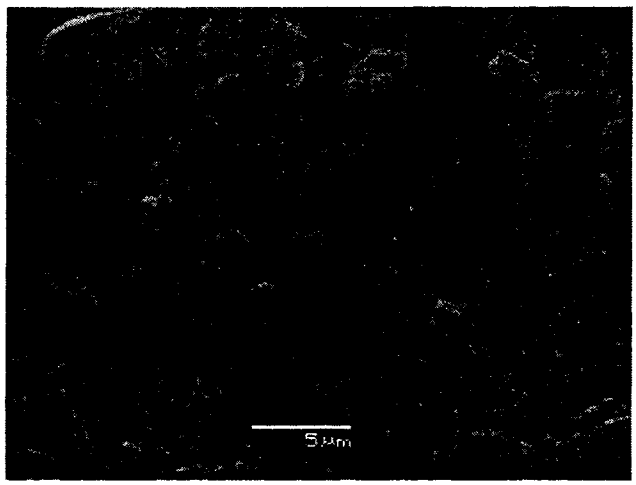

Figure 4-10, TiO_2 particles synthesized with cellulose/$Ti(OBu)_4$ molar ratio 5:1

Figure 4-11 (a-h) shows the TiO_2 nanosized particles shape controlled by SDS at different SDS/$Ti(OBu)_4$ molar ratios. Well shaped TiO_2 nanorods with dimensions of 300-100nm in diameter and 800-500nm in length were formed when SDS was used (Figure 4-11 (a) to (d)). The shape uniformity of nanorods was improved with an increase in the SDS/$Ti(OBu)_4$ molar ratio from 0.01:1 to 0.025:1. The best uniformity was formed at an SDS/$Ti(OBu)_4$ molar ratio of 0.025:1.When the SDS/$Ti(OBu)_4$ molar ratio was set at 0.01:1 (Figure 4-11 (a)), the nanorods aggregated and the morphology of the nanorods was not clear. Figure 4-12 is the portion magnified image of the cross-section of the TiO_2 nanorods. It shows that the nanorods synthesized with an SDS/$Ti(OBu)_4$ molar ratio of 0.025:1 are symmetrical and hexagonal.

Cubic TiO_2 nanosized particles were obtained when the SDS/$Ti(OBu)_4$ molar ratio was higher than 0.08:1 (Figure 4-11 (d-h)). Cubic TiO_2 nanosized particles with an average dimension of about 500nm were obtained when the SDS/$Ti(OBu)_4$ molar ratio was set at 0.08:1 and 0.5:1. Uniformity of the shape was improved, and the size of the cubic nanosized particles was decreased, when the SDS/$Ti(OBu)_4$ molar ratio was increased. Uniform cubic TiO_2 nanosized particles were obtained at an SDS/$Ti(OBu)_4$ molar ratio of 5:1. These results, as

shown in Figures 4-8 to 4-11, indicate that the shape evolution of the TiO_2 nanorods and nanosized particles depends on not only surfactant composition but also surfactant concentration.

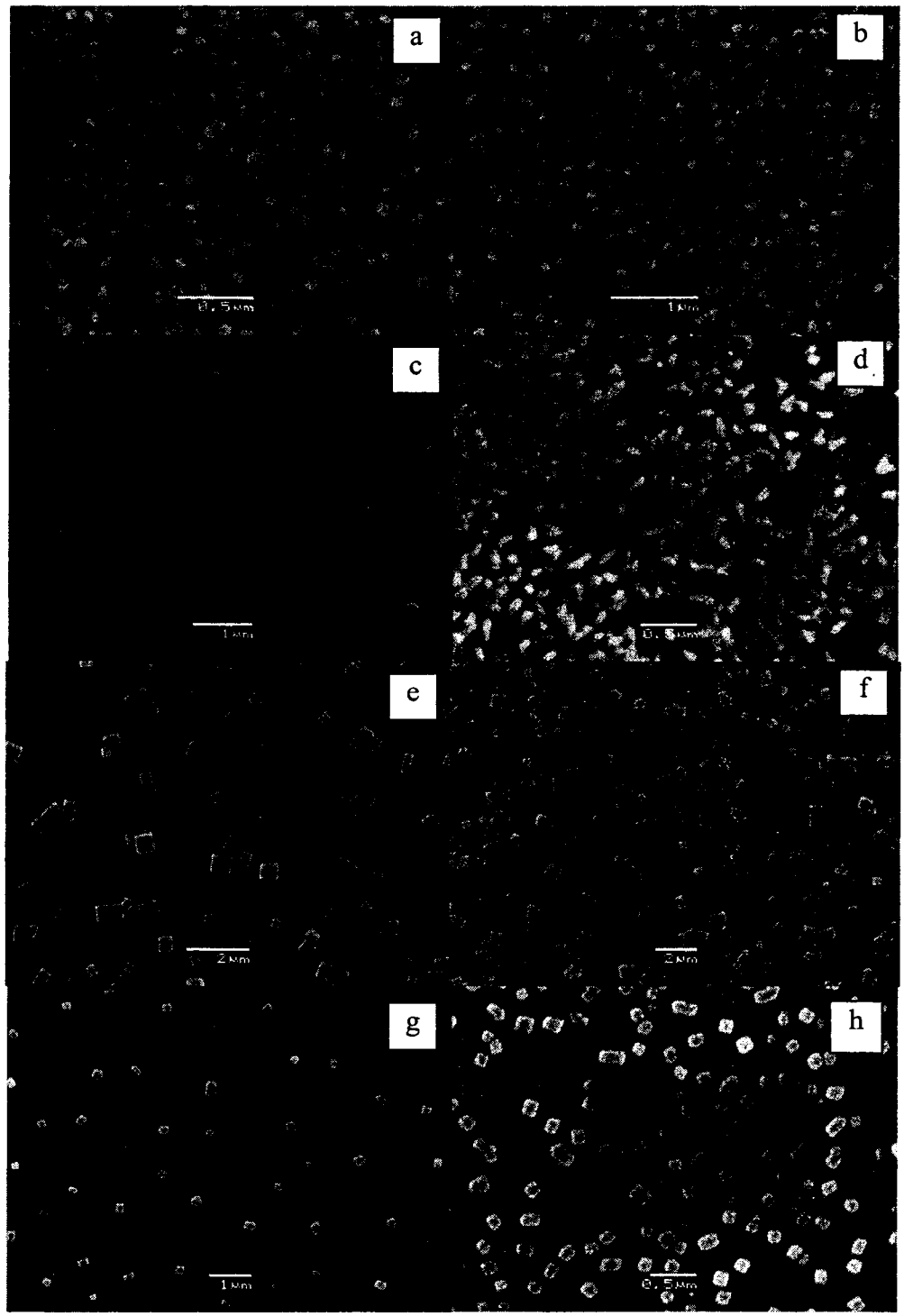

Figure 4-11, Shape evolution of TiO_2 nanosized particles by increasing SDS/$Ti(OBu)_4$ molar ratio (calcined at 600^0C):
(a) 0.01:1, (b) 0.02:1, (c) 0.025:1, (d) 0.04:1, (e) 0.08:1, (f) 0.5:1, (g) 2.5:1, (h) 5:1.

Figure 4-12, Magnified image of TiO_2 nanorod

4.1.3 Shape and size evolution of TiO_2 nanosized particles synthesized from $TiCl_4$

Shape and size evolution of the TiO_2 nanosized particles synthesized from $TiCl_4$ with different DBS/$TiCl_4$ molar ratio are shown in Figure 4-13. Figure 4-13 (a-d) shows the SEM images of the elliptical TiO_2 nanosized particles synthesized with an increase in the DBS/$TiCl_4$ molar ratio. The size of the nanosized particles decreased as the DBS/$TiCl_4$ molar ratio was increased. The shape of nanosized particles synthesized from $TiCl_4$ in Figure 4-13 is obviously different from the nanosized particles synthesized from $Ti(OBu)_4$. Better shape uniformity and size distribution were obtained when the DBS/$TiCl_4$ molar ratio was increased.

Figure 4-14 (a)-(d) shows the size evolution of TiO_2 nanorods when the cellulose/$TiCl_4$ molar ratio was increased from 1×10^{-4}:1 to 1×10^{-3}:1. The dimensions of the TiO_2 nanorods ranged from 1000nm to 300nm in diameter and 10μm to 5μm in length. Figure 4-14 (d) shows the morphology of the TiO_2 disks synthesized at a cellulose/$TiCl_4$ molar ratio of $1x10^{-3}$:1. TiO_2 disks of ~50nm in thickness were formed. The disks piled together and formed large aggregates. When the cellulose/$TiCl_4$ molar ratio was set at 5:1, large aggregates were formed and no uniform nanosized particles were obtained as shown in Figure 4-15.

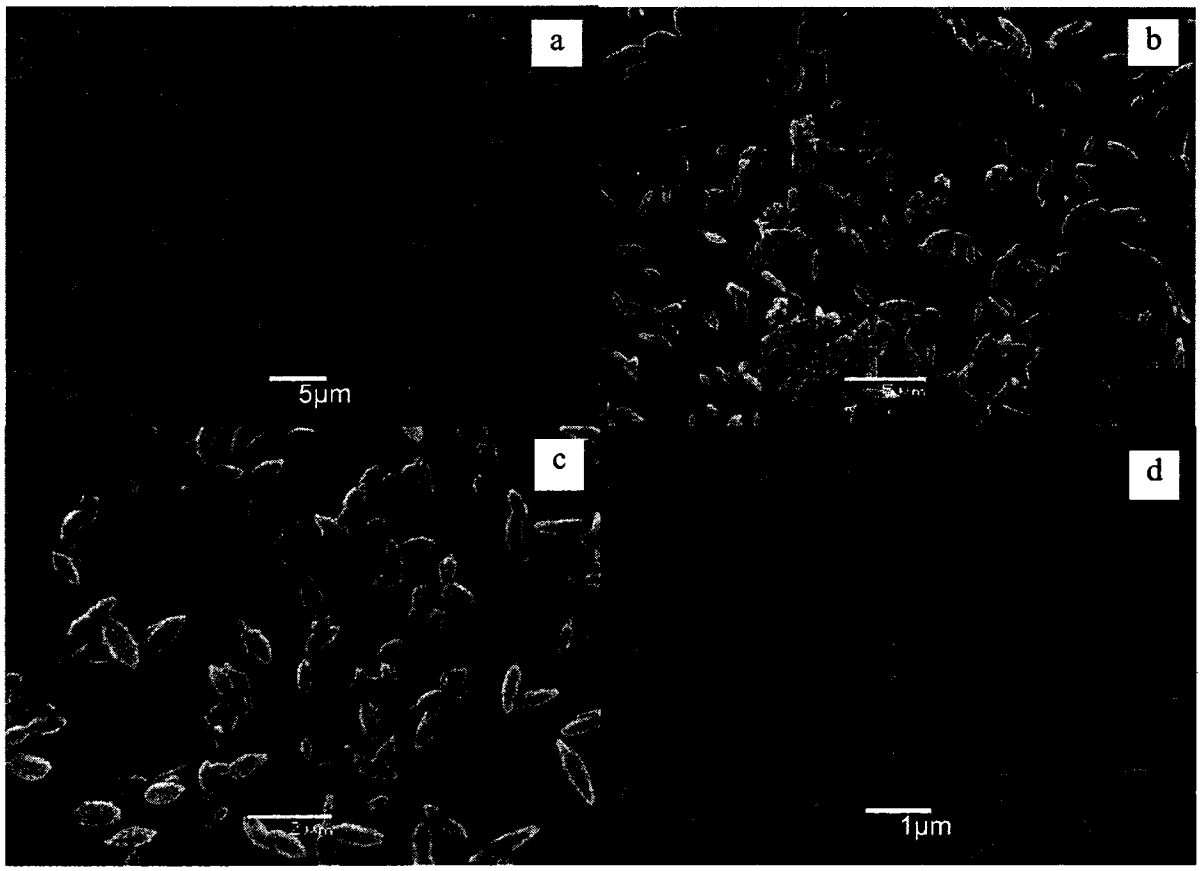

Figure 4-13, Size evolution of TiO_2 nanosized particles with increasing DBS/$TiCl_4$ molar ratio
(a) 0.2:1, (b) 0.4:1, (c) 1:1, (d) 5:1

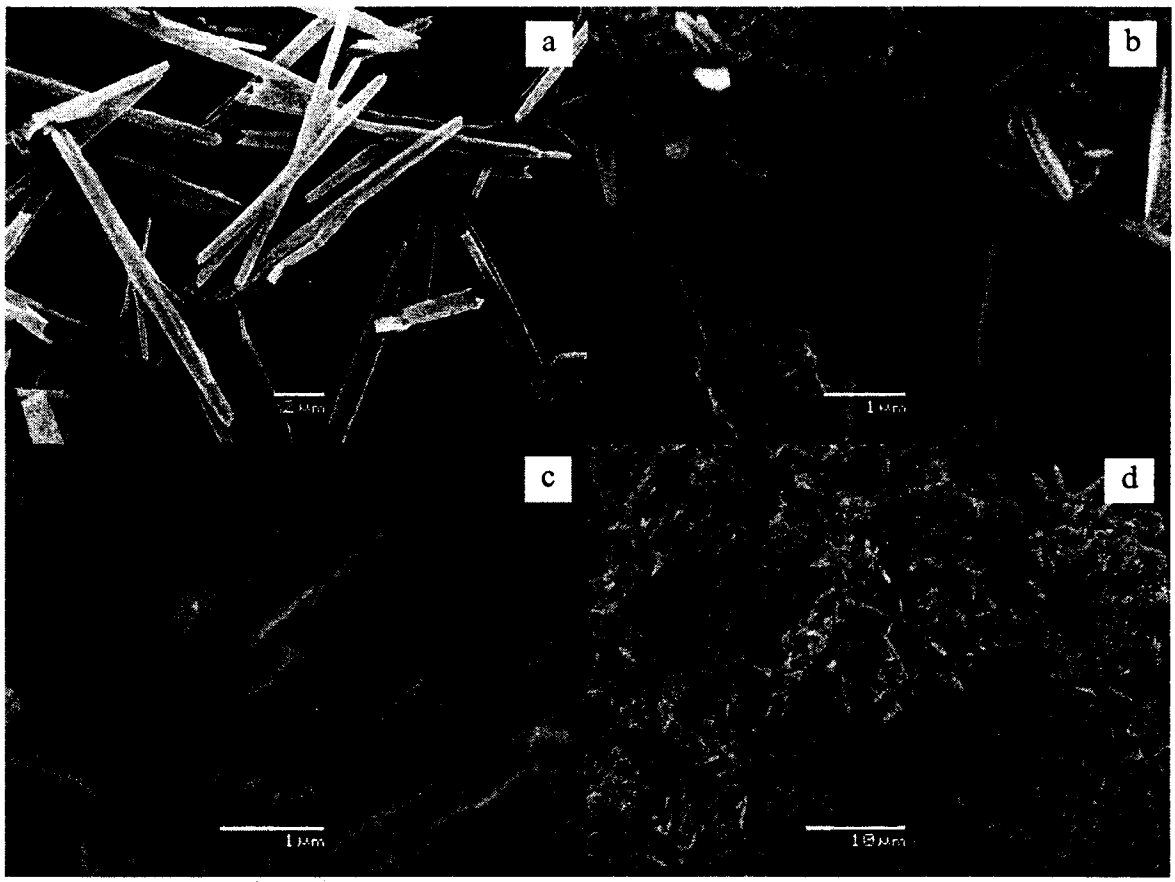

Figure 4-14, Size evolution of TiO_2 nanosized particles with increasing Cellulose/ $TiCl_4$ molar ratio (calcined at 500^0C):
(a) 1×10^{-4}:1, (b) 5×10^{-4}:1, (c) 7×10^{-4}:1, (d) 1×10^{-3}:1.

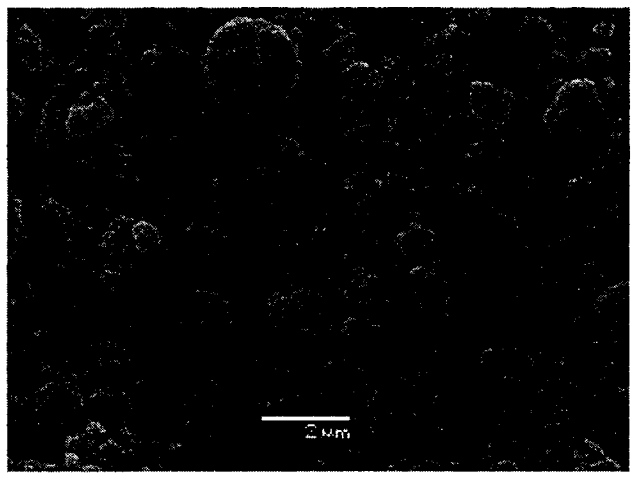

Figure 4-15, TiO_2 particles synthesized with a cellulose/$TiCl_4$ molar ratio of 5:1.

Figure 4-16 (a) to (d) show the size evolution of the hexagonal nanorods with an increase in the $SDS/TiCl_4$ molar ratio. When $TiCl_4$ and SDS were used, hexagonal nanorods were obtained. Shape uniformity was improved when the $SDS/TiCl_4$ molar ratio was increased from 0.001:1 (Figure 4-16 (a)) to 0.025:1 (Figure 4-16 (b)). Complete and well crystallized hexagonal TiO_2 nanorods of ~800nm in diameter and ~2μm in length were obtained (Figure 4-16 (c)). Symmetrical and hexagonal nanorods with a uniform morphology and uniform size of ~500nm in diameter and ~2μm in length were formed at an $SDS/TiCl_4$ molar ratio of 0.025:1 (Figure 4-16 (d)). When $TiCl_4$ was used, there were fewer organic molecules and links to constrain the movement of the TiO_2 monomers. The $TiCl_4$ hydrolyzed vigorously, thus larger dimension nanorods could be formed than the nanosized particles synthesized from $Ti(OBu)_4$.

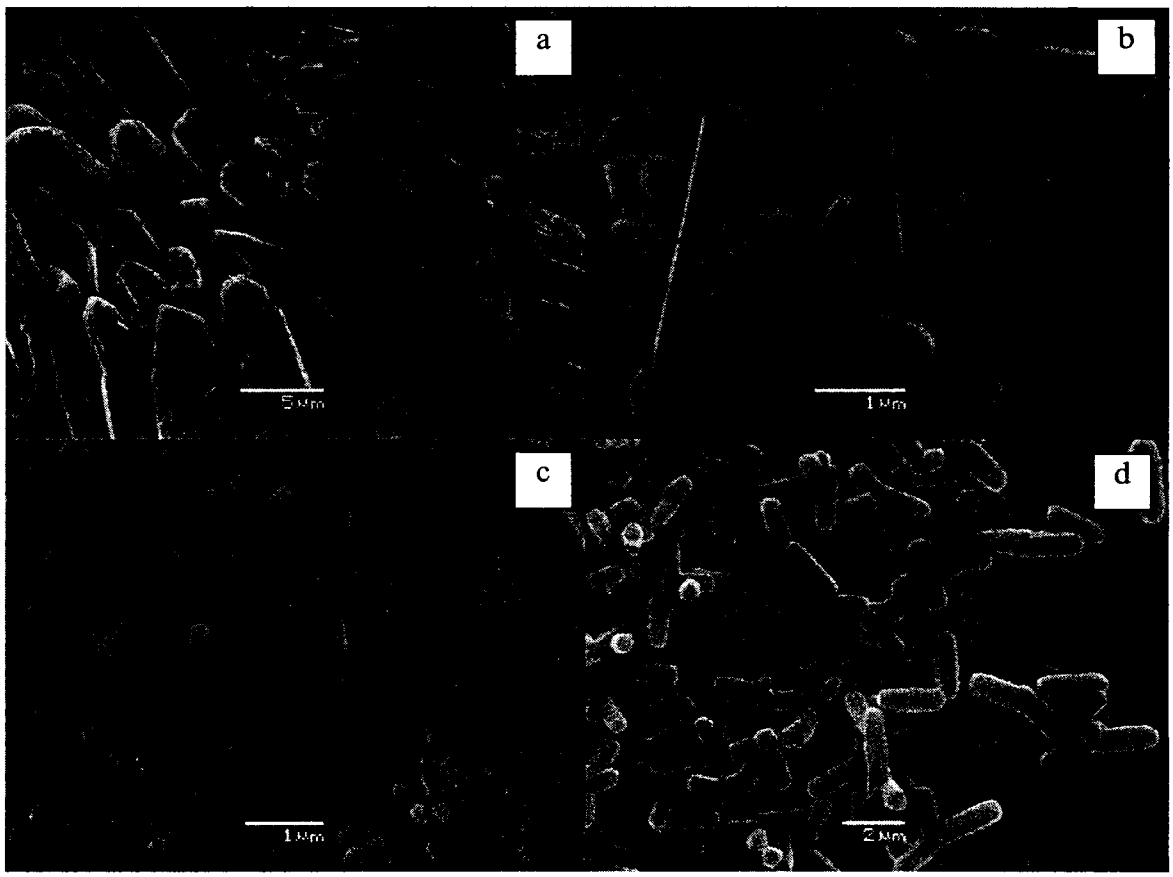

Figure 4-16, Size evolution of TiO_2 nanorods synthesized with different $SDS/TiCl_4$ molar ratio
(a) 0.001:1, (b) 0.002:1, (c) 0.01:1, (d) 0.025:1.

4.1.4 Influence of calcination temperature on the morphologies

Calcination temperature is another important factor that can affect the morphology of the nanosized particle formation. Figure 4-17 (a) to (e) show the different morphologies of the nanosized particles synthesized at an SDS/$Ti(OBu)_4$ molar ratio of 0.02:1 and calcined at different temperatures (400^0C to 800^0C). When the gel was calcined at 400^0C, the size of formed particles was larger and the shape was poorly formed because the surfactants and residual carbon could not be completely removed. Uniform nanorods were shown in Figure 4-17 (b) when the nanosized particles were calcined at 500^0C. Well shaped nanorods were obtained when the calcination temperature was 600^0C. The size of the nanorods calcined at 600^0C was similar to that of the nanorods calcined at 500^0C. At high temperature, the diffusion and the surface energy of the small particles increases. The small particles trend to agreegate together to lower the total surface energy of the particles at high temperature [174], small agglomerates or larger sizes of TiO_2 nanorods were formed when the calcination temperature was increased from 700^0C to 800^0C (Figure 4-17 (c-e)).

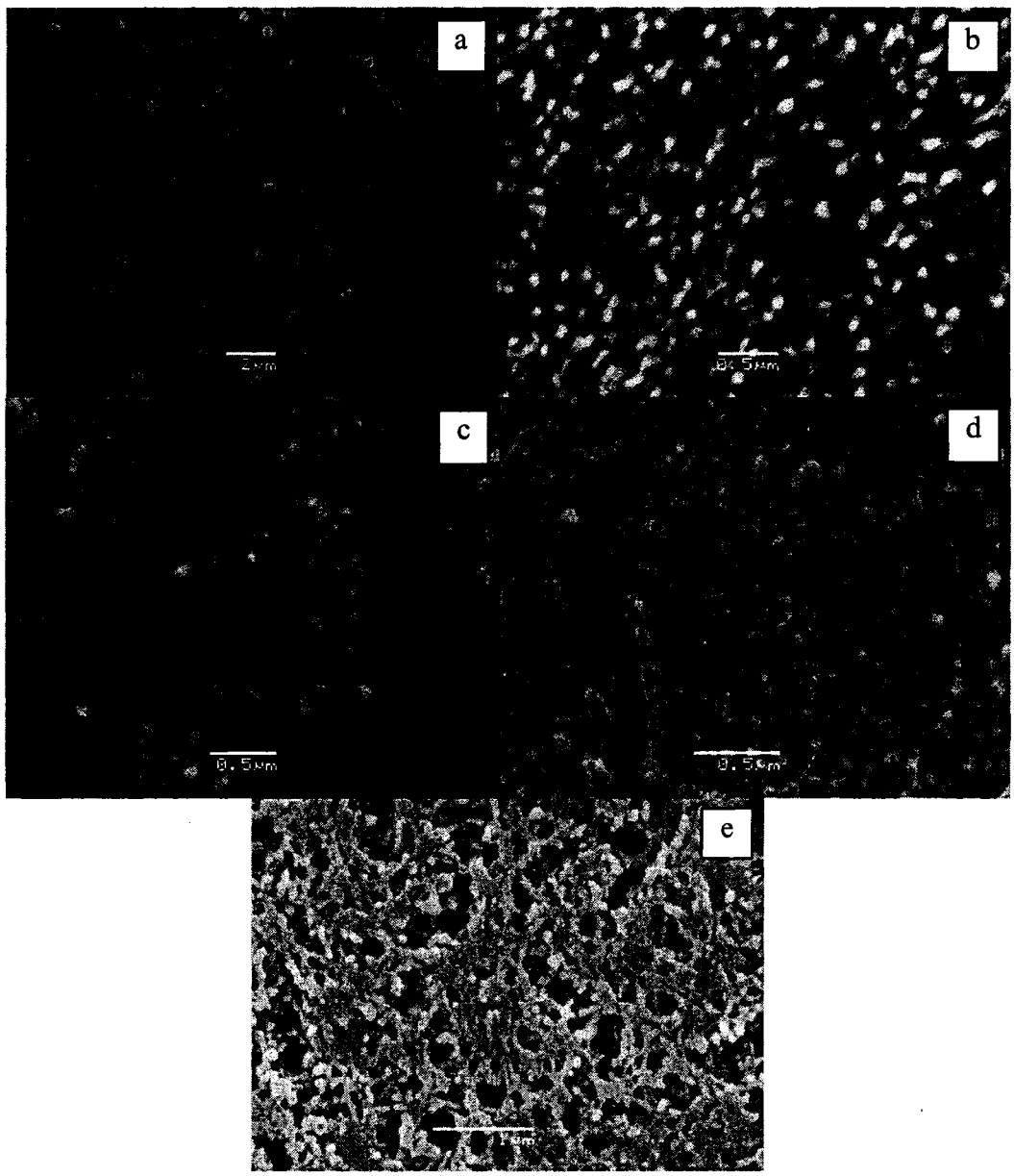

Figure 4-17, Shape evolution of TiO_2 nanosized particles with increasing calcination temperature ($SDS/Ti(OBu)_4$= 0.02:1):
(a) 400^{0}C, (b) 500^{0}C, (c) 600^{0}C, (d) 700^{0}C, (e) 800^{0}C.

4.1.5 Hypothesized mechanism of the isotropic growth of TiO_2 nanosized particles

In the formation of nanocrystals, different crystal facets are characterized by different surface energies. In the anatase TiO_2 nanosized particles, the surface free energy of the (001) facets is 1.4 times larger than that of the (101) facets, according to the Donnay-Harker rules [160]. The structure of anatase TiO_2 nanosized particles is tetragonal and the nucleate octagonal bipyramid works as truncate seeds. Selective surfactant adhesion occurs symmetrically during crystal growth according to the symmetry structure of the anatase TiO_2 nanosized particles. The selective adsorption of surfactants on the different crystal facets controls the growth rate of nanocrystals in different facet directions.

The mechanism of the growth of TiO_2 nanorods and nanosized particles under the action of different concentrations of surfactants is proposed and shown in Figure 4-18. This mechanism is based on the "oriented attachment" and anisotropic and isotropic growth mechanism suggested by Cozzoli et al [29].

The formation and growth of TiO_2 nanosized particles can be described as a two-step process: Formation of hydrolysis monomer $Ti(OH)_x(OR)_{4-x}$, (as shown in Figure 4-18, monomer structure) and then the polycondensation reactions leading to the formation of a Ti-O-Ti network. Studies have shown that in the absence of surfactant or other additives, titanium alkoxides vigorously react with water at a low temperature, and thus amorphous TiO_2 precipitation can be obtained. With the presence of surfactants, the surfactant molecules typically comprise a compact Ti-O-Ti network of hexa-coordinated Ti atoms. The Ti nanocrystals are surrounded by carboxylate ligands, which have the propensity to bridge Ti centers. The contact of precursor

monomers with water can be hindered when surrounded by surfactants, thus the growth of cross-linking of Ti-O-Ti bonds occurs directionally [161-163].

Directional growth of the nanosized particles took place at low surfactant/titanium precursor molar ratios because the monomers directly contacted with water without hindrance by surfactants in all directions. In such a case, rapid hydrolysis takes place in the direction without surfactant and the system is kinetically controlled by the high monomer concentration [31]. The growth rate in a specific direction of nanocrystal facets is accentuated, thus nanorods were formed (Figure 4-9 (a-d), Figure 4-11 (a-c)). These results are in agreement with the hydrolysis mechanism of anisotropic and isotropic growth of nanocrystals suggested by Cozzoli et al [29].

On the other hand, if some of the conditions favouring directional growth of TiO_2 nanosized particles are retarded, the nanosized particle is nearly spherical or cubic. At high surfactant/titanium precursor molar ratios, Ostwald Ripening favours the formation of spherical particles [72]. Anisotropic growth is suppressed when monomer concentration is low. In the early growth stage, the monomers are consumed as soon as they are produced. The growth rate in a specific direction of nanocrystal facets cannot be accentuated, thus the overall growth rate of monomers is slow and isotropic. High surfactant/titanium precursor molar ratios resulted in spherical and cubic TiO_2 nanosized particles (Figure 4-9 (e-h) and Figure 4-11 (e-h)). On the basis of this, desired shape and size of TiO_2 nanosized particles can be obtained by adjusting the molar ratio of surfactant/titanium precursor to a proper value.

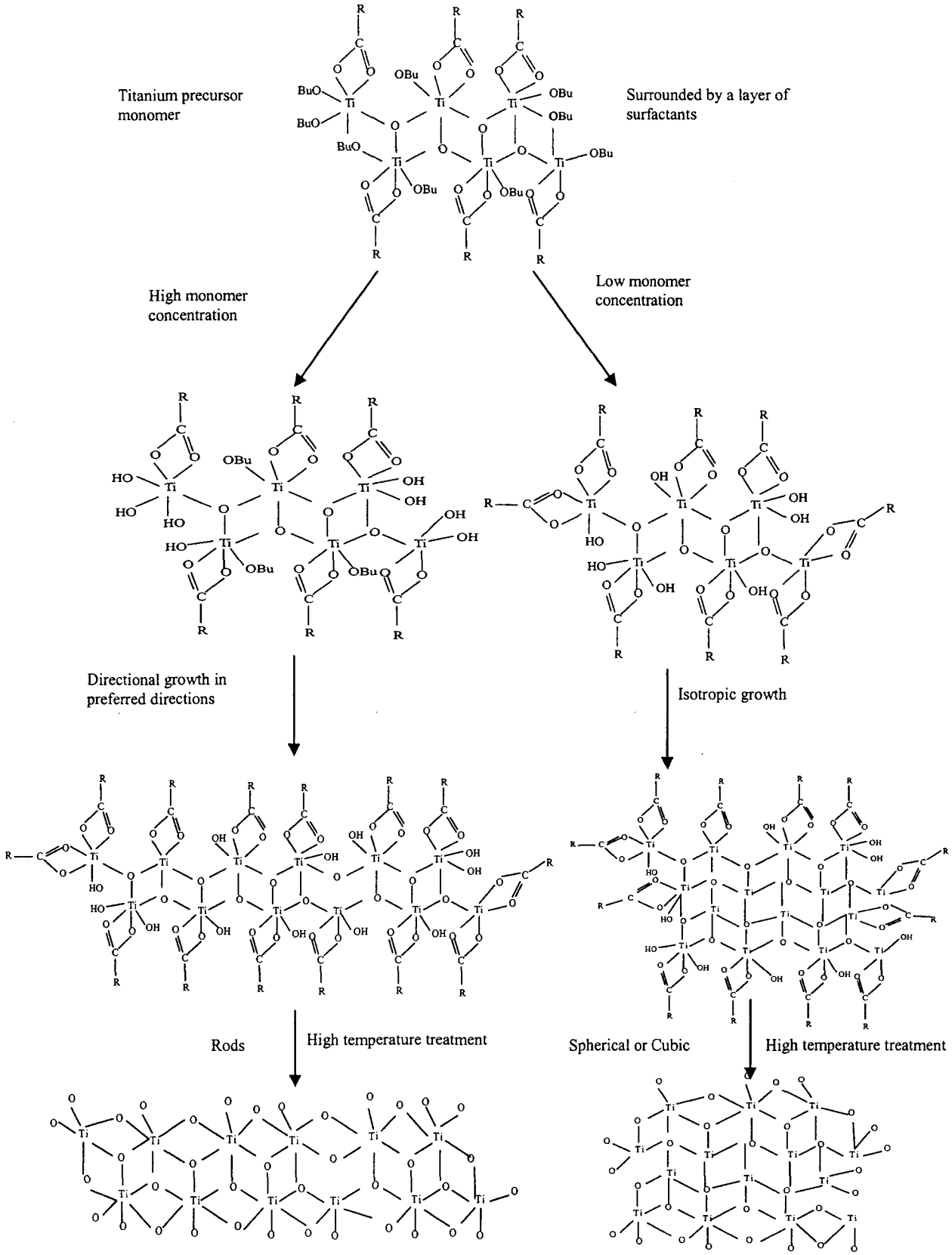

Figure 4-18, Hypothesis of shape evolution of TiO_2 nanosized particles

4.2 X-ray diffraction characterization of TiO_2 nanosized particles.

4.2.1 XRD patterns of the nanosized particles synthesized from $Ti(OBu)_4$

Figure 4-19 shows the XRD patterns of nanosized particles synthesized with different surfactants and calcined at 400^0C. XRD patterns of the TiO_2 nanosized particles indicate the presence of anatase crystal with a typical anisotropic growth pattern along the (001) direction. All the nanosized particles consist of anatase as a unique phase. Surfactants had no obvious effect on the phase formation of the nanosized particles. The main reason is that the formation of phases is mainly determined by the calcination temperature [7].

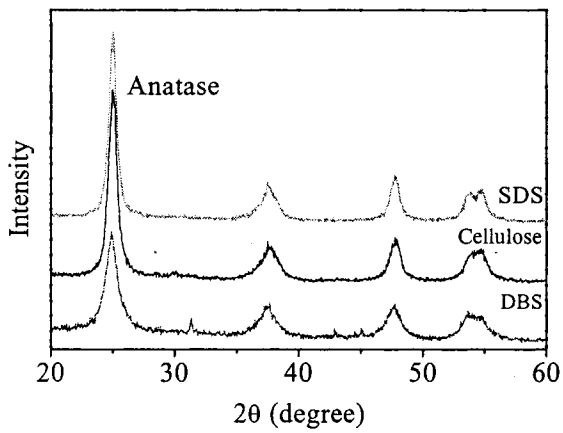

Figure 4-19, XRD patterns of the TiO_2 nanosized particles synthesized from $Ti(OBu)_4$ (Calcined at 400^0C).

XRD patterns of TiO_2 nanosized particles shape-controlled by different surfactants and calcined at different temperatures (400^0C to 800^0C) are shown in Figure 4-20. The degree of crystallinity of TiO_2 was improved with an increase in the calcination temperature which could be represented by a higher diffraction intensity. Characteristic peaks of anatase phase became sharper and narrower when the calcination temperature was increased. Rutile TiO_2 component

appeared when nanosized particles were calcined at 500^{0}C. A rutile reflection appeared in the diffraction pattern when the calcination temperature was higher than 500^{0}C.

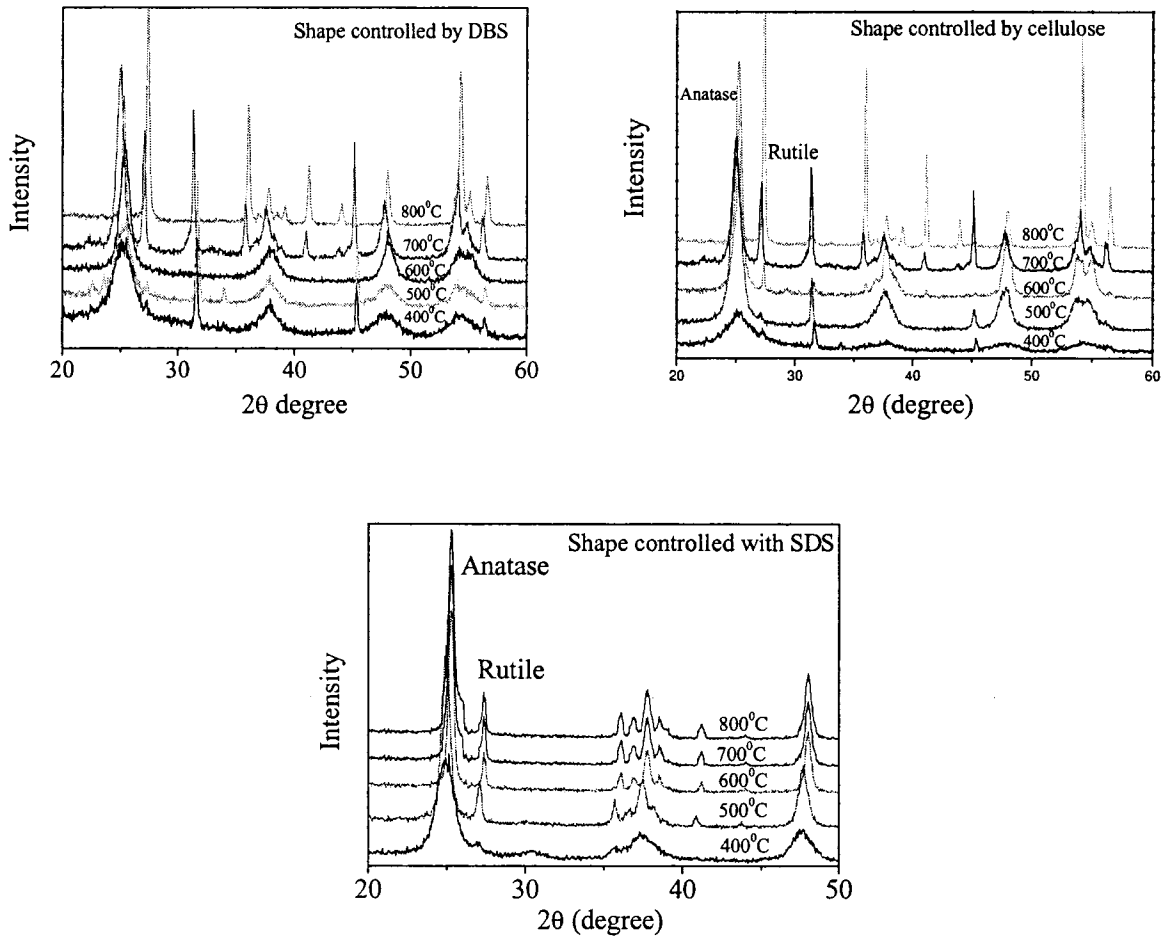

Figure 4-20, XRD patterns of nanosized particles synthesized from Ti(OBu)$_4$ calcined at different temperatures
(a) shape controlled by DBS, (b) shape controlled by cellulose, (c) shape controlled by SDS.

4.2.2 XRD patterns of the nanosized particles synthesized from $TiCl_4$

Figure 4-21 shows the XRD patterns of TiO_2 nanosized particles synthesized from $TiCl_4$ with different surfactants and calcined at 400^{0}C. The XRD patterns show typical anatase crystal structure. All the nanosized particles consist of anatase as a unique phase after being calcined at

400^{0}C. The XRD pattern of the nanosized particles shape-controlled by SDS shows best crystalline represented by the highest intensity and a sharper characteristic peak for anatase phase.

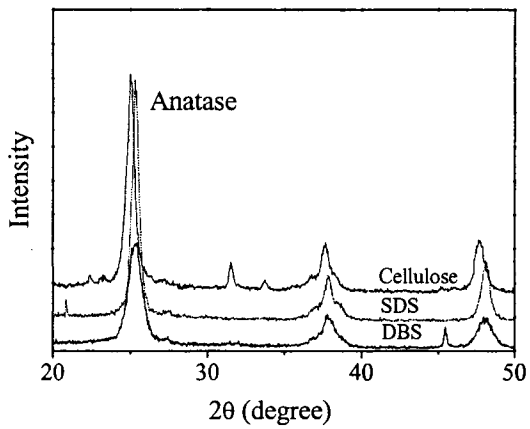

Figure 4-21, XRD patterns of the TiO_2 nanosized particles synthesized from $TiCl_4$ (calcined at 400^{0}C).

XRD patterns of TiO_2 nanosized particles shape-controlled by SDS and calcined at different temperatures (500^{0}C to 800^{0}C) are shown in Figure 4-22. A better crystallinity of TiO_2, which was represented by a higher diffraction intensity of the characteristic peaks, was obtained when the calcination temperature was increased. Characteristic peaks of anatase phase became sharper and narrower when the calcination temperature was increased. The rutile peaks also increased. When compared to the XRD patterns of nanosized particles synthesized from $Ti(OBu)_4$, as shown in Figure 4-21, the nanosized particles synthesized from $TiCl_4$ showed an obvious peak of $TiCl_2$ complex at 31.70^{0}C [164]. $TiCl_x$ complex will be formed when $TiCl_4$ was used. The nanosized particles synthesized from $TiCl_4$ with the use of DBS and cellulose and

calcined at different temperatures have XRD patterns similar to the patterns of the nanosized particles synthesized with SDS.

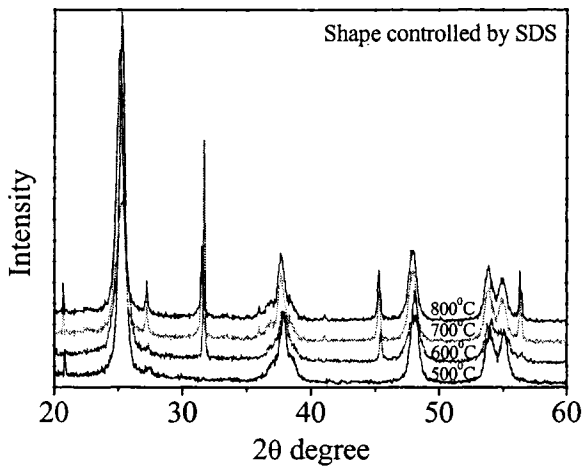

Figure 4-22, XRD patterns of the TiO_2 nanosized particles synthesized from $TiCl_4$ calcined at different temperatures.

4.2.3 XRD patterns of TiO_2 nanosized particles synthesized with different surfactant/$Ti(OBu)_4$ molar ratios

XRD patterns of the TiO_2 nanosized particles show that the TiO_2 nanosized particles calcined at 600^0C are typical anatase TiO_2 nanosized particles. The percentage of anatase composition is different in the TiO_2 nanosized particles synthesized with different surfactants. The dominant crystal phase of the nanorods and nanosized particles is anatase as shown in Figures 4-23 and 4-24.

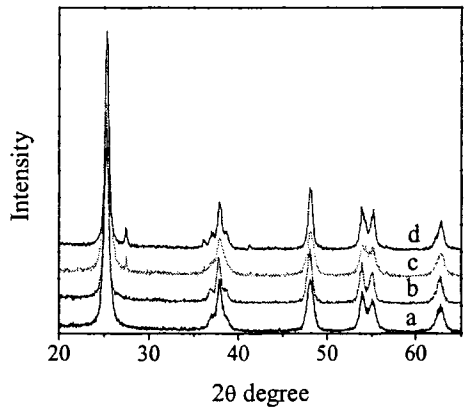

Figure 4-23, XRD patterns of TiO_2 nanosized particles synthesized with different cellulose/$Ti(OBu)_4$ molar ratios
(calcined at 600^0C):
(a) $5x10^{-4}$:1, (b) $1x10^{-3}$:1, (c) 0.01:1, (d) 0.04:1.

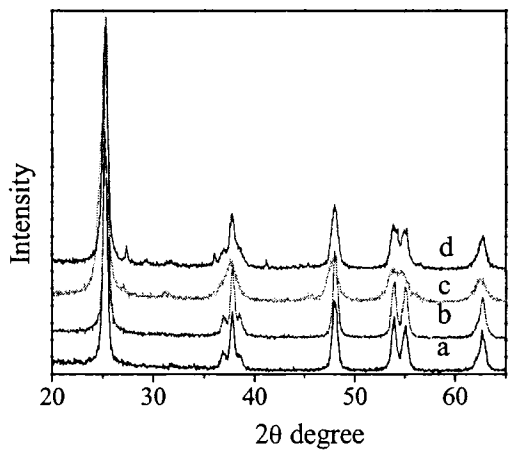

Figure 4-24, XRD patterns of TiO_2 nanosized particles synthesized with different SDS/$Ti(OBu)_4$ molar ratios
(calcined at 600^0C):
(a) 0.01:1, (b) 0.02:1, (c) 0.5:1, (d) 2.5:1.

4.3 FTIR spectrum analysis

Figure 4-25 (a-c) shows the FT-IR spectrum of the shape-controlled TiO_2 nanosized particles. Spectrum 1 represents the nanosized particles calcined at 400^0C whereas spectrum 2 represents the nanosized particles dried at 70^0C. The absorption from 2500-3600cm^{-1} could be assigned to the stretching vibration of the hydrogen-bond from -OH groups of the adsorbed water

and carboxylic acids and –COOH groups of the adsorbed carboxylic acids. The absorption around 1650, 1460 and 1065 cm^{-1} could be assigned to the stretch vibration of –C=C–, asymmetric C-CH_3, and –C–O bond, respectively. A comparison between spectrum 1 and 2 suggests that most of the decomposition of the organic functional groups from surfactants were complete by calcination at 400^0C for one hour. In the shape-controlled TiO_2 nanosized particles with DBS and SDS, there was still some –C-O residual left as indicated in spectrum 1 at 1065cm^{-1}. The FTIR spectrums suggest that the nanosized particles after calcination at 400°C are pure TiO_2 nanosized particles without attached organic molecules. The surface composition of the nanosized particles was similar after high temperature (400^0C) calcination.

Figure 4-26 shows the FTIR spectrums of the TiO_2 nanosized particles synthesized with SDS and calcined at 500^0C to 800^0C. The spectrums show that there were no obvious differences between the nanosized particles calcined at various high temperatures. The surface organic residuales had been removed completely at 500^0C.

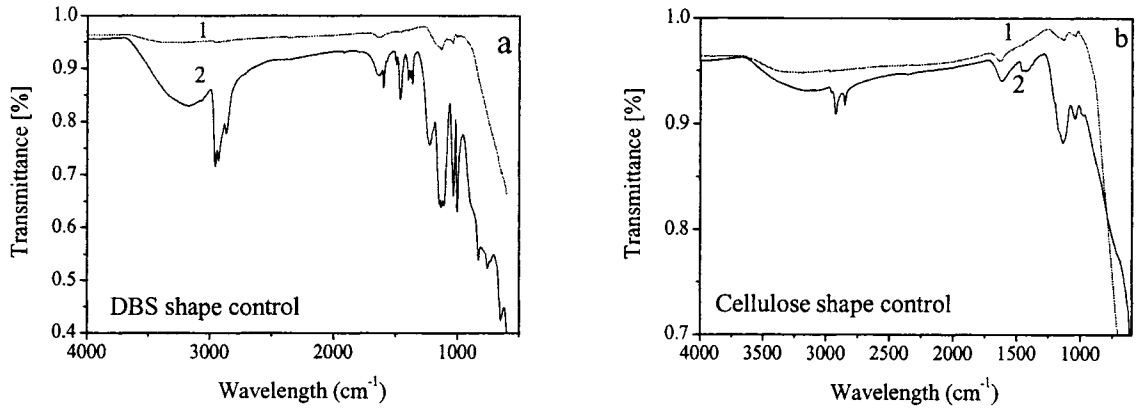

Figure 4-25, FTIR spectrum of the TiO_2 nanosized particles synthesized from $Ti(OBu)_4$.
a. Nanosized particles with DBS, b. Nanosized particles with cellulose, c. Nanosized particles with SDS.
1. Nanosized particles after calcined at 400°C, 2. Nanosized particles dried in oven at 70°C.

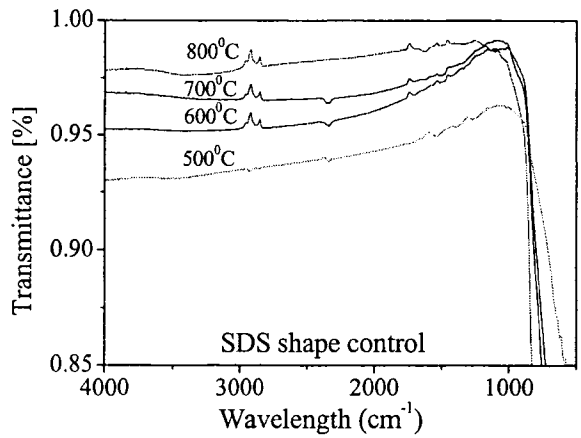

Figure 4-26, FTIR spectrum of TiO_2 nanosized particles calcined at different temperatures.

Figure 4-27 (a-c) shows the FTIR spectrums of TiO_2 nanosized particles synthesized from $TiCl_4$. As shown in the spectrums, there were no obvious characteristic peaks of organic functional groups or bonding existing in the nanosized particles after being calcined at 400^0C. When compared with the nanosized particles synthesized from $Ti(OBu)_4$, there was no significant difference in the surface chemical composition between the nanosized particles synthesized from different precursors.

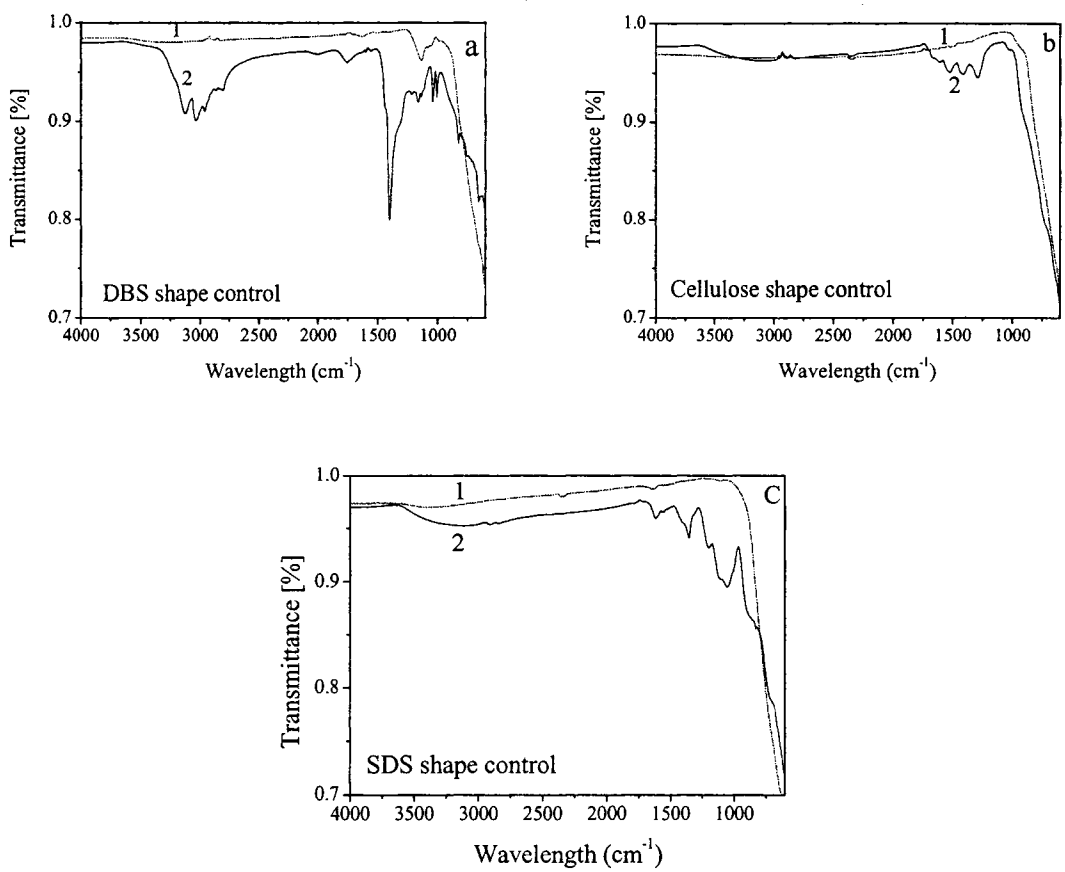

Figure 4-27, FTIR spectrum of shape-controlled TiO_2 nanosized particles synthesized from $TiCl_4$
(a) Nanosized particles with DBS, (b) Nanosized particles with cellulose, (c) Nanosized particles with SDS. 1, Nanosized particles after calcined at 400^0C, 2, Nanosized particles dried in oven at 70^0C.

4.4 UV-Vis spectrum analysis

4.4.1 UV-Vis reflectance of shape-controlled TiO_2 nanosized particles

UV-Vis reflectance of TiO_2 nanosized particles is shown in Figure 4-28 (a-b). An obvious red shift of UV-Vis reflectance spectra of shape-controlled TiO_2 nanosized particles (spectra 1, 2 and 3) was observed when compared to the spectra of a commercial anatase TiO_2 nanoparticle Degussa P-25 (spectrum 4) and non-shape controlled anatase TiO_2 nanosized particles obtained without the use of surfactants (spectrum 5). Shape-controlled TiO_2 nanosized particles strongly absorbed UV light within a wavelength below 380nm, while the non-shape controlled anatase TiO_2 nanosized particles and P-25 absorbed most of the UV light with a lower wavelength (<350nm). This suggests that the shape-controlled TiO_2 nanosized particles have a lower band gap than the neat anatase TiO_2 nanosized particles and P-25. This result is consistent with the observation of Petroski et al. [165].

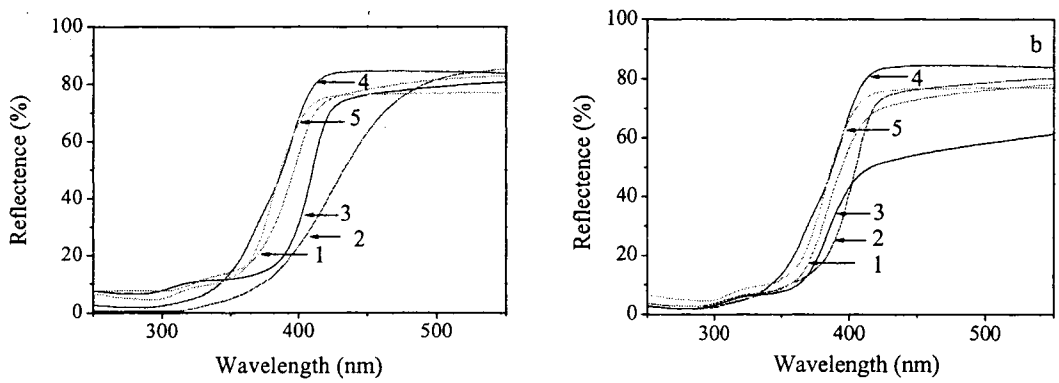

Figure 4-28, UV-Vis reflectance spectra of the TiO_2 nanosized particles calcined at 500^0C
(a) Nanosized particles synthesized from $Ti(OBu)_4$, (b) Nanosized particles synthesized from $TiCl_4$.
1: TiO_2-DBS 2: TiO_2-SDS , 3: TiO_2-Cellulose, 4: P-25, 5: Non-shape controlled TiO_2

The lower band gap has a positive effect on the photocatalytic activity because lower source energy is needed to induce a photocatalytic reaction. The red shift of light reflectance of shape-controlled nanosized particles might be due to a large amount of surface defects on

particle surfaces which give the shape-controlled nanosized particles a higher ability to capture electron-hole pairs [63]. According to the theory of quantum size effect [91, 166, 167], Louis Brus [166] suggested that the light absorption of nanosized particles is similar to the absorption by bulk materials when the size of particles is larger than 100nm. With the morphologies shown in Figures 4-2 to 4-7, shape-controlled TiO_2 nanosized particles have average dimensions between 100 and 500nm, so the size difference of the nanosized particles might not be the main reason for the lower band gap energy for the shape-controlled TiO_2 nanosized particles. The light absorption occurs at higher wavelengths and thus a lower band gap energy exists in the shape-controlled TiO_2 nanosized particles. Therefore, less energy is needed to activate the shape-controlled TiO_2 nanosized particles to generate excited electrons and then induce photocatalytic reactions.

4.4.2 Effect of calcination temperature on the UV-Vis reflectance.

Effect of calcination temperature on the UV-Vis spectra of nanosized particles synthesized from $Ti(OBu)_4$ and $TiCl_4$ is shown in Figures 4-29 and 4-30. The reflectance spectra show that there were red shifts of UV-Vis reflectance spectra with an increase in the calcination temperature. As confirmed by the XRD patterns, TiO_2 nanosized particles transformed from anatase to rutile as the calcination temperature increases. Pure rutile TiO_2 has lower band gap energy (3.0eV) than the anatase TiO_2 (3.2eV). Band gap energy can be represented by the light reflectance spectra. The rutile TiO_2 starts to absorb UV light at the wavelength 420nm, whereas anatase TiO_2 starts to absorb UV light at 365nm. The light reflectance spectra shifted to a higher wavelength because the TiO_2 nanosized particles transformed from anatase to rutile. The percentage of rutile crystal composition was increased with an increase in the calcination

temperature (Figures 4-20 and 4-22), so the band gap energy of the nanosized particles decreased as the calcination temperature was increased.

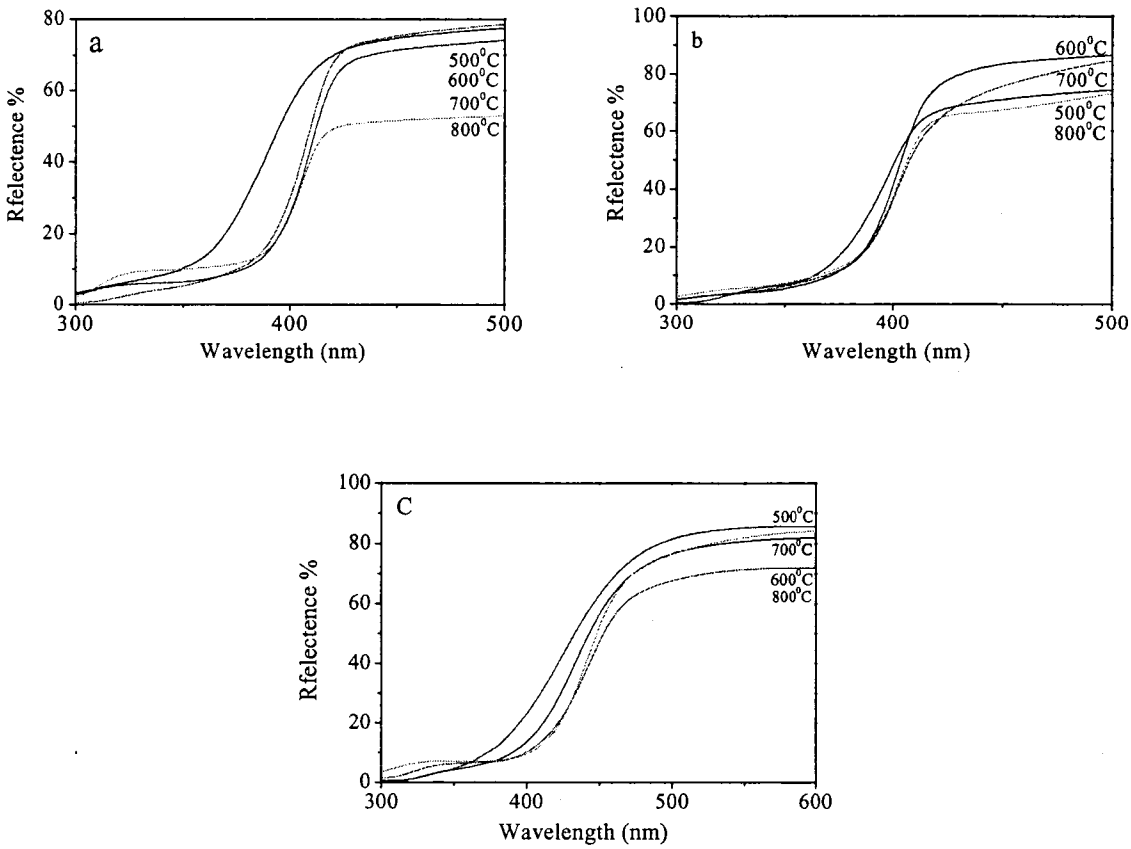

Figure 4-29, UV-Vis light reflectance spectrum of the nanosized particles synthesized form $Ti(OBu)_4$ calcined at different temperatures

(a) shape-controlled by DBS, (b) shape-controlled by cellulose, (c) shape-controlled by SDS.

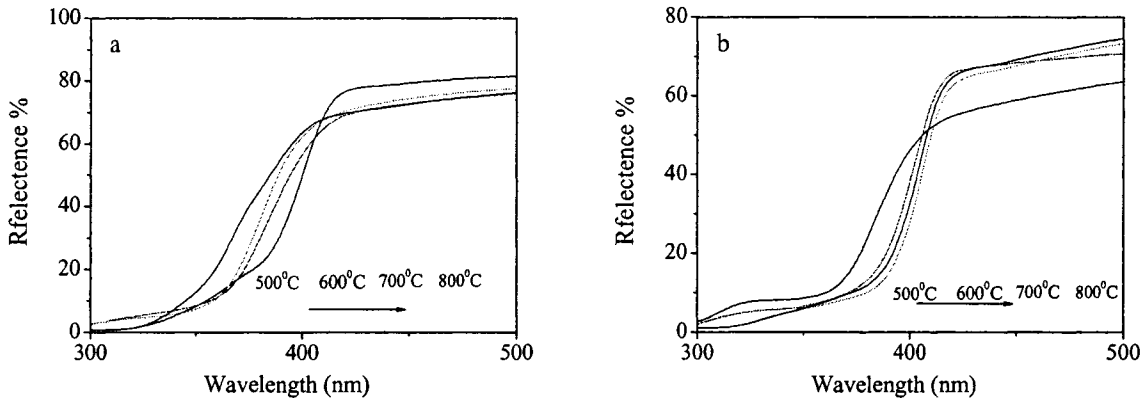

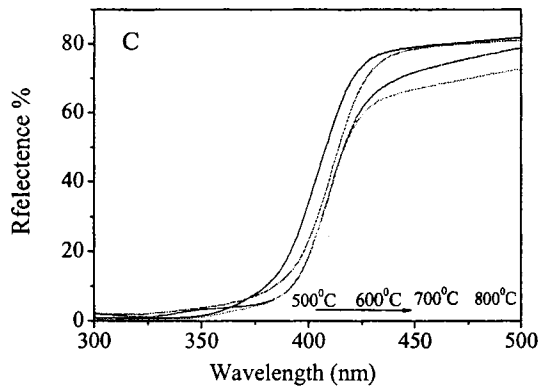

Figure 4-30, UV-Vis light reflectance spectrum of the nanosized particles synthesized form $TiCl_4$ calcined at different temperatures

(a) shape-controlled by DBS, (b) shape-controlled by cellulose, (c) shape-controlled by SDS.

CHAPTER 5 Zeta Potential of TiO_2 Nanosized Particles

5.1 Zeta potential of TiO_2 nanosized particles synthesized from $Ti(OBu)_4$

Figure 5-1 shows the zeta potential vs. pH curves of shape-controlled TiO_2 nanosized particles, non shape-controlled TiO_2 nanosized particles, and P-25. The shape controlled nanosized particles in Figures 4-2 to 4-5 were prepared from $Ti(OBu)_4$. The IEP of non shape-controlled TiO_2 nanosized particles and P-25 in deionized water was 6.5 and 7.4, respectively, which is close to the values reported in the literature [168, 169]. The IEPs of shape-controlled TiO_2 nanosized particles were shifted to a pH of 4.2 and 3, when DBS and cellulose were used, respectively, during the synthesis. The lower IEPs of shape-controlled TiO_2 nanosized particles suggest a better stability of dispersions of particles around neutral pH, as compared the neat TiO_2 and P-25, due to a lager repulsive electrostatic interaction.

Zeta potential of TiO_2 nanosized particles in aqueous suspensions can be affected by a number of factors such as pH, ion concentrations and charges of ions. The zeta potential of TiO_2 nanoparticle in suspensions is probably controlled by the pH through the following process [104]:

$$TiOH_2^+ \underset{+H^+}{\overset{-H^+}{\rightleftharpoons}} TiOH \underset{+H^+}{\overset{-H^+}{\rightleftharpoons}} TiO^-$$

For each shape-controlled nanosized particle, there was a specified zeta potential curve and IEP. The overall zeta potential of shape-controlled nanosized particles decreased as the pH was increased which can be explained by the previous reaction [104]. The shape-controlling process could alter the surface energy of the nanosized particles, which results in different adsorption and affinity of protons on the surface [30]. The difference might be also due to the

changes in surface area and the adsorptive abilities to hydroxyl ions on the surfaces of nanosized particles.

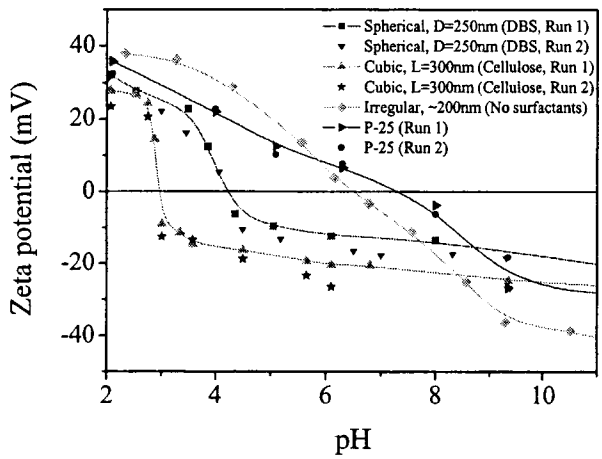

Figure 5-1, Zeta potential of shape-controlled TiO_2 nanosized particles synthesized from $Ti(OBu)_4$

Zeta potential vs. pH curves of TiO_2 nanosized particles shaped by SDS and calcined at different temperatures (500^0C-800^0C) are illustrated in Figure 5-2. A unique finding was that the pH-Zeta potential curves had two IEPs and reentered the positive zeta potential zone. This does not occur with TiO_2 synthesized with $TiCl_4$ and SDS as shown in Figures 5-3 and 5-4. This phenomenon was not limited to a specific sample or preparation condition. A similar trend of pH-Zeta potential curves was observed for the TiO_2 nanosized particles calcined at different temperatures. The zeta potentials of the shape-controlled nanosized particles were positive around neutral pH. Because the shape-controlling processes altered the surface structure and morphology of the nanosized particles, the imperfections such as oxygen vacancies were introduced and this changed the electronic structure of the nanosized particles. Water molecules could then occupy these oxygen vacancies, producing adsorbed -OH groups, which tended to make the nanosized particles positively charged [170]. This phenomenon can not be explained

without knowing what functional groups are attached to the titanium skeleton or surface and other surface analysis evidences. However, it is clear that the overall zeta potential curves shift to the right side as the calcination temperature increases but the IEPs are still lower than the IEP of P-25. The first IEP of the TiO_2 nanosized particles shape-controlled by SDS appears at a pH between 2.7 to 3.9 at the calcination temperature ranged from 500^0C to 800^0C. Zeta potential becomes negative when pH surpasses the first IEP and then reenters the positive charged zone when pH surpasses 4.0. Figures 4-25 to 4-26 suggest that there were no organic functional groups or material residuals attaching on the nanosized particle surface after the nanosized particles were calcined at 400^0C. The results exclude the possibility that the second IEP was caused by the residual functional groups of SDS on the surfaces.

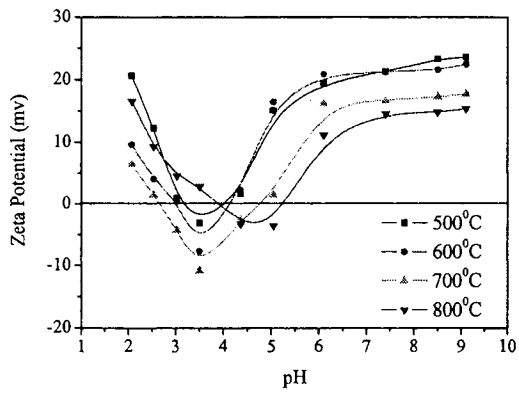

Figure 5-2, Zeta potential of SDS shape controlled TiO_2 nanosized particles synthesized from $Ti(OBu)_4$

5.2 Zeta potential of TiO_2 nanosized particles synthesized from $TiCl_4$

Figure 5-3 shows the pH dependence of zeta potential of shape-controlled TiO_2 nanosized particles prepared from $TiCl_4$. The IEPs of the shape-controlled nanosized particles were at a pH of 5.0, 4.0 and 4.5, respectively, when DBS, cellulose and SDS was used during the preparation. These IEPs were higher than the IEPs of the TiO_2 nanosized particles synthesized from $Ti(OBu)_4$

as shown in Figure 5-1. The results also indicated that the shape-controlled TiO_2 nanosized particles from $TiCl_4$ had a lower IEP as compared to the no shape-controlled TiO_2 nanosized particles and P-25. Figure 5-4 shows the effect of calcination temperature on zeta potential of TiO_2 nanosized particles shape controlled by SDS and prepared from $TiCl_4$. The IEP of the nanosized particles was increased from 4.8 to 8 when the calcination temperature was increased from 500^0C to 800^0C. Studies have shown that the transformation of the anatase TiO_2 to rutile TiO_2 could commence at temperatures higher than 550^0C [38]. It was reported that the anatase has a higher degree of hydroxylation than rutile which generate a larger number of hydroxyl groups (OH^-) on the surface [7]. As shown in Figure 5-4, TiO_2 nanosized particles calcined at a lower temperature had a more negative zeta potential because the number of hydroxyl groups (OH^-) in anatase phase is higher than that in rutile phase obtained at higher calcination temperatures. A comparison of the zeta potential of TiO_2 nanosized particles with the addition of SDS during preparation showed that the nanosized particles prepared from $Ti(OBu)_4$ have two IEPs at a pH of 3.0 and 3.8, respectively, while the nanosized particles prepared from $TiCl_4$ have only one relative higher IEP at pH 4.7. This result further suggests that the second IEP was not caused by a residual SDS on TiO_2 nanosized particle surfaces.

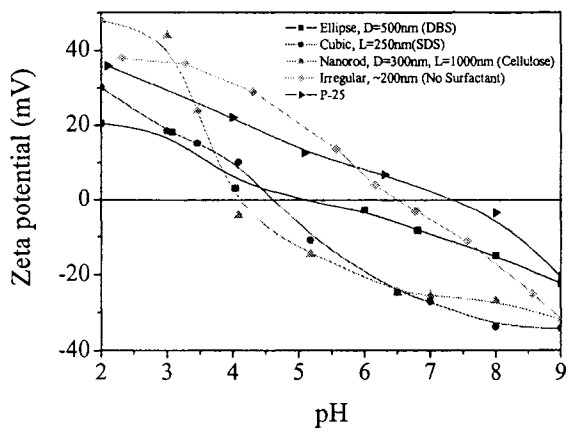

Figure 5-3, Zeta Potential of the shape controlled TiO_2 nanosized particles synthesized from $TiCl_4$.

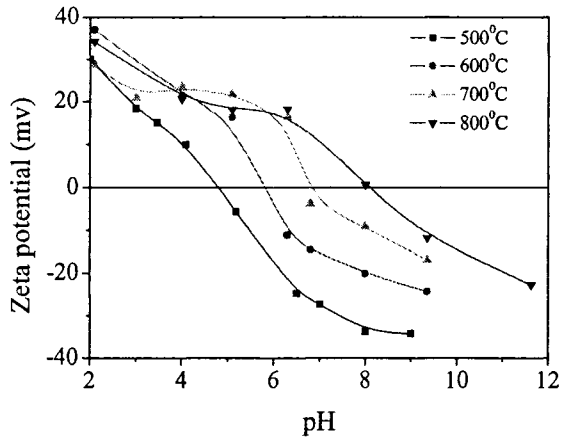

Figure 5-4, Zeta potential of SDS shape controlled TiO_2 nanosized particles synthesized from $TiCl_4$.

5.3 Zeta potential of TiO_2 nanosized particles in SDS solution

In order to further investigate the unique two IEPs, as shown in Figure 5-2, of TiO_2 nanosized particles from $Ti(OBu)_4$ precursor and to improve the stability and homogeneity of TiO_2 nanosized particles in aqueous suspension, zeta potential of TiO_2 nanosized particles in the SDS solution was studied by using a 0.5μM solution of SDS. The results show that the addition of SDS in TiO_2 nanosized particle suspension shifted the IEPs to the left (a lower pH value) and mostly had a smaller magnitude of positive zeta potential and a larger magnitude of negative zeta potential, as shown in Figures 5-5 to 5-7. The results also suggest that the unique two IEPs of TiO_2 nanosized particles was not caused by the adsorption of SDS on the surface of TiO_2 nanosized particles. The available anions and cations from the SDS altered the charge of the double layer and created a new and smaller IEP for the shape-controlled TiO_2 nanosized particles.

The lower zeta potential in SDS solution can be explained by the semi-micelle model [171]. At high pHs, TiO_2 nanosized particles show electro-negativity. SDS is adsorbed on the TiO_2 nanosized particle surface through non-polar physical adsorption. The adsorption volume is

small because of the repulsion between the particles. When SDS concentration increases, SDS micelles will form on the TiO_2 nanosized particle surface, and adsorption volumes increase dramatically in the micelle forming stage. Zeta potential becomes more negative because of the adsorption of surfactant SDS micelles. Repulsion of the surfactant prevents the nanosized particles from flocculation and sedimentation which is the basis for the electrostatic stability of nanosized particles in aqueous suspension.

The effect of SDS concentration on zeta potential of TiO_2 nanosized particles is shown in Figure 5-8. Zeta potential became more negative when SDS concentration was increased at neutral pH. Zeta potential curves became flat when SDS solution reached at 1.5μM. Nanosized particles shape controlled by DBS had a large negative zeta potential than the nanosized particles shape controlled by cellulose and SDS in SDS solutions at neutral pH.

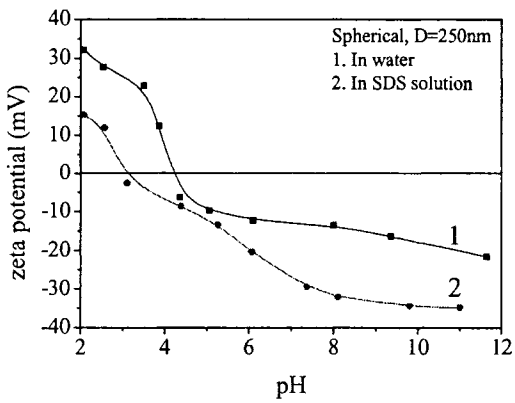

Figure 5-5, Zeta potential of DBS shaped TiO_2 nanosized particles synthesized from $Ti(OBu)_4$ in water and SDS solution
(SDS conc. 0.5μM)

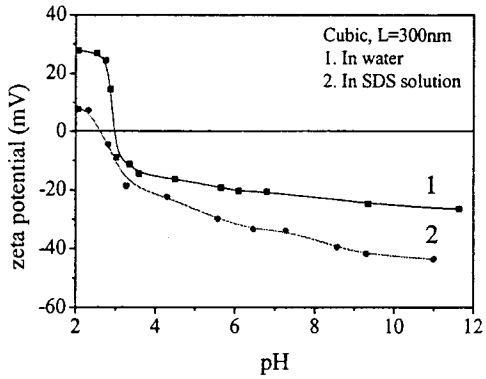

Figure 5-6, Zeta potential of cellulose shaped TiO_2 nanosized particles synthesized from $Ti(OBu)_4$ in water and SDS solution
(SDS conc. 0.5μM)

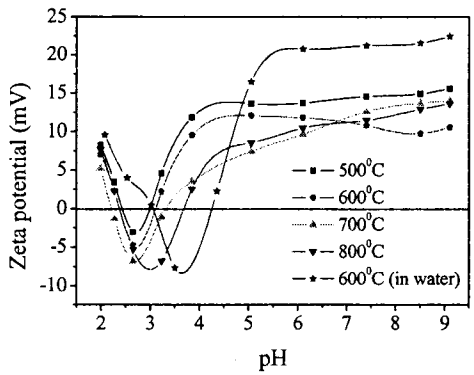

Figure 5-7, Zeta potential of SDS shaped TiO_2 nanosized particles synthesized from $Ti(OBu)_4$ in water and SDS solution
(SDS conc. 0.5μM)

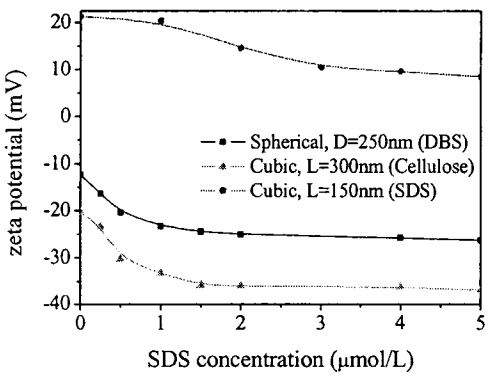

Figure 5-8, Zeta potential of TiO_2 nanosized particles synthesized from $Ti(OBu)_4$ in SDS solutions
(pH=6.5)

CHAPTER 6 Photocatalytic Activity Studies

6.1 Preliminary studies of the photocatalytic reactions

6.1.1 Determination of the loading mass of TiO_2 films

The effect of photocatalyst loading mass on photocatalytic decomposition of methyl orange (MO) in fixed film batch reactors is shown in Figure 6-1. The results show that reaction rate of photocatalytic decomposition was initially increased with an increase in the loading mass and then reached at a relatively stable rate after the loading mass was higher than 1.5 $x10^{-4}$ g/cm^2. There was no significant improvement in the efficiency when the loading mass was increased from $5x10^{-4}g/cm^2$ to $1x10^{-3}g/cm^2$. This might be due to the fact that nanosized particles in the bottom of a thick layer TiO_2 film could not contact with the organic compound to catalyze the decomposition reaction of MO. A further increase in the loading mass could barely improve the reaction rate. Therefore, the loading mass of TiO_2 films was controlled at 5.0 $x10^{-4}g/cm^2$ in the comparative studies reported in this thesis.

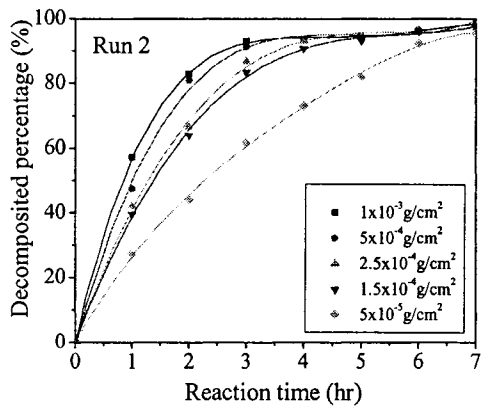

Figure 6-1, Effect of loading mass on photocatalytic reaction of TiO_2 nanosized particles.
(SDS/ $Ti(OBu)_4$=1:1, initial [MO]=500μg/L)

6.1.2 Effect of calcination temperature on the photocatalytic activities

The effect of calcination temperature on the photocatalytic activity of TiO_2 nanosized particles is shown in Figures 6-2 to 6-4. TiO_2 nanosized particles calcined at 600^0C showed the highest photocatalytic activity represented by the highest decomposition rate of MO. Calcination temperature is one of the most important parameters that can affect the photocatalytic activity of the TiO_2 photocatalysts because calcination temperature can determine the crystal composition of TiO_2 nanosized particles. From XRD patterns, as shown in Figure 4-20 and 4-22, a considerable amount of rutile phase was formed when TiO_2 nanosized particles were calcined at 600^0C. According to Equation (3-1), the percentage of anatase composition in the nanosized particles was calculated and summarized in Table 6-1. At the optimal calcination temperature (600^0C), the percentage of anatase composition varied from 62% to 93% in different shape-controlled nanosized particles. Although rutile phase was reported with a lower photocatalytic activity as compared to the anatase phase because of the lower ability to adsorb hydroxyl ions [139, 172-174], some studies also found a composite of the anatase and rutile phase could improve the photocatalytic activity to some degree. Results in this study were in agreement with the conclusions of other studies [172-174] in that an optimal calcination temperature exists for an optimal anatase/rutile ratio for the highest photocatalytic activity.

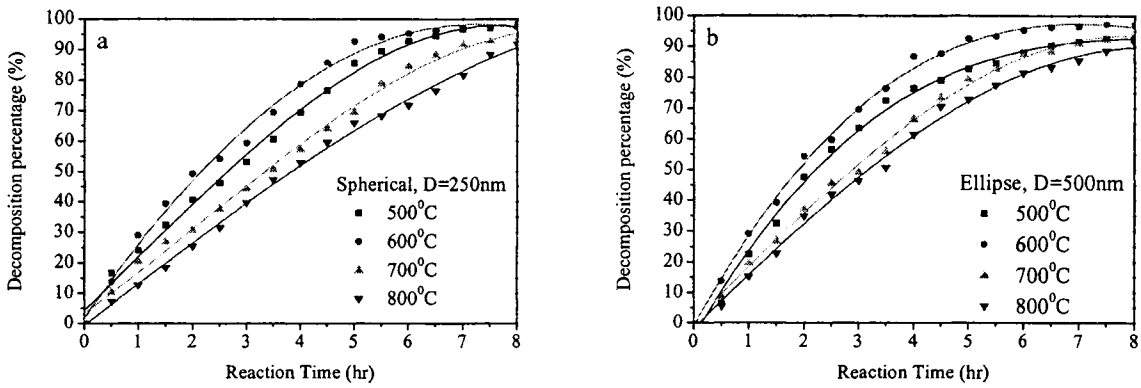

Figure 6-2, Comparison of photocatalytic activities of TiO_2 nanosized particles with DBS.
(initial [MO]=1000μg/L)
(a) Nanosized particles synthesized from $Ti(OBu)_4$, (b) Nanosized particles synthesized from $TiCl_4$.

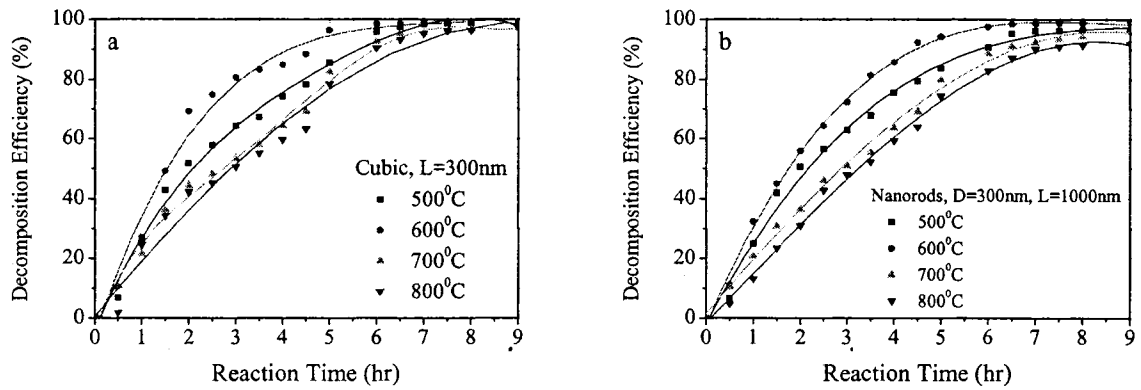

Figure 6-3, Comparison of photocatalytic activities of TiO_2 nanosized particles with cellulose.
(initial [MO]=1000μg/L)
(a) Nanosized particles synthesized from $Ti(OBu)_4$, (b) Nanosized particles synthesized from $TiCl_4$.

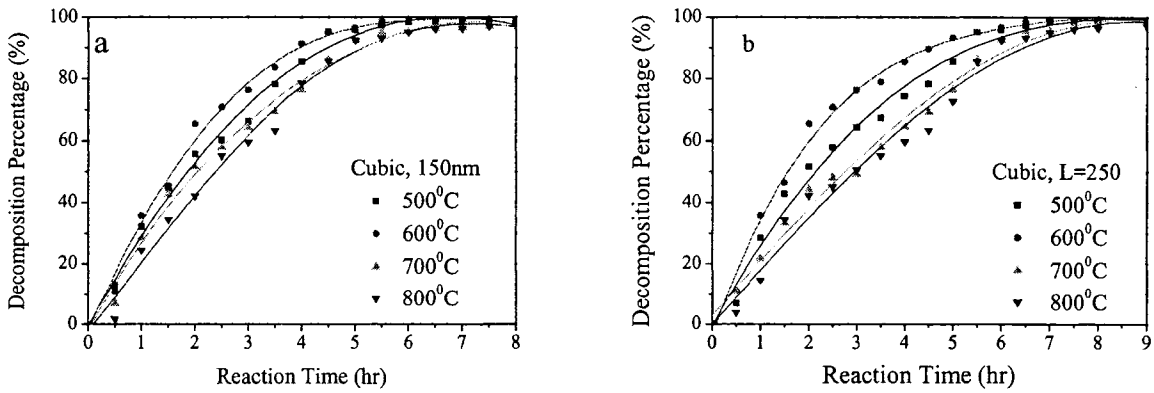

Figure 6-4, Comparison of photocatalytic activities of TiO_2 nanosized particles with SDS.
(initial [MO]=1000ug/L)
(a) Nanosized particles synthesized from $Ti(OBu)_4$, (b) Nanosized particles synthesized from $TiCl_4$.

Table 6-1, Calculations of anatase composition in the shape-controlled nanosized particles

Temperature	$Ti(OBu)_4$+DBS		$Ti(OBu)_4$+cellulose		$Ti(OBu)_4$+SDS		$TiCl_4$+DBS		$TiCl_4$+cellulose		$TiCl_4$+SDS	
	Ia	I_R	Ia	I_R	Ia	I_R	Ia	I_R	Ia	I_R	Ia	I_R
500°C	71.20	28.80	89.98	10.02	80.34	19.66	90.51	9.49	93.63	6.37	93.33	6.67
600°C	62.60	37.40	83.44	16.56	78.19	21.81	88.81	11.19	93.05	6.95	89.43	10.57
700°C	54.16	45.84	54.68	45.32	70.69	29.31	75.18	24.82	73.08	26.92	82.59	17.41
800°C	31.77	68.23	25.87	74.13	67.19	32.81	59.09	40.91	62.78	37.22	77.32	22.68

Figure 6-5 shows the correlation between anatase phase percentage and the initial reaction rate of MO at the first hour of the reaction. As shown in Figure 6-5, the reaction rate increase in general with the anatase phase percentage increase. It is hard to draw a conclusion on the correlation between the crystal phase composition with the photocatalytic activity. The photocatalytic activity of the TiO_2 nanosized particles are determined not only by the crystal phase composition. Shape and size of the particles, band gap energy and surface composition are the other determining factors for the photocatalytic activities.

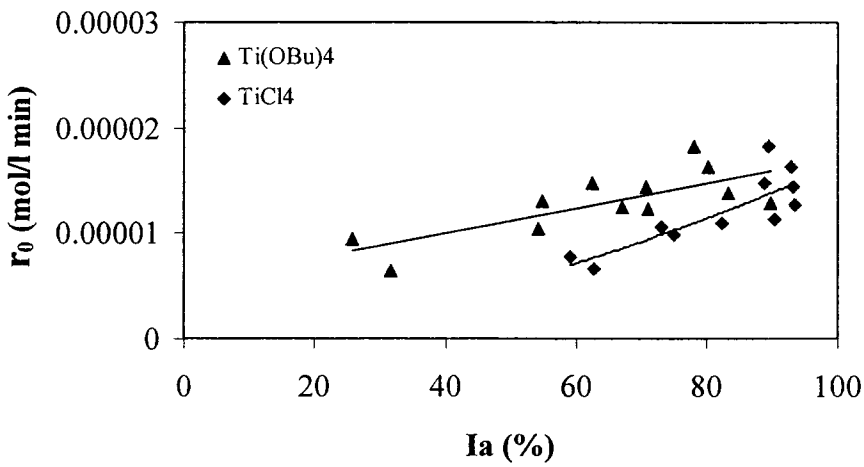

Figure 6-5, Relationship between the initial reacrion rate and crystal phase composition

6.2 Photocatalytic activity of the shape- and size-controlled TiO_2 nanosized particles

The photocatalytic activity of the nanosized particles synthesized from $Ti(OBu)_4$ and $TiCl_4$ with different surfactants was studied. The photocatalytic decomposition rates of phenol and MO on different nanosized particles are shown in Figures 6-6 and 6-7. The morphologies of

the TiO_2 nanosized particles were shown in Figures 4-2 to 4-7. When compared to the neat TiO_2 nanosized particles without using surfactants, shape- and size-controlled nanosized particles had higher photocatalytic activity. The cubic TiO_2 nanosized particles shape-controlled by SDS showed the highest photocatalytic activity. Complete decomposition of phenol and MO could be obtained at 8hours and 1.5hours, respectively, with TiO_2 nanosized particles having the highest photocatalytic activity. Among the shape-controlled nanosized particles, cubic TiO_2 nanosized particles shape-controlled by SDS have the highest photocatalytic activity. This could be attributed to the smallest particle size and best uniformity in shape as observed in SEM images, Figures 4-2 to 4-7. A lower band gap energy could also contribute to the higher photocatalytic activity of the shape-and size-controlled nanosized particles. In Figure 4-28, the UV-Vis spectrum of the TiO_2 nanosized particles shape controlled by SDS suggests that they have a lower band gap than the other nanosized particles. The photocatalytic decomposition reactions on this photocatalyst could be induced by a lower energy.

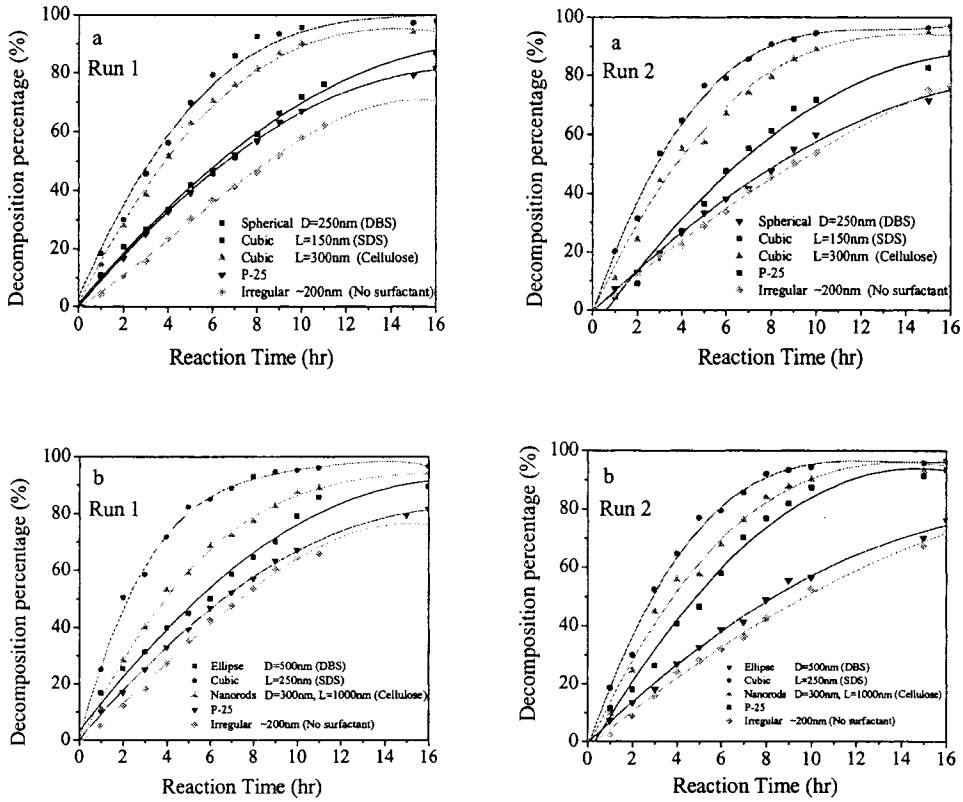

Figure 6-6, Comparison of the photocatalytic activities of the shape-controlled TiO_2 nanosized particles
(calcined at 600^{0}C)
(initial [phenol]=100mg/L, Surfactant/titanium precursor=1:1),
(a) Nanosized particles synthesized from $Ti(OBu)_4$, (b) Nanosized particles synthesized from $TiCl_4$.

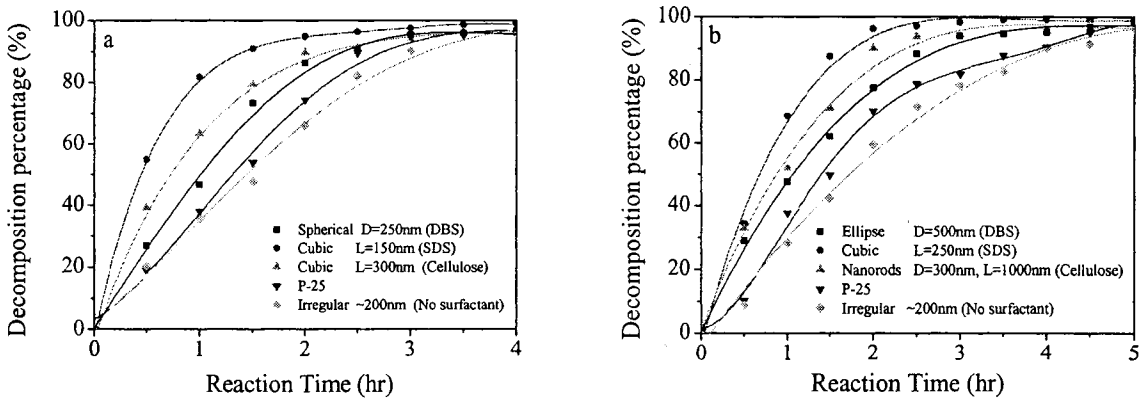

Figure 6-7, Comparison of the photocatalytic activities of the shape-controlled TiO_2 nanosized particles
(calcined at 600^{0}C)
(Initial [MO]=500μg/L; surfactant/titanium precursor=1:1)
(a) Nanosized particles synthesized from $Ti(OBu)_4$, (b) Nanosized particles synthesized from $TiCl_4$.

6.3 Kinetic studies of photocatalytic decomposition reactions

For comparative studies of kinetics reported here, TiO_2 nanosized particles were all calcined at 600°C. For first order reaction kinetics, the dependence of $1/r_0$ on $1/C_0$, where r_0 was the initial reaction rate dC/dt and C_0 was the initial concentrations of phenol and MO solution, should be linear. Based on the variations in concentrations of phenol and MO, the initial reaction rates were calculated. The correlation of $1/C_0$ and $1/r_0$ was then drawn. As shown in Figures 6-8 and 6-9, a linear dependence between $1/r_0$ and $1/C_0$ with a correlation factor $R^2>0.98$ exists rather than other kind of relationship. These results indicate that photocatalytic decomposition reaction of phenol and MO showed first order kinetic behavior. This result is consistent with the findings of previous studies [118, 138, 19] in that photocatalytic reactions of pollutants on TiO_2 photocatalysts can be well described using the first order kinetic.

Kinetics of the photocatalytic reaction of phenol and MO were studied in fixed film batch reactors. The values of k_{app} were obtained from the slope of the plots of $-\ln(C/C_0)$ vs. t, as shown in Figures 6-10 to 6-15. Figures 6-16 and 6-17 show the plots of $1/k_{app}$ versus C_0 for different TiO_2 nanosized particles synthesized from different surfactant/$Ti(OBu)_4$ molar ratios. The calculated results of k_c and K_C were summarized in Table 6-2.

In the photocatalytic decomposition of phenol and MO, the TiO_2 nanosized particles synthesized with different surfactant/$Ti(OBu)_4$ molar ratios showed different photocatalytic activities which are represented by the different k_c values in Table 6-2. Similar trends of the changes in photocatalytic activities were observed in both cases of phenol and MO. For the same shape of nanosized particles and nanorods, photocatalytic activity was improved with a decrease

in their sizes. This is consistent with the findings of Zhang et al. [25], because a decrease in particle size results in an increase in specific surface area and reaction sites. However, the change in k_c showed that the photocatalytic activity of the nanosized particles did not always increase with a decrease in the size of the nanosized particles when nanosized particle shape changed. Larger nanorods had higher photocatalytic activities than smaller cubic and spherical nanosized particles (Table 6-2). These results suggest that the shape and morphology of TiO_2 nanosized particles are more important than the size in determining the photocatalytic activity. These results also indicated that the photocatalytic decomposition of substrates was non-selective on the same nanosized particles.

Adsorption of the substrate on the photocatalysts is another important factor affecting the photocatalytic efficiency [118]. Significant differences in *Kc* values were observed for the TiO_2 nanosized particles synthesized with different surfactant composition and concentrations. In general, the K_C values for phenol decomposition were about 10-20 times larger than that of MO decomposition (Table 6-2). In contrast, the k_c values for phenol decomposition were much smaller (10-20 times) than that for MO decomposition (Table 6-2). These results suggest that a smaller k_c was associated with a larger K_C. This is general true for the decomposition of the same pollutant (phenol or MO) with TiO_2 nanosized particles obtained from the use of different surfactant composition and concentrations (Table 6-2). These results might not be surprise, as this might be explained by the competition of adsorbed hydroxyl radical concentration and pollutant on the TiO_2 nanoparticle surfaces. The heterogeneous photocatalytic decomposition of organic substrates proceeds in two elementary mechanisms: oxidation of the successive contact with the hydroxyl radicals and direct oxidative reaction with the photo-generated holes in a

process similar to the photo-Kolbe reaction [118]. The adsorbed OH^-, H_2O molecules are very important for the k_c values because they are the main sources of hydroxyl radicals. In addition, the adsorbed oxygen containing species can also contribute to the formation of hydroxyl radicals on the TiO_2 surface [175]. Because of the tiny sizes of the nanosized particles, the adsorption of phenol and MO on the TiO_2 surface could block the diffusion of oxygen containing species and H_2O molecules to the TiO_2 surface to generate hydroxyl radicals. Active sites and surrounding space are occupied by the adsorbed phenol and MO molecules on the nanosized particles. In the case of MO, the blockage of adsorbed hydroxyl radicals by MO molecules might be less significant than by phenol because the larger and longer molecular chain of MO might lead to a lower adsorption capacity (lower K_C). It is challenge to give an in-depth explanation of the changes in K_C values on different shape-controlled nanosized particles without the information of physical and chemical properties, such as specific surface area, pore size and volume. These results indicated that the photocatalytic activity was not always improved by a higher adsorptive capacity.

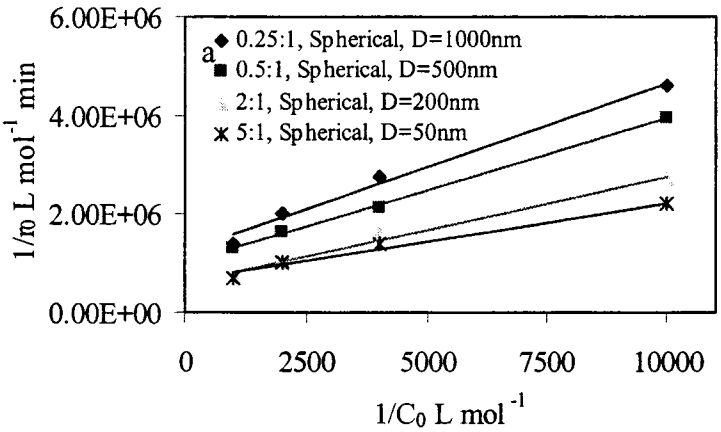

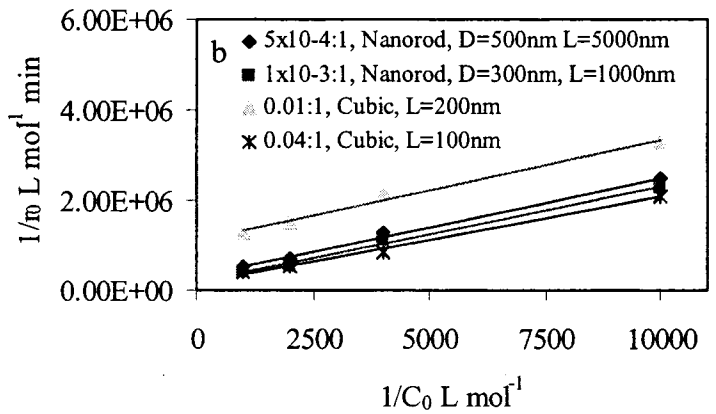

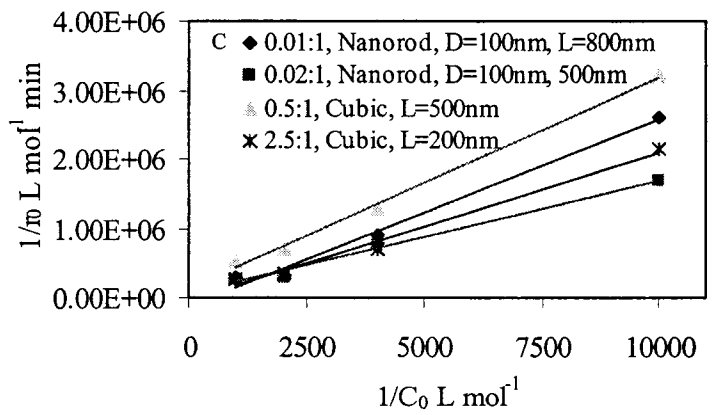

Figure 6-8, Relationship between initial reaction rate r_0 and initial concentration C_0 of phenol
(a) Shape-controlled by DBS with different DBS/$Ti(OBu)_4$ molar ratios.
(b) Shape-controlled by cellulose with different cellulose/$Ti(OBu)_4$ molar ratios.
(c) Shape-controlled by SDS with different SDS/$Ti(OBu)_4$ molar ratios.

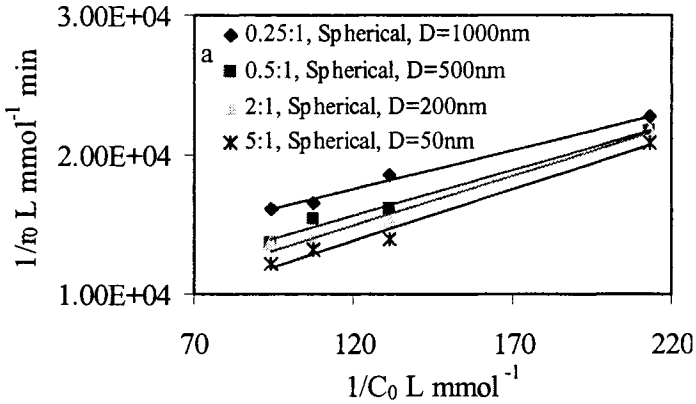

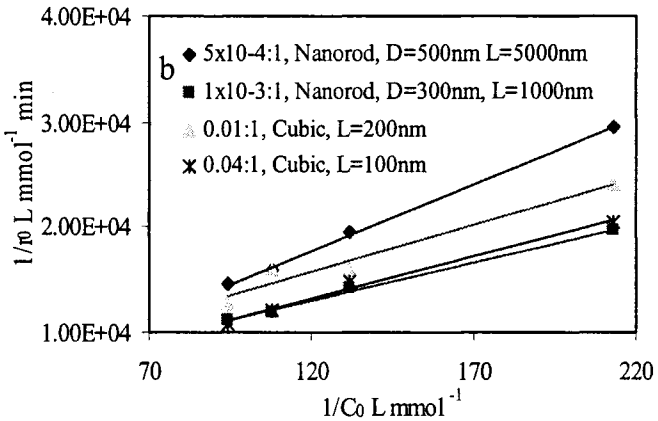

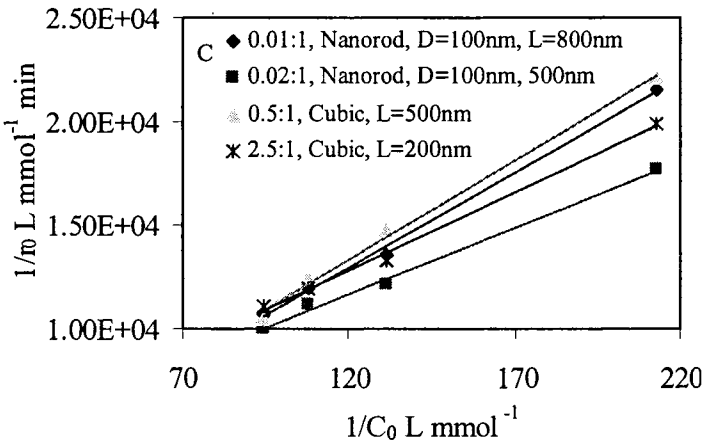

Figure 6-9, Relationship between initial reaction rate r_0 and initial concentration C_0 of MO
(a) Shape-controlled by DBS with different DBS/$Ti(OBu)_4$ molar ratios.
(b) Shape-controlled by cellulose with different DBS/$Ti(OBu)_4$ molar ratios.
(c) Shape-controlled by SDS with different DBS/$Ti(OBu)_4$ molar ratios.

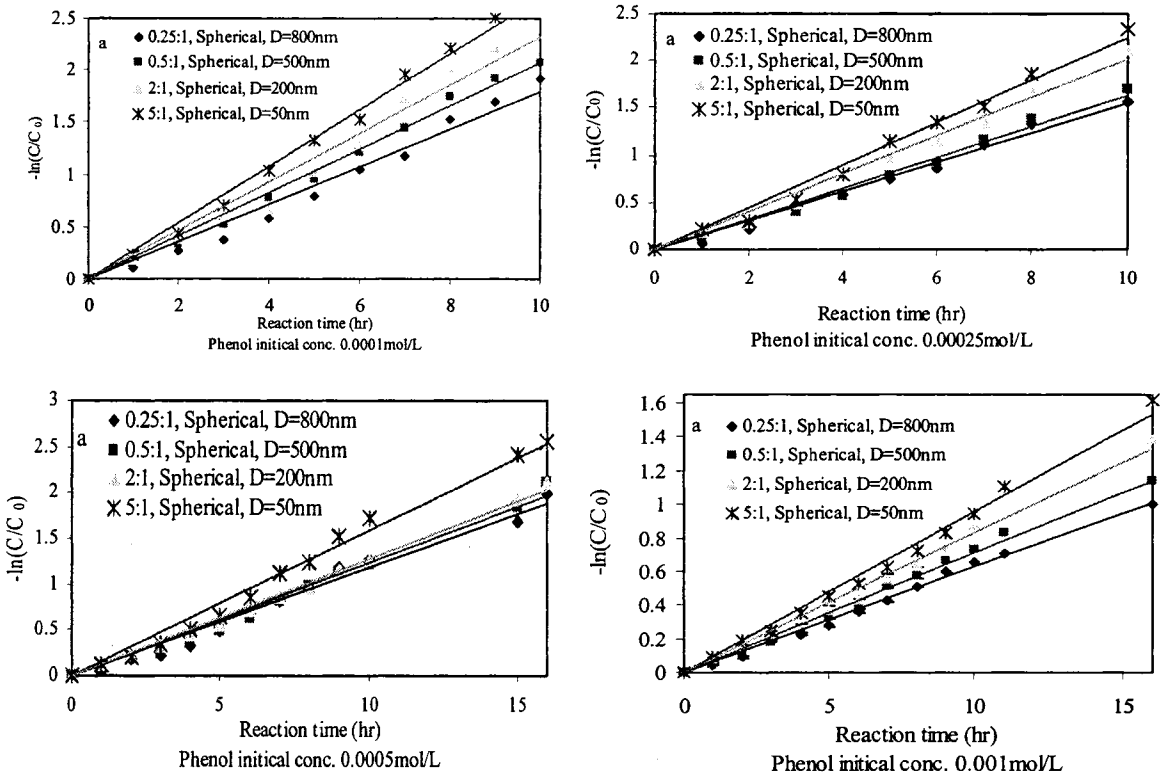

Figure 6-10, Relationship of -ln(C/C$_0$) and time of phenol on TiO$_2$ nanosized particles synthesized with DBS

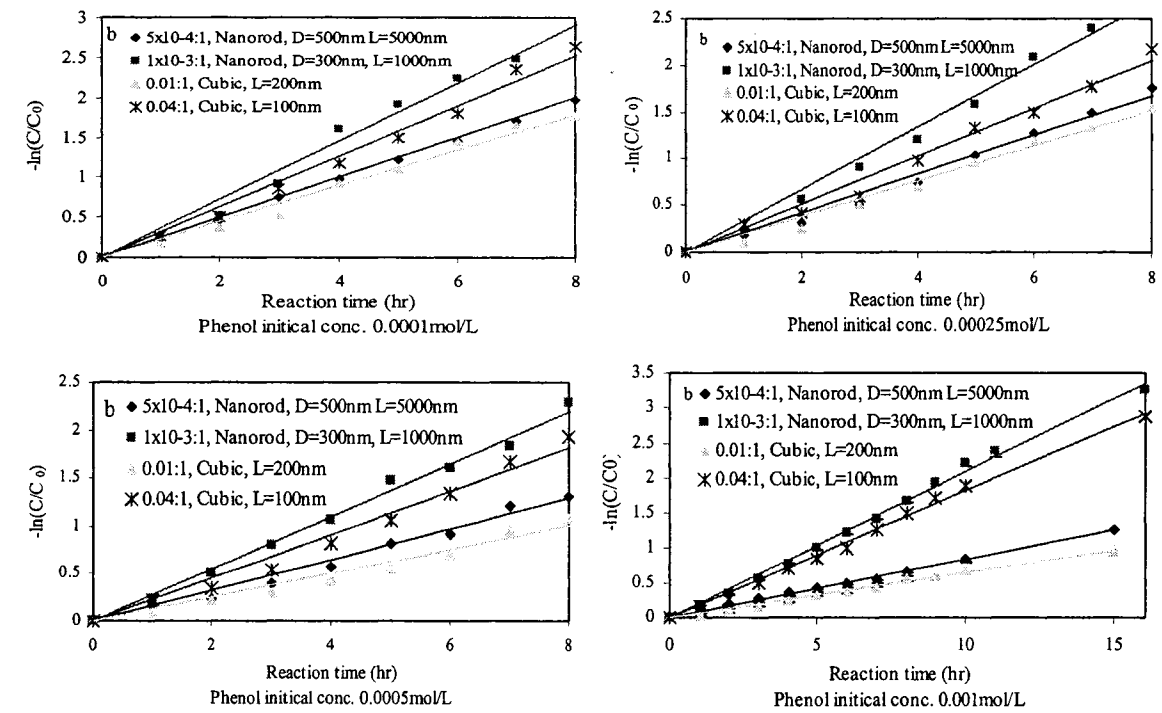

Figure 6-11, Relationship of -ln(C/C$_0$) and time of phenol on TiO$_2$ nanosized particles synthesized with cellulose

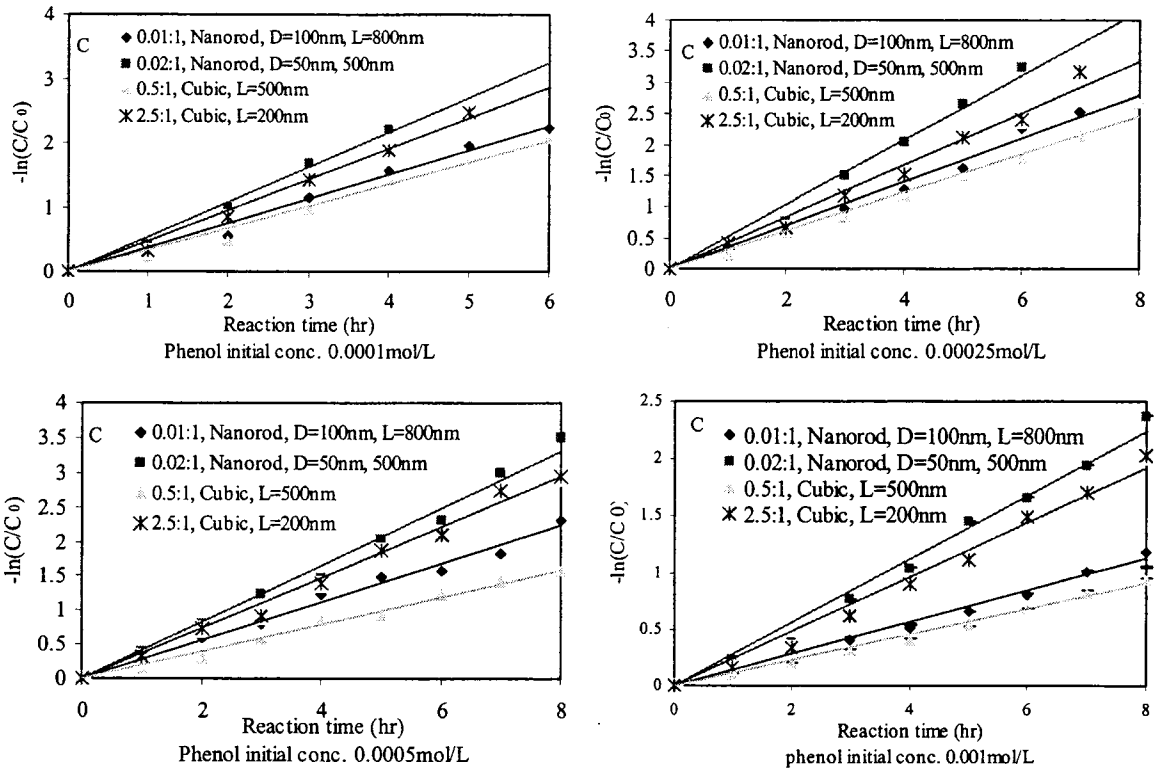

Figure 6-12, Relationship of -ln(C/C$_0$) and time of phenol on TiO$_2$ nanosized particles synthesized with SDS

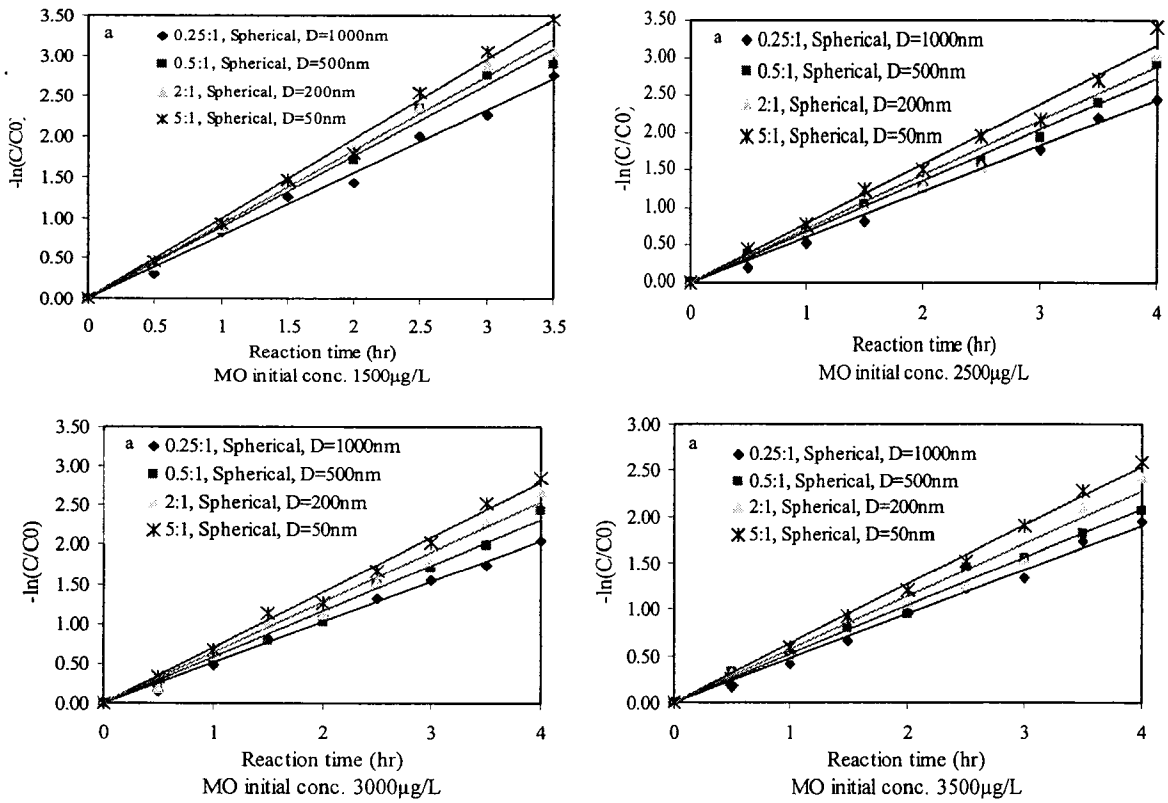

Figure 6-13, Relationship of -ln(C/C$_0$) and time of MO on TiO$_2$ nanosized particles synthesized with DBS

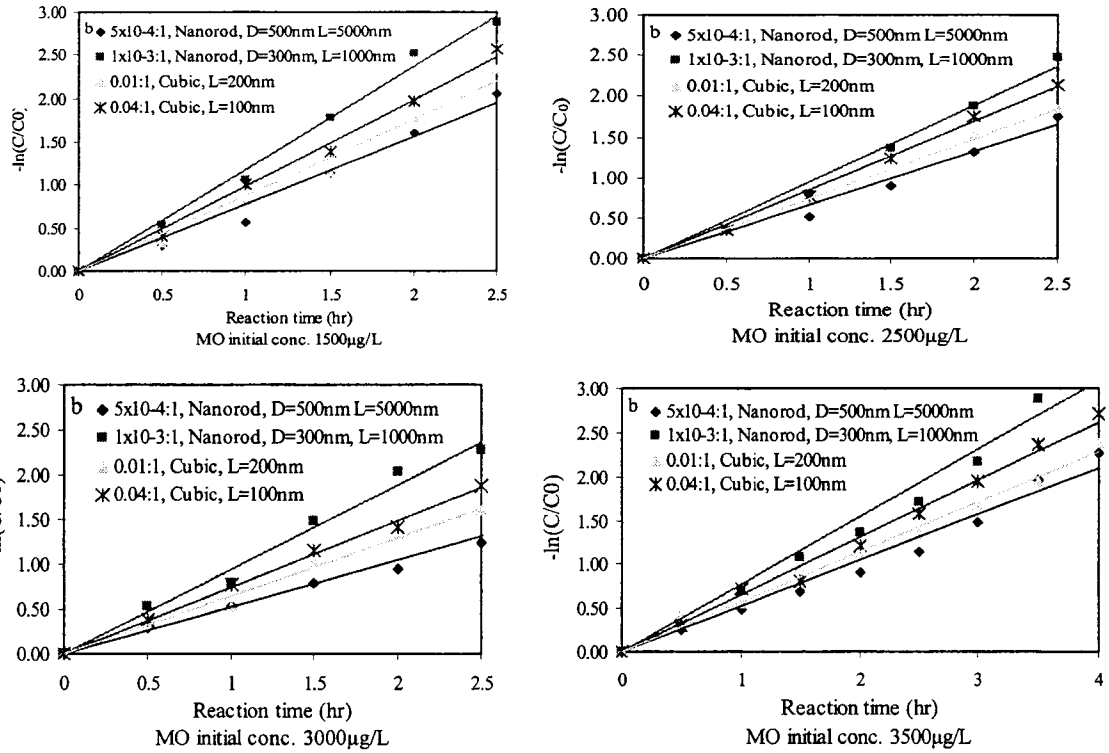

Figure 6-14, Relationship of -ln(C/C$_0$) and time of MO on TiO$_2$ nanosized particles synthesized with cellulose

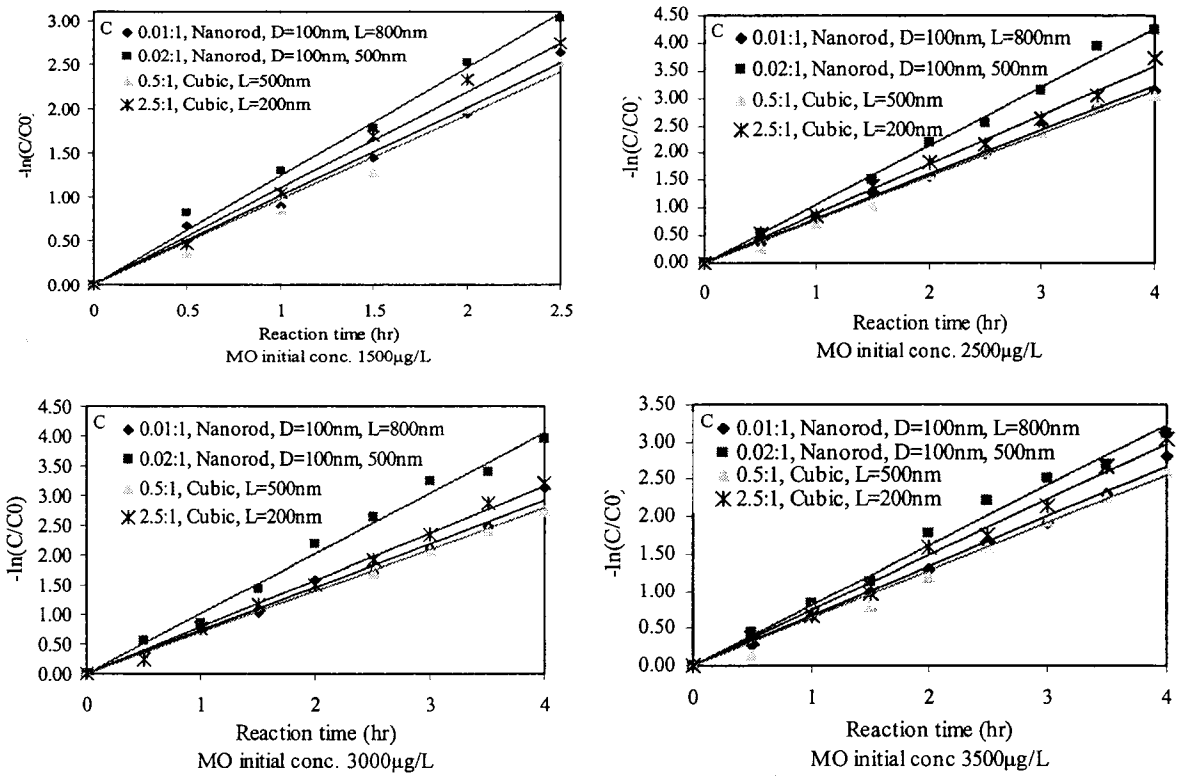

Figure 6-15, Relationship of -ln(C/C$_0$) and time of MO on TiO$_2$ nanosized particles synthesized with SDS

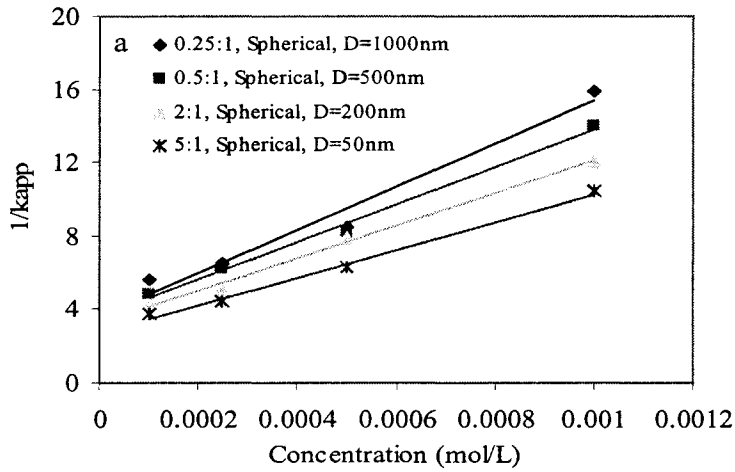

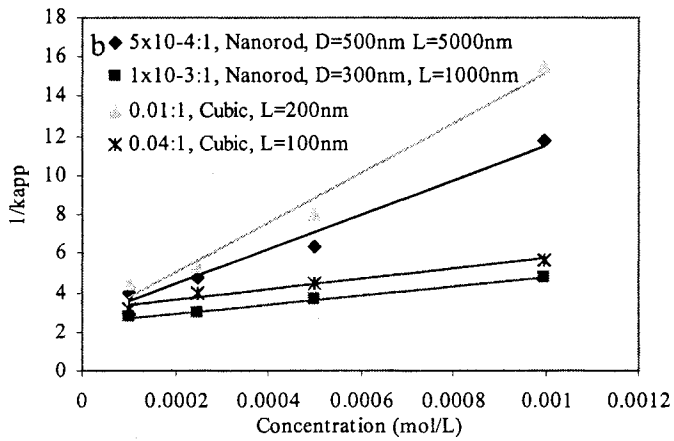

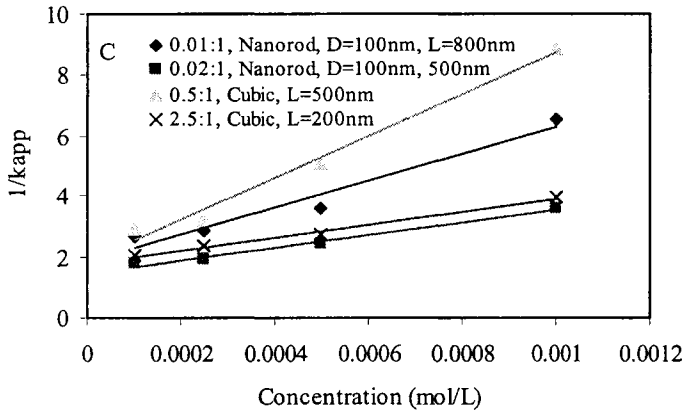

Figure 6-16, Correlation between $1/k_{app}$ and initial concentration of phenol
(a) Shape-controlled by DBS with different DBS/$Ti(OBu)_4$ molar ratios.
(b) Shape-controlled by cellulose with different cellulose/$Ti(OBu)_4$ molar ratios.
(c) Shape-controlled by SDS with different SDS/$Ti(OBu)_4$ molar ratios.

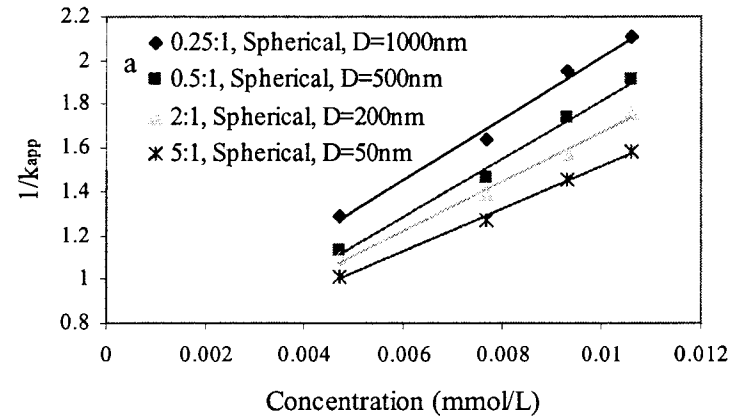

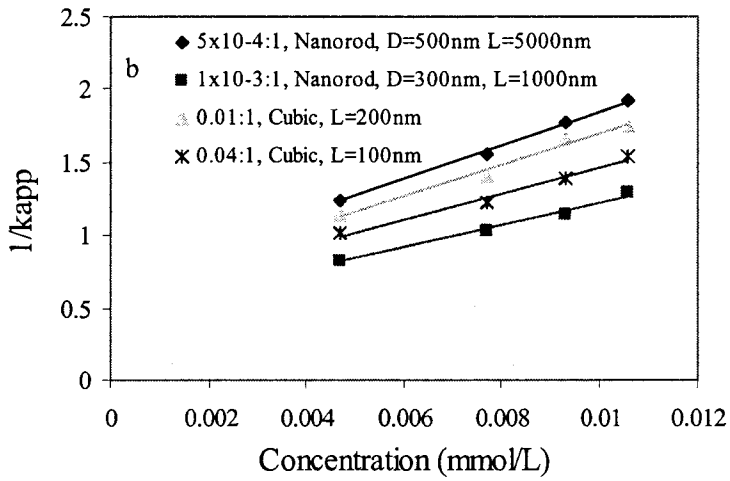

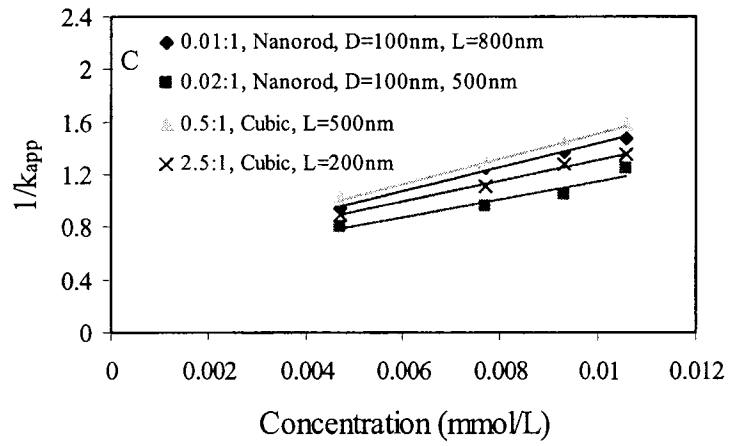

Figure 6-17, Correlation between $1/k_{app}$ and initial concentration of MO
(a) Shape-controlled by DBS with different DBS/$Ti(OBu)_4$ molar ratios.
(b) Shape-controlled by cellulose with different cellulose/$Ti(OBu)_4$ molar ratios.
(c) Shape-controlled by SDS with different SDS/$Ti(OBu)_4$ molar ratios.

Table 6-2, Reaction rate constants (k_c) and constants of adsorption equilibrium (K_C) for the photocatalytic decomposition of phenol and MO on different TiO_2 photocatalysts

Surfactant used	surfactant /$Ti(OBu)_4$	Shape and Size	Phenol		MO	
			k_c (mmol L^{-1} hr^{-1})	K_C (L mol^{-1})	k_c (mmol L^{-1} hr^{-1})	K_C (L mol^{-1})
DBS	0.2:1	Spherical, D*=1000nm	0.0855	3168.472	7.082	223.2411
	0.5:1	Spherical, D=500nm	0.0982	2841.277	7.498	274.1982
	2:1	Spherical, D=200nm	0.113	2742.961	8.893	206.0656
	5:1	Spherical, D=50nm	0.132	2783.808	10.408	174.1174
Cellulose	5×10^{-4}:1	Nanorods, D=500nm, L**=5000nm	0.114	3295.076	8.621	174.4211
	1×10^{-3}:1	Nanorods, D=300nm, L=1000nm	0.436	924.1826	13.133	141.3421
	0.01:1	Cubic, L=200nm	0.0792	4018.336	9.248	175.7069
	0.04:1	Cubic, L=100nm	0.377	1082.755	11.421	150.3124
SDS	0.01:1	Nanorods, D=100nm, L=800nm	0.226	2380.829	11.119	169.4949
	0.02:1	Nanorods, D=100nm, L=500nm	0.492	1343.186	14.725	145.4197
	0.5:1	Cubic, L=500nm	0.145	3805.927	10.592	179.2179
	2.5:1	Cubic, L=200nm	0.477	1123.788	12.803	139.0741

* Where D is the diameter, ** L is the length.

6.4 Influence of light intensity on the photocatalytic decomposition rates

The correlation between the light intensity (mW/cm^2) and the initial reaction rate (r_0, mM L^{-1} min^{-1}) calculated from variations of concentrations in the first hour of photocatalytic reaction is shown in Figure 6-18. The initial reaction rate increased with an increase in the light intensity. The TiO_2 nanosized particles synthesized with SDS have the highest photocatalytic activity for both substrates. From the fitting equations shown in Figure 6-18, it was found that the light intensity (I) could not be linearly related to the initial reaction rates. The dependence of the initial reaction rate on the light intensity was proportional to I^X (x ranged from 0.55 to 0.65). In the classic semiconductor photocatalysis experiment conducted by Egerton et al, the dependence of kinetics to I was ranged from first order to half-order [176]. Some studies also reported that the initial rates of photocatalytic decomposition of organic pollutants were proportional to $I^{0.5}$ [177] or $I^{0.6}$ [178]. The results in this work are consistent with the work of other studies. The

kinetics fell in the transition range between the first and half-order dependence upon the light intensity.

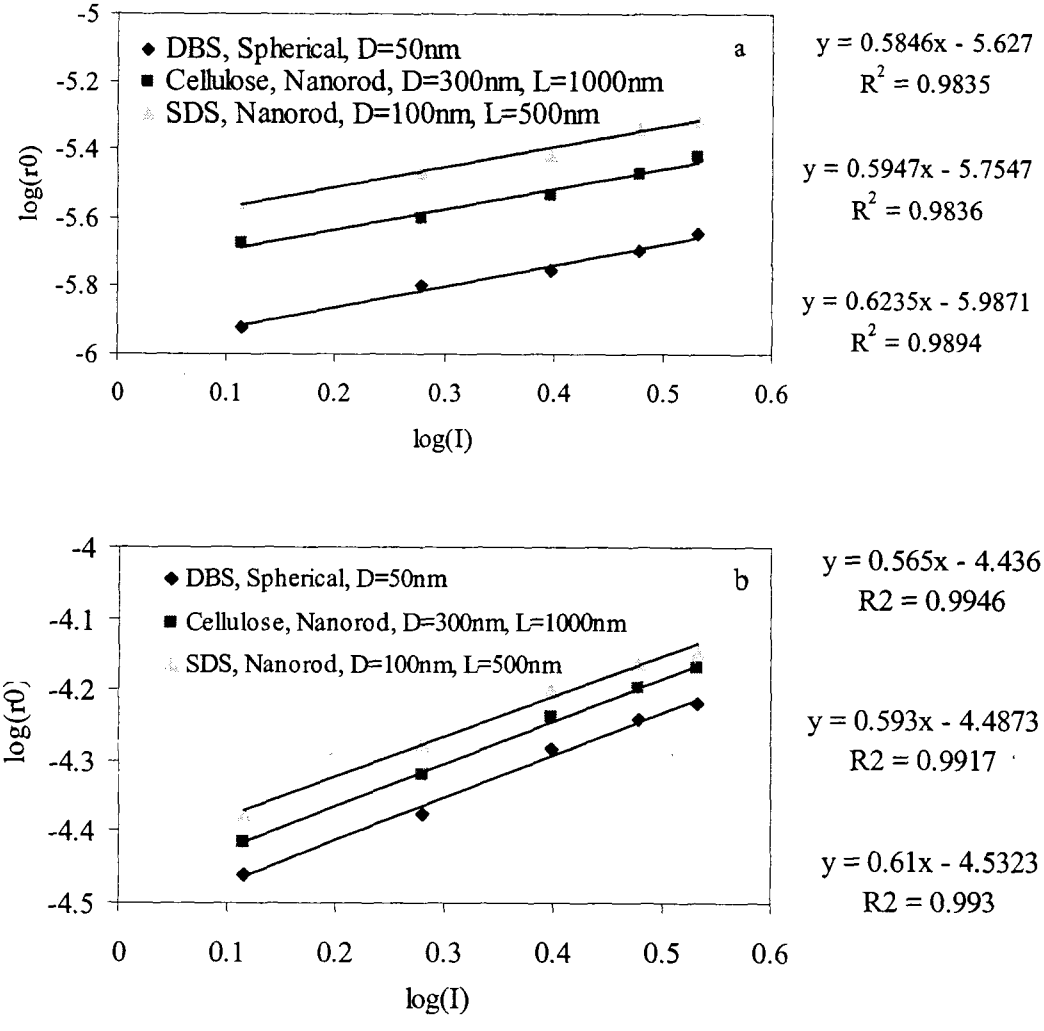

Figure 6-18, Relationship between initial reaction rate r_0 and light intensity
(a) Photocatalytic decomposition of phenol (Initial concentration 0.001mol/L),
(b) Photocatalytic decomposition of MO (Initial concentration 0.004mmol/L).

CHAPTER 7 Conclusions and Recommendations

7.1 Conclusions

Surfactants including sodium dodecyl benzene sulfonate (DBS), sodium dodecyl sulfate (SDS) and hydroxypropyl methyl cellulose were employed, during preparation, to control the shape and size of the TiO_2 nanosized particles. Various shapes of TiO_2 nanosized particles, including spherical, cubic, rod, ellipse and leaf-like shapes were obtained by using different surfactant composition and concentrations. Spherical TiO_2 nanosized particles were formed when DBS was used. Nanorods and cubic nanosized particles were obtained when SDS and cellulose were used, respectively.

It was found that the shape and size of nanosized particles depends on not only surfactant composition but also surfactant concentration. The shape and size evolution of the TiO_2 nanosized particles synthesized with different surfactant/titanium precursor molar ratios were studied. Nanosized particle size decreases with an increase in the surfactant/titanium precursor molar ratio. The results shows that nanorods tended to form at high surfactant/titanium precursor molar ratios while cubic nanosized particles were favored at low surfactant/titanium precursor molar ratios. The mechanism of the formation of various shapes of TiO_2 nanosized particles was proposed.

Zeta potential of shape- and size-controlled TiO_2 nanosized particles was measured at different pH values. A unique finding is that TiO_2 nanosized particles shaped by sodium dodecyl sulfate (SDS) have two isoelectric points (IEPs), while other shape-controlled TiO_2 nanosized

particles have only one IEP. At neutral pH, shape-and size-controlled TiO_2 nanosized particles have a more negative zeta potential than TiO_2 nanosized particles obtained without the addition of surfactants during synthesis and commercial anatase TiO_2 nanosized particles Duggase P-25. The IEP value of TiO_2 nanosized particles increases with an increase in calcination temperature. Different zeta potential values were observed for TiO_2 nanosized particles obtained with the addition of different surfactants during preparation. The addition of SDS in TiO_2 nanosized particle suspensions causes a shift of the IEPs to lower pH values. The results suggest that the zeta potential of TiO_2 nanosized particles can be manipulated with the addition of surfactants during the synthesis process or after dispersion in aqueous phase.

The photocatalytic activity of prepared TiO_2 nanosized particles was evaluated in fixed film batch reactors with phenol and methyl orange as model compounds. The results indicate that the photocatalytic activity of shape- and size-controlled TiO_2 nanosized particles can be controlled and improved through the manipulation of shape and size using surfactants during preparation. Shape is more important than size in controlling the photocatalytic activity of shape- and size-controlled TiO_2 nanosized particles. Kinetic studies show that the photocatalytic decomposition of MO and phenol follows the first order kinetic. An optimal calcination temperature at 600°C exists for the highest photocatalytic activity.

7.2 Recommendations

Although extensive studies on photocatalytic reactions of TiO_2 nanosized particles have been done, tremendous opportunities exist for the improvement of their photocatalytic activity. Further studies should be concentrated on the mechanism of the formation of different shapes

and sizes of TiO_2 nanosized particles with different surfactant composition and concentrations. The potential correlation between the shape and size and photocatalytic activity of TiO_2 nanosized particles is not clear and needs further studies. More evidence through surface analysis should be collected to provide an in-depth understanding of the variations in photocatalytic activity of various shape- and size-controlled TiO_2 nanosized particles. New approaches, such as a combination of the use of surfactant and metal ions dopping during preparation should be studied to further improve the photocatalytic activity of shape- and size- controlled TiO_2 nanosized particles.

References:

[1] J. F. Banfield, Nanoparticles and the Environment, 2001.

[2] Y. Jun, J. Seo, J. Cheon, Recent Advances in the Shape Control of Inorganic Nano-building Blocks, Coordination Chemistry Review, 249 (2005) 1766-1775.

[3] G. A Ozin, A.C Arsenault, Nanochemistry, A Chemical Approach to Nanomaterials, RSC Publishing, 2005.

[4] A. P. Alivisatos, Semiconductor clusters, nanocrystals, and quantum dots, Science, 271 (1996) 933-938.

[5] L. Brus, Chemical approaches to semiconductor nanocrystals, Journal of Physics and Chemistry of Solids, 59 (1998) 459-465.

[6] A. Fujishima, T.N. Rao, D.A. Tryk, Titanium dioxide photocatalysis, Journal of Photochemistry and Photobiology C: Photochemistry Reviews, 1 (2000) 1-21.

[7] O. Carp, C.L. Huisman, A. Reller, Photoinduced reactivity of titanium dioxide, Progress in Solid State Chemistry, 32 (2004) 33-177.

[8] D. A. Tryk a, A. Fujishima, K. Honda, Recent topics in photoelectrochemistry: achievements and future prospects, Electrochimica Acta, 45 (2000) 2363-2376.

[9] L. E. Brus, Quantum crystallites and nonlinear optics, Applied Physics A-Materials Science and Processing, 53 (1991) 465-474.

[10] A. P. Alivisatos, Semiconductor clusters, nanocrystals, and quantum dots, Science, 271 (1996) 933-937.

[11] N. A. Anderson, T. Lian, Ultrafast electron transfer at the molecule-semiconductor nanoparticle interface, Annual Review of Physical Chemistry, 56 (2005) 491-519.

[12] D. Chen, A.K. Ray, Photocatalytic kinetics of phenol and its derivatives over UV irradiated TiO_2, Applied Catalysis B: Environmental, 23 (1999) 143-157.

[13] W. Wang, L.W. Chiang, Y. Ku, Decomposition of benzene in air streams by UV/TiO_2 process, Journal Hazardous Materials, 101 (2003) 133-146.

[14] A.M. Braun, E. Oliveros, How to evaluate photochemical methods for water treatment, Water Science and Technology, 35 (1997) 17-23.

[15] M.A. Fox, M.T. Dulay, Heterogeneous Photocatalysis, Chemical Review, 95 (1993) 341-357.

[16] I.K. Konstantinou, V.A. Sakkas, T.A. Albanis, Photocatalytic degradation of propachlor in aqueous TiO_2 suspensions. Determination of the reaction pathway and identification of intermediate products by various analytical methods, Water Research, 36 (2002) 2733-2742.

[17] M. Muneer, D. Bahnemann, Semiconductor-mediated photocatalyzed degradation of two selected pesticide derivatives, terbacil and 2,4,5-tribromoimidazole, in aqueous suspension, Applied Catalysis B: Environmental, 36 (2002) 95-111.

[18] L. Manna, E. Scher, A.P. Alivisatos, Synthesis of Soluble and Processable Rod-, Arrow-, Teardrop-, and Tetrapod-Shaped CdSe Nanocrystals, Journal of American Chemical Society, 122 (2000) 12700-12706.

[19] D.J. Milliron, S.M. Hughes, A.P. Alivisatos, et al., Colloidal nanocrystal heterostructures with linear and branched topology, Nature, 430 (2004) 190-195.

[20] D. Chatterjee, S. Dasgupta, Visible light induced photocatalytic degradation of organic pollutants, Journal of Photochemistry and Photobiology C: Photochemistry Review, 6 (2005) 186-205.

[21] D.G. Shchukin, D.V. Sviridov, Photocatalytic processes in spatially confined micro- and nanoreactors, Journal of Photochemistry and Photobiology C: Photochemistry Review, 7 (2006) 23-39.

[22] J.C. Yu, X. Wang, X. Fu, Pore-Wall Chemistry and Photocatalytic Activity of Mesoporous Titania Molecular Sieve Films, Chemistry of Materials, 16 (2004) 1523-1530.

[23] Z.B. Zhang, C.C. Wang, R. Zakaria, J.Y. Ying, Role of Particle Size in Nanocrystalline TiO_2-Based Photocatalysts, Journal of Physical Chemistry B, 102 (1998) 10871-10878.

[24] Z. A. Peng, X. Peng, Mechanism of the Shape Evolution of CdSe Nanocrystals, Journal of the American Chemical Society, 123 (2001) 1389-1395.

[25] P.D. Cozzoli, A. Kornowski, H.J. Weller, Low-temperature synthesis of solution of soluble and processable organic-capped anatase TiO_2 nanorods, Journal of American Chemical Society,125 (2003), 14539-14548.

[26] R.L. Penn and J.F. Banfield, Imperfect oriented attachment: Dislocation generation in defect-free nanocrystals, Science, 281 (1998) 969-971.

[27] M.P. Pileni, The role of soft colloidal tempelates in controlling the size and shape of inorganic nanocrystals, Nature materials, 2 (2003) 145-150.

[28] A. Mills, S. Le Hunte., An overview of semiconductor photocatalysis, Journal of Photochemistry and Photobiology A: Chemistry, 108 (1997) 1-35.

[29] A.J. Hoffmann, E.R. Carraway, M.R. Hoffmann, Photocatalytic production of H_2O_2 and organic peroxides on quantum-sized semiconductor colloids, Environmental Science and Technology, 28 (1994) 776-785.
[30] A. Mills, S. Morris, Photomineralization of 4-chlorophenol sensitized by titanium dioxide: a study of the initial kinetics of carbon dioxide, Journal of Photochemistry and Photobiology A: Chemistry, 71 (1993) 75-83.
[31] A. Mills, S. Morris, R. Davies, Photomineralisation of 4-chlorophenol sensitised by titanium dioxide: a study of the intermediates, Journal of Photochemistry and Photobiology A: Chemistry, 70 (1993) 183-191.
[32] Y. Jun, Y. Jung, J. Cheon, Architectural Control of Magnetic Semiconductor Nanocrystals, Journal of the American Chemical Society, 124 (2002) 615-619.
[33] M. Tonejc, I. Djerdj, A. Tonejc, Evidence from HRTEM image processing, XRD and EDS on nanocrystalline iron-doped titanium oxide powders, Materials Science and Engineering: B, 85 (2001) 55-63.
[34] P. Yang, C. Lu, N. Hua, Y. Du, Titanium dioxide nanoparticles co-doped with Fe^{3+} and Eu^{3+} ions for photocatalysis, Materials Letters, 57 (2002) 794-801.
[35] S. Sivakumar, C.P. Sibu, P. Mukundan, P. Krishna Pillai, K.G.K. Warrier, Nanoporous titania-alumina mixed oxides-an alkoxide free sol-gel synthesis, Materials Letters, 58 (2004) 2664-2669.
[36] C. Su, B.Y. Hong, C.M. Tseng, Sol-gel preparation and photocatalysis of titanium dioxide, Catalysis Today, 96 (2004) 119-126.
[37] M. Wu, G. Lin, D. Chen, G. Wang, D. He, S. Feng, R. Xu, Sol-Hydrothermal Synthesis and Hydrothermally Structural Evolution of Nanocrystal Titanium Dioxide, Chemistry of Materials, 14 (2002) 1974-1980.
[38] Q. Zhang, Effects of calcination on the photocatalytic properties of nanosized TiO_2 powders prepared by $TiCl_4$ hydrolysis, Applied catalysis B: Environmental, 26 (2000) 207-215
[39] Y. Shi, X. Zhang, H. Li, Liquid phase deposition templates synthesis of nanostructures of anatase titania, Materials Science and Engineering A, 333 (2002) 239-242.
[40] N.F. Ois, B. Ginzberg, Parameters Involved in the Sol-Gel Transition of Titania in Reverse Micelles, Journal of Sol-Gel Science and Technology, 13 (1998) 341-346.
[41] T. Sugimoto, X.P. Zhou, A. Muramatsu, Synthesis of uniform anatase TiO_2 nanoparticles by gel-sol method - 1. Solution chemistry of $Ti(OH)_n^{(4-n)+}$ complexes, Journal of Colloid and Interface Science, 252 (2002) 339-346.
[42] T. Sugimoto, X.P. Zhou, Synthesis of uniform anatase TiO_2 nanoparticles by the gel-sol method - 2. Adsorption of OH- ions to $Ti(OH)_4$ gel and TiO_2 particles, Journal of Colloid and Interface Science, 252 (2002) 347-353.
[43] T. Sugimoto, X.P. Zhou, A. Muramatsu, Synthesis of uniform anatase TiO_2 nanoparticles by gel-sol method 3. Formation process and size control, 259 (2003) 43-52.
[44] T. Sugimoto, X.P. Zhou, A. Muramatsu, Synthesis of uniform anatase TiO_2 nanoparticles by gel-sol method 4. Shape control, Journal of Colloid and Interface Science, 259 (2003) 53-61.
[45] B. Li, X. Wang, M. Yan, L. Li, Preparation and characterization of nano-TiO_2 powder, Material Chemistry and Physics, 78 (2003) 184-188.
[46] L. Miao, S. Tanemura, S. Toh, K. Kaneko, M. Tanemura, Heating-sol–gel template process for the growth of TiO_2 nanorods with rutile and anatase structure, Applied Surface Science, 238 (2004) 175-179.
[47] N. Uekawa, J. Kajiwara, K. Kakegawa, Y. Sasaki, Low Temperature Synthesis and Characterization of Porous Anatase TiO_2 Nanoparticles, Journal of Colloid and Interface Science, 250 (2002) 285-290.
[48] C. Guillard, B. Beaugiraud, C. Dutriez et al., Physicochemical properties and photocatalytic activities of TiO_2-films prepared by sol-gel methods, Applied Catalysis B: Environmental, 39 (2002) 331-342.
[49] R. Campostrini, M. Ischia, L. Palmisano, Pyrolysis study of sol-gel derived TiO_2 powders-Part III. TiO_2-anatase prepared by reacting titanium(IV) isopropoxide with acetic acid, Journal of Thermal Analysis and Calorimetry, 75 (2004) 13-24.
[50] N.Y. Al-Salim, S. Abagshaw, A. Bittar, T. Kemmett, A.J. McQuilla, A.M. Mills, et al., Characterisation and activity of sol-gel-prepared TiO_2 photocatalysts modified with Ca, Sr or Ba ion additives, Journal of Materials Chemistry, 10 (2000) 2358-2363.
[51] Y. Li, T.J. White, S.H. Lim, Low-temperature synthesis and microstructural control of titania nano-particles, Journal of Solid State Chemistry, 177 (2004) 1372-1381.
[52] C.-S. Kim, B.K. Moon, J.-H. Parka, S.T. Chungc, S.-M. Sond, Synthesis of nanocrystalline TiO_2 in toluene by a solvothermal route, Journal of Crystal Growth, 254 (2003) 405-410.
[53] Y.X. Zhang, G.H. Li, L.D. Zhang, Hydrothermal synthesis and photoluminescence of TiO_2 nanowires, Chemical Physics Letters, 365 (2002) 300-304.
[54] Y.V. Kolen'ko, A.A. Burukhin, B.R. Churagulov, N.N. Oleynikov, Synthesis of nanocrystalline TiO_2 powders from aqueous $TiOSO_4$ solutions under hydrothermal conditions, Material Letters, 57 (2003) 1124-1129.
[55]H. Kominami, J.-I. Kato, S.-Y. Murakami, Solvothermal syntheses of semiconductor photocatalysts of ultra-high activities, Catalysis Today, 84 (2003) 181-189.

[56] B. L. Cushing, V. L. Kolesnichenko, C. J. O'Connor, Recent Advances in the Liquid-Phase Syntheses of Inorganic Nanoparticles, Chemical Reviews, 104 (2004) 3893-3946.
[57] R. M. Tromp, J. B. Hannon, Thermodynamics of nucleation and growth, Surface Review and Letters, 9 (2002) 1565-1593.
[58] R. Chu, J. Yan, S. Lian, Y. Wang, F. Yan, D. Chen, Shape-controlled synthesis of nanocrystalline titania at low temperature, Solid State Communication, 130 (2004) 789-792.
[59] P.H. Borse, L.S. Kankate, F. Dassenoy, W. Vogel, J. Urban, S. K. Kulkarni, Synthesis and investigations of rutile phase nanoparticles of TiO_2, Journal of Materials Science, Materials in Electronics, 13 (2002) 553-559.
[60] S. Eriksson, U. Nylén, S. Rojas, M. Boutonnet, Preparation of catalysts from microemulsions and their applications in heterogeneous catalysis, Applied Catalysis A: General 265 (2004) 207-219.
[61] N. Nagaveni, M.S. Hegde, N. Ravishankar, G.N. Subbanna, G. Madras, Synthesis and Structure of Nanocrystalline TiO2 with Lower Band Gap Showing High Photocatalytic Activity, Langmuir, 20 (2004) 2900-2907.
[62] M. Adachi, K. Okuyama, T. Fujimoto, Film formation by a new chemical vapor deposition process using ionization of tetraethylorthosilicate, Japanese Journal of Applied Physics, 34 (1995) 1148-1150.
[63] K. Nakaso, T. Fujimoto, T. Seto, M. Shimada, K. Okuyama, M. M. Lunden, Size distribution change of titania nanoparticle agglomerates generated by gas phase reaction, Aerosol Science and Technology, 35 (2001) 929-947.
[64] K. Nakaso, K. Okuyama, M. Shimada, S. E. Pratsinis, Effect of reaction temperature on CVD-made TiO_2 primary particle diameter, Chemical Engineering and Science, 58 (2003) 3227-3335.
[65] C. S. Kim, K. Okuyama, K. Nakaso, M. Shimada, Direct measurement of nucleation and growth modes in titania nanoparticles generation by a CVD method, Journal of Chemical Engineering of Japan, 37 (2004) 1379-1389.
[66] K. Nakaso, B. Han, K. H. Ahn, M. Choi, K. Okuyama, Synthesis of non-agglomerated nanoparticles by an electrospray assisted chemical vapor deposition (ES-CVD) method, Journal of Aerosol Science, 34 (2003) 869-881.
[67] R. van de Krol, A. Goossens, J. Schoonman, Mott-Schottky Analysis of Nanometer-Scale Thin-Film Anatase TiO_2, Journal of the Electrochemical Society, 144 (1997) 1723-1727.
[68] M.T. Swihart, Vapor-phase synthesis of nanoparticles, Current Opinion in Colloid and Interface Science, 8 (2003) 127-133.
[69] A. Peng and X.G. Peng, Formation of High-Quality CdTe, CdSe, and CdS Nanocrystals Using CdO as Precursor, Journal of American Chemical Society, 123 (2001) 183-184.
[70] R. L. Penn, J.F. Banfield, Oriented attachment and growth, twinning, polytypism, and formation of metastable phases: Insights from nanocrystalline TiO_2, American Mineralogist, 83 (1998) 1077-1082.
[71] N. M. Dimitrijevic, B.M. Rabatic and T. Rajh, Assembly and Charge Transfer in Hybrid TiO_2 Architectures Using Biotin-Avidin as a Connector, Journal of American Chemical Society, 127 (2005) 1344-1345.
[72] Z. V. Saponjic, D. M. Tiede and A.S. Barnard, Shaping nanometer-scale architecture through surface chemistry, Advanced Materials, 17 (2005) 965-971.
[73] A. Chemseddine, T. Moritz, Nanostructuring titania: Control over nanocrystal structure, size, shape, and organization, European Journal of Inorganic Chemistry, 2 (1999) 235-245.
[74] J. Joo, S.G. Kwon and T.Y. Yu, Large-Scale Synthesis of TiO_2 Nanorods via Nonhydrolytic Sol-Gel Ester Elimination Reaction and Their Application to Photocatalytic Inactivation of E. coli, Journal of Physical Chemistry B, 109 (2005)15297-15302.
[75] Y. W. Jun, M. F. Casula and J.H. Sim, Surfactant-Assisted Elimination of a High Energy Facet as a Means of Controlling the Shapes of TiO_2 Nanocrystals, Journal of American Chemical Society, 125 (2003) 15981-15985.
[76] Z. R. Tian, J. A. Voigt, J. Liu, B. McKenzie and H.F. Xu, Large Oriented Arrays and Continuous Films of TiO_2-Based Nanotubes, Journal of American Chemical Society, 125 (2003) 12384-12385.
[77] L. Manna, E.C. Scher, A.P. Alivisatos, Shape Control of Colloidal Semiconductor Nanocrystals, Journal of Cluster Science, 13 (2002) 521-532.
[78] Y. C. Zhu, C. X. Ding, Oriented growth of nano-TiO_2 whiskers, Nanostructured Materials, 11 (1999) 427-431.
[79] B. M. Rabatic, N. M. Dimitrijevic, R.E. Cook, Spatially confined corner defects induce chemical functionality of TiO2 nanorods, Advanced Materials, 18 (2006) 1033-1037.
[80] J. H. Lee, I. C. Leu, M. C. Hsu, Y.-W. Chung, Frabricatioin of aligned TiO_2 one-dimensional nanostructured arrays using a one-step templating solution approach, Journal of Physical Chemistry B: Letters, 109 (2005)13056-13059.
[81] T. Kasuga, M. Hiramatsu, A. Hoson, T. Sekino, Formation of titanium dioxide nanotube, Langmuir, 14 (1998) 3160-3163.
[82] X. H. Li, W. M. Liu, H. L. L[illegible] Template synthesis of well-aligned titanium dioxide nanotubes, Applied Physics A, 80 (2005) 317-320.

[83] Y. Q. Wang, G. Q. Hu, X. F. Duan, Microstructure and formation mechanism of titanium dioxide nanotubes, Chemical Physics Letters, 365 (2002) 427-431.
[84] M. Wei, Y. Konishi, H. Zhou, Formation of nanotubes TiO_2 from layered titanate particles by a soft chemical process, Solid State Communications, 133 (2005) 493-497.
[85] M.K. Aminian, N. Taghavinia, A. Iraji-zad, S.M. Mahdavi, Highly porous TiO_2 nanofibres with a fractal structure, Nanotechnology, 17 (2006) 520-525.
[86] H. Y. Zhu, Y. Lan, X. P. Gao, S. P. Ringer, Z. F. Zheng, Phase transition between nanostructures of titanate and titanium dioxide via simple wet-chemical reactions, Journal of American Chemical Society, 127 (2005) 6730-6736.
[87] N. Uekawa, J. Kajiwara, K. Kakegawa, Y. Sasaki, Low temperature synthesis and characterization of porous anatase TiO_2 nanoparticles, Journal of Colloid and Interface Science, 250 (2002) 285-290.
[88] S. Yin, R. Li, Q. He, T. Sato, Low temperature synthesis of nanosize rutile titania crystal in liquid media, Materials Chemistry and physics, 75 (2002) 76-80.
[89] F. J. Vidal-Iglesias, J. Solla-Gullon, A. Aldaz, Shape-dependent Electrocatalysis, Electrochemistry Communications, 6 (2004) 1080-1084.
[90] T. Teranishi, R. Kurita, M. Miyake, Shape Control of Pt Nanoparticles, Journal of Inorganic and Organometallic Polymers, 10 (2000) 145-157.
[91] O. Margeat, F. Dumestre, C. Amiens, Synthesis of iron nanoparticles: Size effects, shape control and organization, Progress in Solid State Chemistry, 33 (2005) 71-79.
[92] Z. Liu, S. Li, Y. Qian, Complex-Surfactant-Assisted Hydrothermal Route to Ferromagnetic Nickel Nanobelts, Advanced Materials, 15 (2003) 1946-1948.
[93] Y. Jun, C. S. Choi, J. Cheon, Size and shape controlled ZnTe nanocrystals with quantum confinement effect, Chemical Communications, 1 (2001) 101-106.
[94] R. Vijaya Kumar, Y. Diamant, A. Gedanken, Sonochemical synthesis and characterization of nanometer-size transition metal oxides from metal acetates, Chemistry of Materials, 12 (2000) 2301-2305.
[95] D. Zitoun, N. Pinna, N. Frolet, Single Crystal Manganese Oxide Multipods by Oriented Attachment, Journal of American Chemical Society, 127 (2005) 15034-15035.
[96] F.X. Redl, K.S. Cho, C.B. Murray, S. O'Brien, Three-dimensional Binary Superlattices of Magnetic Nanocrystals and Semiconductor Quantum Dots, Nature, 423 (2003) 968-971.
[97] D. Beydoun, R. Amal, G. Low, S. McEvoy, Role of nanoparticles in photocatalysis, Joural of Nanoparticle Research 1(1999) 439-458.
[98] C. Burda, X. Chen, R. Narayanan, Chemistry and Properties of Nanocrystals of Different Shapes, Chemical Reviews, 105 (2005) 1025-1102.
[99] C.B. Murray; C.R. Kagan; M.G. Bawendi, Synthesis and characterization of monodisperse nanocrystals and close-packed nanocrystal assembles, Annual Review of Materials Science, 30 (2000) 545-610.
[100] R. Wang, K. Hashimoto, A. Fujishima, M. Chikuni, E. Kojima, A. Kitamura, M. Shimohigoshi, T. Watanabe, Light-induced amphiphilic surfaces, Nature, 388 (1997) 431-432.
[101] R. Wang, K. Hashimoto, A. Fujishima, M. Chikuni, E. Kojima, A. Kitamura, M. Shimohigoshi, T. Watanabe, Photogeneration of highly amphiphilic TiO_2 surfaces, Advanced Materials, 10 (1998) 135–138.
[102] B.P. Nelson, R. Candal and M.A. Anderson, Control of Surface and Potentials on Nanoporous TiO_2 Films by Potential-Determining and Specifically Adsorbed Ions, Langmuir, 16 (2000) 6094-6101.
[103] S. Liufu, H. Xiao and Y. Li, Adsorption of poly(acrylic acid) onto the surface of titanium dioxide and the colloidal stability of aqueous suspension, Journal of Colloid and interface Science, 281 (2005) 155-163.
[104] G.Xu, J. Zhang and G. Song, Effect of Complexation on the Zeta Potential of Titanium Dioxide Dispersions, Journal of Dispersion Science and Technology, 24 (2003) 527-535.
[105] M. Miyauchi, A. Ikezawa and K. Hashimoto, Zeta potential and photocatalytic activity of nitrogen doped TiO2 thin films, Physical Chemistry Chemical Physics, 6 (2004) 865-870.
[106] F. Molino, J. M. Barthez and J. Marignan, Influence of surfactants on the structure of titanium oxide gels: Experiments and simulations, Physical Review E, 53 (1996) 921-925.
[107] T. Sato, S. Kohnosu, Effect of polyvinylpyrrolidone on the physical properties of titanium dioxide suspensions, Colloid Surface. A, 88 (1994) 197-205.
[108] N. Mandzy, E. Grulke and T. Druffel, Breakage of TiO_2 agglomerates in electrostatically stabilized aqueous dispersions, Powder Technology, 16 (2005) 121-126.
[109] D. Gumy, C. Morais and P. Bowen, Catalytic activity of commercial of TiO_2 powders for the abatement of the bacteria (E. coli) under solar simulated light: Influence of the isoelectric point, Applied Catalysis B: Environmental, 63 (2006) 76-84.

[110] J. Palarcik, J. Jandera and L. Svoboda, A study of an influence of pH on zeta potential of titanium dioxide particles in different dispersion environments, CHISA 2004-16th International Congress of Chemical and Process Engineering, 2004, 8133-8145.
[111] S. Lebrette, C. Pagnoux, Stability of aqueous TiO_2 suspensions: influence of ethanol Journal of Colloid and Interface Science, 280 (2004) 400-408.
[112] M.R. Hoffmann, S.T. Martin, W. Choi, Detlef W. Bahnemann, Environmental applications of Semiconductor Photocatalysis, Chemical Reviews, 95 (1995) 69-96.
[113] M.A. Fox, M.T. Dulay, Hetergeneous Photocatalysis, Chemical Reviews, 93 (1993) 341-357.
[114] Y. Mao, C. Schoneich, K.D. Asmus, Identification of organic acids and other intermediates in oxidative degradation of chlorinated ethanes on titania surfaces en route to mineralization: a combined photocatalytic and radiation chemical study, Journal of Physical Chemistry, 95 (1991) 80-89.
[115] U. Stanford, K.A. Gray, P.V. Kamat, An in situ diffuse reflectance FTIR investigation of photocatalytic degradation of 4-chlorophenol on a TiO_2 powder surface, Chemical Physics Letters, 205 (1993) 55-61.
[116] A. V. Vorontsov, E. N. Kurkin, E. N. Savinon, Study of TiO_2 Deactivation during Gaseous Acetone Photocatalytic Oxidation, Journal of Catalysis, 186 (1999) 318-324.
[117] S.B. Kim, S.C. Hong, Kinetic study for photocatalytic degradation of volatile organic compounds in air using thin film TiO_2 photocatalyst, Applied Catalysis B: Environmental 35 (2002) 305-315.
[118] Y. Li, Xiaodong Li, J. Li and J. Yin, Photocatalytic degradation of methyl orange by TiO_2-coated activated carbon and kinetic study, Water Research, 40 (2006) 1119-1126.
[119] B. Serrano, H. de Lasa, Photocatalytic Degradation of Water Organic Pollutants.Kinetic Modeling and Energy Efficiency, Industrial and Engineering Chemistry Research, 36 (1997) 4705-4711.
[120] M. H. Priya, G. Madras, Kinetics of Photocatalytic Degradation of Chlorophenol, Nitrophenol, and Their Mixtures, Industrial and Engineering Chemistry Research, 45 (2006) 482-486.
[121] M. H. Priya, G. Madras, Kinetics of Photocatalytic Degradation of Phenols with Multiple Substituent Groups, Journal of Photochemistry and photobiology A: Chemistry 179 (2006) 256-262.
[122] H. Park, W. Choi, Photocatalytic conversion of benzene to phenol using modified TiO_2 and polyoxometalates, Catalysis Today, 101 (2005) 291–297.
[123] T. Ohno, Y. Masaki, S. Hirayama, M. Matsumura., TiO_2-Photocatalyzed Epoxidation of 1-Decene by H_2O_2 under Visible Light, Journal of Catalysis, 204 (2001) 163-168.
[124] H. Maeda, H. Miyamoto, K. Mizuno, Synthesis of 3,3,6,6-tetraaryl-1,2-dioxanes via TiO2-catalyzed photooxygenation of 1,1-diarylethenes in the presence of $Mg(ClO_4)_2$, Chemistry Letters, 33 (2004) 462-463.
[125]O.S. Mohamed, A. El-Aal, M. Gaber, A.A. Abdel-Wahab, Photocatalytic oxidation of selected aryl alcohols in acetonitrile, Journal of Photochemistry and Photobiology A: Chemistry, 148 (2002) 205-210.
[126] R. Wang, K. Hashimoto, A. Fujishima, M. Chikuni, E. Kojima, A. Kitamura, et al., Photogeneration of highly amphiphilic TiO_2 surfaces, Advanced Materials, 10 (1998) 135-138.
[127] G.S. Shepharda, S. Stockenstr .oma, D. de Villiersb, W.J. Engelbrechtb, G.el F.S. Wesselsb, Degradation of microcystin toxins in a falling film photocatalytic reactor with immobilized titanium dioxide catalyst, Water Research, 36 (2002) 140-146.
[128] R.S. Sonawane , S.G. Hegde , M.K. Dongare, Preparation of titanium(IV) oxide thin film photocatalyst by sol–gel dip coating, Materials Chemistry and Physics, 77 (2002) 744-750.
[129] K. Sunada, T. Watanabe, K. Hashimoto, Studies on photokilling of bacteria on TiO_2 thin film, Journal of Photochemistry and Photobiology A: Chemistry, 156 (2003) 227-233.
[130] Y. Shioya, K. Ikeue, M. Ogawa and M. Anpo, Synthesis of transparent Ti-containing mesoporous silica thin film materials and their unique photocatalytic activity for the reduction of CO_2 with H_2O, Applied Catalysis A: General, 254 (2003) 251-259.
[131] A. Mills, J. Wang, Photobleaching of methylene blue sensitized by TiO_2: an ambiguous system, Journal of Photochemistry and Photobiology A: Chemistry, 127 (1999) 123-134.
[132] A. Mills, N. Elliott, I.P. Parkin, S.A. O'Neill, R.J. Clark, Novel TiO_2 CVD films for semiconductor photocatalysis, Journal of Photochemistry and Photobiology A: Chemistry, 151 (2002) 171-179.
[133] A. Mills, J. Wang, Simultaneous monitoring of the destruction of stearic acid and generation of carbon dioxide by self-cleaning semiconductor photocatalytic films, Journal of Photochemistry and Photobiology A: Chemistry, (2006) in press.
[134] J. Araña, E. Tello Rendón, J.M. Doña Rodríguez, High concentrated phenol and 1,2-propylene glycol water solutions treatment by photocatalysis: Catalyst recovery and re-use , Applied Catalysis B: Environmental, 30 (2001) 1-10.

[135] D. Chen, A.K. Ray, Photocatalytic kinetics of phenol and its derivatives over UV irradiated TiO_2, Applied Catalysis B: Environmental, 23 (1999) 143-157.
[136] S. Tasai , S. Cheng , Effect of TiO_2 crystalline structure in photocatalytic degradation of phenolic contaminants, Catalysis Today, 33 (1997) 227-237.
[137] S. Parra, J. Olivero, L. Pacheco, C. Pulgarin, Structural properties and photoreactivity relationships of substituted phenols in TiO2 suspensions, Applied Catalysis B: Environment, 43 (2003) 293-301.
[138] A. Sobczynski, Ł. Duczmal, W. Zmudzi´nski, Phenol destruction by photocatalysis on TiO2: an attempt to solve the reaction mechanism, Journal of Molecular Catalysis A: Chemical 213 (2004) 225-230.
[139] B. Neppolian, H.C. Choi, S. Sakthivel, Solar/UV-induced photocatalytic degradation of three commercial textile dyes, Journal of Hazardous Materials B, 89 (2002) 303-317.
[140] V. Augugliaro, C. Baiocchi, A.B. Prevot, Azo-dyes photocatalytic degradation in aqueous suspension of TiO_2 under solar irradiation, Chemosphere, 49 (2002) 1223-1230.
[141] E. Vulliet, C. Emmelin, J.-M. Chovelon, Chantal Guillard and Jean-Marie Herrmann, Photocatalytic degradation of sulfonylurea herbicides in aqueous TiO_2, Applied Catalysis B: Environmental, 38 (2002) 127-137.
[142] M. Muneera, D. Bahnemannb, Semiconductor-mediated photocatalyzed degradation of two selected pesticide derivatives, terbacil and 2, 4, 5-tribromoimidazole, in aqueous suspension, Applied Catalysis B: Environmental, 36 (2002) 95-111.
[143] M.S. Vohra, A.P. Davis, TiO_2-assisted photocatalysis of Lead-EDTA, Water Research, 34 (2000) 952-964.
[144] R. Zhang, L. Gao, Photodegradation of surfactants on the nanosized TiO_2 prepared by hydrolysis of the alkoxide titanium, Chemosphere, 54 (2004) 405-411.
[145] B. Bems, F.C. Jentoft, R. Schlogl, Photoinduced decomposition of nitrate in drinking water in the presence of titania and humic acids, Applied Catalysis B: Environmental, 20 (1999) 155-163.
[146] S. Kataoka, E. Lee, M.I. Tejedor-Tejedor and M.A. Anderson, Photocatalytic degradation of hydrogen sulfide and in situ FT-IR analysis of reaction products on surface of TiO_2, Applied Catalysis B: Environmental, 61 (2005) 159-163.
[147] T. Furuzono, M. Iwasaki, S. Yasuda, A. Korematsu, T. Yoshioka, S. Ito, et al., Photoreactivity and cell adhesiveness of amino-group-modified titanium dioxide nano-particles on silicone substrate coated by covalent linkage, Journal of Materials Science Letters, 22 (2003) 1737-1740.
[148] M. Stevenson, K. Bullock, W.Y. Lin, K. Rajeshwar, Sonolytic enhancement of the bactericidal activity of irradiated titanium dioxide suspensions in water, Research on Chemical Intermediates, 23 (1997) 311-323.
[150] A. Shah, P. Torres, T. Tscharner, N. Wyrsch, H. Keppner, Photovoltaic Technology: The Case for Thin-Film Solar Cells, Science, 285 (1999) 692-698.
[151] H. Tseng, W.-C. Chang, J.C.S. Wu, Photoreduction of CO_2 using sol–gel derived titania and titania-supported copper catalysts, Applied Catalysis B: Environmental 37 (2002) 37-48.
[152] H. Harada, Sonophotocatalytic decomposition of water using TiO_2 photocatalyst, Ultrasonics Sonochemistry, 8 (2001) 55-58.
[153] R. Abe, K. Sayama, K. Domen, A new type of water splitting system composed of two different TiO_2 Photocatalysts (anatase, rutile) and a IO_3-/I- shuttle redox mediator, Chemical Physics Letters, 344 (2001) 339-344.
[154] L.B. Khalil, M.W. Rophael, W.E. Mourad, The removal of the toxic Hg(II) salts from water by photocatalysis, Applied Catalysis B: Environmental, 36 (2002) 125-130.
[155] A. Mills, S.-K. Lee, A. Lepre, Photodecomposition of ozone sensitised by a film of titanium dioxide on glass, Journal of Photochemistry and Photobiology A: Chemistry 155 (2003) 199-205.
[156] A. Nakajima, S.I. Koizumi, T. Watanabe, K. Hashimoto, Effect of repeated photo-illumination on the wettability conversion of titanium dioxide, Journal of Photochemistry and Photobiology A: Chemistry, 146 (2001) 129-132.
[157] J.G. Yu, X.J. Zhao, Effect of surface microstructure on the super-hydrophilic property of the sol-gel derived porous TiO_2 thin films, Journal of Materials Science Letters, 20 (2001) 671-673.
[158] A. Nakajima, A. Fujishima, K. Hashimoto, T. Watanabe, Preparation of transparent superhydrophobic boehmite and silica films by sublimation of aluminum acetylacetonate, Advanced Materials, 11 (1999) 1365-1368.
[159] A. Dobosz, A. Sobczy'nski, The influence of silver additives on titania photoactivity in the photooxidation of phenol, Water Research, 37 (2003) 1489-1496.
[160] W. Lu, J. Fang, J. Lin, Shape Evolution and Self Assembly of Monodisperse PbTe Nanocrystals, Journal of American Chemical Society, 126 (2004) 11798-11799.
[161] J.N. Hay, H.M. Raval, Synthesis of organic-inorganic hybrids via the non-hydrolytic sol-gel process, Chemistry of Materials, 13 (2001) 3396-3403.

[162] G. Oskam, A. Nellore, R.L. Penn, The Growth Kinetics of TiO_2 Nanoparticles from Titanium(IV) Alkoxide at High Water/Titanium Ratio, Journal of Physical Chemistry B, 107 (2003) 1734-1738.
[163] T. J. Boyle, R. P. Tyner, T. M. Alam, Implications for the Thin-Film Densification of TiO_2 from Carboxylic Acid-Modified Titanium Alkoxides. Syntheses, Characterizations, X-ray Structures of $Ti_3(\mu_3\text{-}O)(O_2CH)_2(ONep)_8$, $Ti_3(\mu_3\text{-}O)(O_2CMe)_2(ONep)_8$, $Ti_6(\mu_3\text{-}O)_6(O_2CCHMe_2)_6(ONep)_6$, $[Ti(\mu\text{-}O_2CCMe_3)(ONep)_3]_2$, and $Ti_3(\mu_3\text{-}O)(O_2CCH_2CMe_3)_2(ONep)_8(ONep{=}OCH_2CMe_3)$, Journal of the American Chemical Society, 121 (1999) 12104-12112.
[164] International Center for Diffraction Data, 1-50, Release 2000.
[165] J.M. Petroski, Z.L. Wang, T.C. Green, Kinetically Controlled Growth and Shape Formation Mechanism of Platinum Nanoparticles, Journal of Physical Chemistry B, 102 (1998) 3316-3320.
[166] L. E. Brus, Electron-electron and electron-hole interactions in small semiconductor crystallites: the size dependence of the lowest excited electronic state, Journal of Physical Chemistry, 80(9) (1984) 4403-4409.
[167] C. B. Murray, C.R. Kagan, M.G. Bawendi, Synthesis and characterization of monodisperse nanocrystals and close-packed nanocrystal assemblies, Annual Review Materials Science, 30 (2000) 545.
[168] V. Nikolakis, Understanding interactions in zeolite colloidal suspensions: A review, Current Opinion in Colloid & Interface Science, 2005, 10, 203-210.
[169] J. Moser, S. Punchihewa and P.P. Infelta, Surface complexation of colloidal semiconductors strongly enhances interfacial electron-transfer rates, Langmuir, 7 (1991) 3012-3018.
[170] M. Ramamoorthy, R.D. King-Smith, D. Vanderbilt, Defects on TiO_2 (110) surfaces, Physical Review B, 49(1994) 7709-7716.
[171] T. Imae, K. Muto, S. Ikeda, The pH dependence of dispersion of TiO_2 particles in aqueous surfactant solutions, Colloid & Polymer Science, 269 (1991), 43-48.
[172] T. Ivanova, A. Harizanova, M. Surtchev, Investigation of sol-gel derived thin films of titanium dioxide doped with vanadium oxide, Solar Energy Materials and Solar Cells, 76 (2003) 591-598.
[173] R. E. Tanner, Y. Liang, Structure and chemical reactivity of adsorbed carboxylic acids on anatase TiO_2 (001), Surface Science, 506 (2002) 251-271.
[174] G. Medeiros-Ribeiro, D.A.A. Ohlberg, D.R. Bowler, R.E. Tanner, Titanium disilicide nanostructures: two phases and their surfaces, Surface Science, 431 (1999) 116-127.
[175] J. Matos, J. Laine, J. M. Hermann, Effect of the Type of Activated Carbons on the Photocatalytic Degradation of Aqueous Organic Pollutants by UV-Irradiated Titania, Journal of Catalysis, 200 (2001) 10-20.
[176] T.A. Egerton, C.J. King, The Influence of Light Intensity on Photocactivity in TiO_2 Pigmented Systems, J. Oil Col. Chem. Assoc. 62 (1979) 386-391.
[177] G. Al-Sayyed, J. C. D'Oliveira, P. Pichat, Journal of Photochemistry and Photobiology A: Chemistry, 58 (1991) 99-114.
[178] A. Mills, M.A. Valenzuela, The photo-oxidation of water by sodium persulfate, and other electron acceptors, sensitized by TiO_2, Journal of Photochemistry and Photobiology A: Chemistry, 165 (2004) 25-34.

Appendix I Evaluation of methodology

Effect of loading mass on the reaction decomposition efficiency

Jan 2-4/2006

Concentration (μg/L) / Time (hr)	Run 1 Loading mass (g/cm^2)				
	$1x10^{-3}$	$5x10^{-4}$	$2.5x10^{-4}$	$1.5x10^{-4}$	$5x10^{-5}$
0	484	484	484	484	484
1	219.7	265.9	285.3	259.3	376.7
2	89.3	103.5	155.7	116.9	275
3	30.3	29.6	72.5	79.4	198.1
4	25.6	24.3	32.9	45.6	141.2
5	23.1	19.4	24.8	34.1	93.4
6	16.5	7.5	16.5	19.7	46.3
7	6.7	5.2	13.2	12.3	23.5

Feb 1-3/2006

Concentration (μg/L) / Time (hr)	Run 2 Loading mass (g/cm^2)				
	$1x10^{-3}$	$5x10^{-4}$	$2.5x10^{-4}$	$1.5x10^{-4}$	$5x10^{-5}$
0	494.5	494.5	494.5	494.5	494.5
1	211.85	260.4	286.5	299	360.75
2	84.7	94.75	166	178.25	276.5
3	34.25	43.75	66	82.65	190.25
4	30.75	32.5	33.95	45.6	133
5	26	27.65	26.6	34.1	89.25
6	19.5	17	18	19.2	38.2
7	7.5	5.2	13.2	12.3	21.5

Concentration change of phenol (mg/L) and MO (μg/L) in blank experiments

May 8-9/2006 for phenol, Feb 7-8/2006 for MO

Concentration / Time (hr)	UV without TiO_2				TiO_2 without UV			
	Phenol (mg/L)		MO (μg/L)		Phenol (mg/L)		MO (μg/L)	
0	7.60	7.74	2826	2937	7.60	7.74	2826	2937
0.5	7.60	7.60	2826	2937	7.60	7.60	2814	2937
1	7.60	7.53	2814	2937	7.47	7.47	2802	2913
1.5	7.47	7.47	2802	2913	7.47	7.47	2789	2900
2	7.47	7.47	2789	2900	7.40	7.47	2777	2900
2.5	7.47	7.47	2777	2888	7.40	7.40	2765	2888
3	7.40	7.47	2765	2888	7.40	7.40	2765	2876
3.5	7.40	7.47	2765	2876	7.40	7.40	2752	2876
4	7.40	7.47	2765	2876	7.33	7.40	2752	2863

Photocatalysts loss by the shear force

Stirring bar 1.5cm length, stirring speed 60rpm

	$Ti(OBu)_4$+DBS Photocatalytic calcination temperatures			
Photocatalysts mass	500^{0}C	600^{0}C	700^{0}C	800^{0}C
Before reactions (g)	0.0492	0.0499	0.0512	0.0506
After reactions (g)	0.0475	0.0484	0.0494	0.0490
Loss (%)	3.46	2.95	3.52	3.16
	$Ti(OBu)_4$+Cellulose Photocatalytic calcination temperatures			
Photocatalysts mass	500^{0}C	600^{0}C	700^{0}C	800^{0}C
Before reactions (g)	0.0511	0.0502	0.0498	0.0506
After reactions (g)	0.0487	0.0485	0.0478	0.0489
Loss (%)	4.70	3.39	4.02	3.36
	$Ti(OBu)_4$+SDS Photocatalytic calcination temperatures			
Photocatalysts mass	500^{0}C	600^{0}C	700^{0}C	800^{0}C
Before reactions (g)	0.0522	0.0499	0.0508	0.0507
After reactions (g)	0.0503	0.0476	0.0491	0.0491
Loss (%)	3.64	4.55	3.35	3.16
	$TiCl_4$+DBS Photocatalytic calcination temperatures			
Photocatalysts mass	500^{0}C	600^{0}C	700^{0}C	800^{0}C
Before reactions (g)	0.0501	0.0497	0.0507	0.0504
After reactions (g)	0.0485	0.0478	0.0488	0.0479
Loss (%)	3.19	3.82	3.75	4.96
	$Ti(OBu)_4$+Cellulose Photocatalytic calcination temperatures			
Photocatalysts mass	500^{0}C	600^{0}C	700^{0}C	800^{0}C
Before reactions (g)	0.0506	0.0504	0.0508	0.0498
After reactions (g)	0.0489	0.0478	0.0490	0.0478
Loss (%)	3.26	5.16	3.54	4.02
	$TiCl_4$+SDS Photocatalytic calcination temperatures			
Photocatalysts mass	500^{0}C	600^{0}C	700^{0}C	800^{0}C
Before reactions (g)	0.0510	0.0502	0.0505	0.0503
After reactions (g)	0.0492	0.0477	0.0489	0.0487
Loss (%)	3.53	4.98	3.17	3.18

Effect of calcination temperature on the decomposition efficiency

MO concentration change of Figure 6-2.

Jan 5-9/2006

Conc. (μg/L) / Time (hr) (a)	Calcination temperature				Conc. (μg/L) / Time (hr) (b)	Calcination temperature			
	500°C	600°C	700°C	800°C		500°C	600°C	700°C	800°C
0	989	989	989	989	0	1002	1002	1002	1002
0.5	823.91	852.43	886.71	916.74	0.5	937.47	863.63	916.43	947.59
1	750.77	702.29	786.69	863.27	1	776.85	711.52	806.81	848.49
1.5	669.94	601.99	724.74	806.25	1.5	677.05	609.91	733.97	773.84
2	587.39	503.31	687.60	737.53	2	525.45	459.24	630.86	653.50
2.5	531.84	454.11	618.80	676.28	2.5	434.47	404.26	545.79	581.46
3	464.18	402.34	551.01	597.81	3	365.43	306.32	510.12	537.63
3.5	391.13	305.07	488.89	521.72	3.5	277.25	237.71	442.18	495.49
4	303.22	212.24	422.44	466.52	4	236.97	133.97	338.38	386.37
4.5	231.75	142.96	356.14	400.30	4.5	210.62	124.80	266.33	296.09
5	144.93	73.78	302.18	338.00	5	172.74	74.75	205.61	272.74
5.5	104.49	57.82	209.15	313.95	5.5	154.91	68.60	172.85	226.15
6	71.33	47.97	155.31	279.35	6	119.94	48.60	124.95	187.07
6.5	53.74	38.33	117.96	232.11	6.5	96.89	38.84	116.03	169.14
7	33.99	35.07	83.95	181.51	7	85.67	35.53	91.08	146.29
7.5	29.54	28.15	71.11	115.29	7.5	74.75	28.52	76.85	114.53
8	24.13	15.29	63.85	82.32	8	69.24	30.19	54.61	88.08

MO concentration change of Figure 6-3.

Jan 12-16/2006

Conc. (μg/L) / Time (hr) (a)	Calcination temperature				Conc. (μg/L) / Time (hr) (b)	Calcination temperature			
	500°C	600°C	700°C	800°C		500°C	600°C	700°C	800°C
0	995	995	995	995	0	998	998	998	998
0.5	928.04	889.09	887.54	977.44	0.5	932.37	886.89	894.86	951.39
1	741.39	725.60	779.68	751.37	1	749.44	677.56	791.33	866.40
1.5	569.85	508.31	634.41	653.57	1.5	581.32	551.46	691.82	763.52
2	481.63	308.67	555.21	575.72	2	494.86	441.81	635.76	689.58
2.5	419.70	251.93	517.40	546.35	2.5	434.16	356.75	539.59	571.86
3	355.19	194.35	466.06	492.45	3	370.94	277.47	490.31	520.67
3.5	325.82	167.87	419.70	446.85	3.5	322.19	188.07	445.81	477.36
4	256.74	152.32	355.19	402.90	4	244.51	144.06	363.94	405.67
4.5	217.35	117.17	306.92	366.62	4.5	205.90	78.34	307.62	361.23
5	143.63	37.23	176.66	213.53	5	163.59	58.64	202.56	255.74
6	41.55	16.41	73.99	94.13	6	93.48	25.41	113.99	172.27
6.5	25.33	14.53	48.30	68.12	6.5	47.65	15.43	89.34	127.60
7	15.38	12.38	45.20	48.26	7	37.90	14.36	76.38	98.76
7.5	14.32	14.37	35.28	38.57	7.5	36.85	12.42	66.86	89.56
8	12.38	2.43	34.42	35.28	8	34.95	14.41	56.05	86.44
9	14.37	0.00	28.61	28.32	9	36.90	12.42	40.49	79.82

MO concentration change of Figure 6-4.
Jan 17-22/2006

Conc. (μg/L) / Time (hr) (a)	Calcination temperature				Conc. (μg/L) / Time (hr) (b)	Calcination temperature			
	500^{0}C	600^{0}C	700^{0}C	800^{0}C		500^{0}C	600^{0}C	700^{0}C	800^{0}C
0	1009	1009	1009	1009	0	1003	1003	1003	1003
0.5	896.67	877.02	941.10	991.20	0.5	935.50	891.87	894.68	965.25
1	685.03	649.39	721.55	761.95	1	717.26	645.53	785.95	857.72
1.5	557.54	551.72	577.87	662.77	1.5	574.43	538.41	669.60	658.82
2	446.69	349.92	488.41	583.82	2	485.50	347.84	559.67	580.36
2.5	401.04	295.44	425.60	453.14	2.5	423.08	293.68	521.56	550.75
3	341.07	240.14	360.19	408.57	3	358.05	238.71	509.93	496.40
3.5	220.41	166.03	311.24	371.78	3.5	328.44	213.44	423.08	450.45
4	145.65	89.26	239.69	216.53	4	258.80	148.44	358.05	406.13
4.5	48.94	48.90	139.85	145.85	4.5	219.11	104.86	309.39	369.57
5	42.14	34.87	75.03	75.27	5	144.78	68.67	238.26	275.42
5.5	25.69	14.73	48.98	69.08	5.5	48.65	48.61	139.02	144.98
6	15.60	12.55	45.84	48.94	6	41.89	34.66	74.58	74.82
6.5	14.52	14.57	35.77	39.11	6.5	25.54	14.64	48.70	68.67
7	12.55	2.46	34.90	35.78	7	15.51	12.48	45.57	48.65
7.5	14.57	0.00	29.01	28.72	7.5	14.43	14.48	31.54	38.88
8	12.55	0.00	21.65	20.31	8	12.48	2.45	24.66	35.57

Appendix II Zeta potential of shape- and size-controlled TiO_2 nanosized particles

Zeta potential of shape-controlled TiO_2 nanosized particles synthesized from $Ti(OBu)_4$

Titanium source and surfactants									
$Ti(OBu)_4$+DBS		$Ti(OBu)_4$+Cellulose				P-25			No surfactant	
		Run 1		Run 2			Run 1	Run 2		
pH	Zeta potential (mV)	pH	Zeta potential (mV)	pH	Zeta potential (mV)	pH	Zeta potential (mV)	Zeta potential (mV)	pH	Zeta potential (mV)
2.07	32.11	2.07	27.75	2	30.56	2.1	35.8	32.4	2.32	37.76
2.53	27.62	2.75	24.39	3	22.16	4	21.97	22.65	3.27	36.24
3.5	22.8	2.87	14.43	3.46	16.16	5.09	12.48	10.2	4.3	28.93
3.86	12.45	3.01	-9.06	4.06	5.4	6.3	6.6	7.56	5.57	13.56
4.36	-6.25	3.35	-11.34	4.49	-10.5	8.0	-3.75	-6.32	6.16	3.83
5.05	-9.65	3.58	-14.55	5.18	-13.23	9.35	-26.7	-18.25	6.78	-3.29
6.1	-12.35	4.5	-16.32	6.5	-16.55	11.64	-28.45	-21.54	7.56	-11.34
8.0	-13.56	5.65	-19.15	7	-17.7	11.8	-29.45	-23.47	8.57	-25.15
11.64	-21.56	6.1	-20.34	8.32	-17.4				9.3	-36.19
11.8		6.8	-20.57	9.32	-18.45				10.5	-38.67
		9.35	-24.77						11.6	-42.34

Zeta potential of SDS shaped TiO_2 nanosized particles synthesized from $Ti(OBu)_4$ in water and SDS solution

Zeta potential (mV) / pH	$Ti(OBu)_4$+SDS							
	In distilled water				In 5μM SDS solution			
	500^0C	600^0C	700^0C	800^0C	500^0C	600^0C	700^0C	800^0C
2.07	20.61	9.56	6.39	16.61	8.23	6.99	5.23	7.65
2.53	12.23	3.98	1.41	9.3	3.44	2.32	-1.32	2.28
3.02	0.98	0.45	-4.23	4.56	-3.06	-4.7	-6.78	-5.32
3.5	-3.11	-7.65	-10.77	2.83	4.6	2.21	-1.05	-6.76
4.36	1.62	2.27	-2.58	-3.29	11.84	9.54	3.54	2.56
5.05	15.09	16.46	1.5	-3.53	13.59	12.05	7.44	8.54
6.1	19.46	20.77	16.17	11.1	13.67	11.76	9.64	10.45
7.4	21.32	21.23	16.75	14.56	14.56	10.75	12.55	11.45
8.5	23.23	21.56	17.23	14.82	14.88	9.74	13.67	12.87
9.1	23.56	22.45	17.76	15.34	15.56	10.54	13.98	13.56

Zeta Potential of the shape controlled TiO_2 nanosized particles synthesized from $TiCl_4$

$TiCl_4$+DBS		$TiCl_4$+Cellulose		$TiCl_4$+SDS		P-25		No surfactant	
pH	Zeta potential (mV)	pH	Zeta potential (mV)	pH	Zeta potential (mV)	pH	Zeta potential (mV)	pH	Zeta potential (mV)
2	20.37	2	47.9	2	30.01	2.1	35.8	2.32	37.76
3.08	17.99	3	43.85	3	18.29	3	27.34	3.27	36.24
4.04	3.15	3.46	23.84	3.46	14.99	4	21.97	4.3	28.93
6	-2.97	4.09	-4.3	4.09	9.9	5.09	12.48	5.57	13.56
6.8	-8.46	5.18	-14.69	5.18	-11	5.54	9.65	6.16	3.83
8	-15.08	6.5	-24.78	6.5	-24.75	6.3	6.6	6.78	-3.30
9	-22.45	7	-25.59	7	-27.28	8	-3.75	7.56	-11.34
		8	-26.95	8	-33.76	9	-20.7	8.57	-25.15
		9	-31.96	9	-34.33	9.35	-26.57	9.3	-36.20
								10.5	-38.67
								11.6	-42.35

Zeta potential of SDS shape controlled TiO_2 nanosized particles synthesized from $TiCl_4$

$TiCl_4$+SDS					
Zeta potential (mV) / pH	500^{0}C	Zeta potential (mV) / pH	600^{0}C	700^{0}C	800^{0}C
2	30.01	2.1	37.03	28.77	34.23
3	18.29	3		20.86	
3.46	14.99	4	21.39	23.49	20.53
4.09	9.9	5.09	16.28	21.61	18.01
5.18	-5.65	6.3	-11.22	16.36	18.18
6.5	-24.75	6.8	-14.54	-3.79	
7	-27.28	8	-20.19	-9.21	0.63
8	-33.76	9.35	-24.33	-17.05	-11.88
9	-34.33	11.64			-22.82

Zeta potential of shape-controlled TiO_2 nanosized particles synthesized from $Ti(OBu)_4$ in water and SDS solution (SDS conc. 0.5μM)

$Ti(OBu)_4$+DBS				$Ti(OBu)_4$+Cellulose			
In water		In SDS		In water		In SDS	
pH	Zeta potential (mV)	pH	Zeta potential (mV)	pH	Zeta potential (mV)	pH	Zeta potential (mV)
2.07	32.11	2.07	15.26	2.07	27.75	2.07	7.645
2.53	27.62	2.56	11.98	2.53	26.83	2.32	7.2
3.5	22.8	3.1	-2.62	2.75	24.39	2.8	-4.54
3.86	12.45	4.37	-8.6	2.87	14.43	3.27	-18.61
4.36	-6.25	5.26	-13.45	3.01	-9.06	4.3	-22.46
5.05	-9.65	6.07	-20.44	3.35	-11.34	5.57	-29.93
6.1	-12.35	7.37	-29.54	3.58	-14.55	6.46	-33.33
8	-13.56	8.1	-32.15	4.5	-16.32	7.27	-33.91
9.35	-16.34	9.8	-34.54	5.65	-19.15	8.57	-39.43
11.64	-21.57	11	-34.87	6.1	-20.34	9.3	-41.8
				6.8	-20.56	11	-43.54
				9.35	-24.77		
				11.64	-26.45		

Zeta potential of TiO_2 nanosized particles synthesized from $Ti(OBu)_4$ in SDS solutions

Zeta potential (mV) / SDS Concentration (μM)	$Ti(OBu)_4$+DBS	$Ti(OBu)_4$+Cellulose	$Ti(OBu)_4$+SDS
0	-12.35	-20.34	21.234
0.25	-16.34	-23.45	--
0.5	-20.44	-30.23	--
1	-23.34	-33.23	20.34
1.5	-24.45	-35.76	14.56
2	-25.06	-35.89	10.42
4	-25.76	-36.12	9.56
5	-26.3	-36.9	8.47

Appendix III Evaluation of photocatalytic activity of the shape-controlled TiO_2 nanosized particles

Phenol concentration change on the TiO_2 nanosized particles synthesized from $Ti(OBu)_4$
June 1-7/2006

Conc. (mg/L) / Time (hr)	(a) Run 1 Surfactants				
	SDS	Cellulose	DBS	P-25	Neat TiO_2
0	97.67	97.67	97.67	97.67	97.67
1	79.76	83.41	86.90	87.72	93.45
2	68.52	70.36	77.44	81.25	87.34
3	53.02	60.08	71.71	73.01	82.37
4	42.76	47.37	64.92	65.44	74.68
5	29.55	36.32	56.72	59.28	68.07
6	20.27	28.82	52.84	51.73	61.81
7	13.86	23.75	47.55	46.61	57.40
8	7.33	18.40	39.74	42.04	52.43
9	6.50	12.99	32.84	35.81	47.01
10	4.30	9.63	27.56	32.24	41.26
15	2.69	5.74	23.43	20.21	36.78
16	2.06	4.26	12.63	17.89	28.89
Conc. (mg/L) / Time (hr)	(a) Run 2 Surfactants				
	SDS	Cellulose	DBS	P-25	Neat TiO_2
0	95.61	95.61	95.61	95.61	95.61
1	76.38	85.42	87.66	88.62	90.87
2	65.63	72.51	80.40	83.07	83.74
3	44.38	53.22	76.97	78.15	77.73
4	33.76	43.03	69.78	70.14	74.19
5	22.43	40.72	60.72	63.63	67.86
6	20.10	31.69	50.07	59.06	63.41
7	13.83	24.78	42.75	55.75	56.52
8	8.99	19.61	37.02	49.96	52.30
9	7.34	13.97	29.96	42.97	47.70
10	5.21	10.54	27.03	38.28	44.17
15	3.50	4.93	16.65	27.27	23.94
16	2.75	4.37	11.59	23.05	22.40

Phenol concentration change on the TiO_2 nanosized particles synthesized from $TiCl_4$
June 8-11/2006

Conc. (mg/L) / Time (hr)	(b) Run 1 Surfactants				
	SDS	Cellulose	DBS	P-25	Neat TiO_2
0	96.34	96.34	96.34	96.34	96.34
1	72.21	85.54	80.20	86.52	91.51
2	47.85	69.03	71.85	80.15	84.52
3	40.02	57.74	66.00	72.01	78.83
4	27.36	45.24	57.84	64.55	70.04
5	17.05	39.39	52.94	58.47	62.47
6	14.44	30.18	48.04	51.02	55.31
7	10.72	26.54	39.82	45.97	50.27
8	6.73	21.79	34.04	41.46	44.58
9	5.22	16.71	28.66	35.32	38.38
10	4.70	12.03	20.16	31.80	34.70
11	3.82	10.59	13.76	19.93	32.72
16	3.10	5.47	9.94	17.65	22.84
Conc. (mg/L) / Time (hr)	(b) Run 2 Surfactants				
	SDS	Cellulose	DBS	P-25	Neat TiO_2
0	97.56	97.56	97.56	97.56	97.56
1	79.67	87.87	86.18	90.32	95.39
2	68.44	73.71	79.92	84.34	88.92
3	46.43	53.83	71.96	79.81	82.21
4	34.55	43.22	57.74	71.19	74.13
5	22.52	41.41	52.18	65.62	70.19
6	20.23	31.63	41.04	59.57	66.40
7	14.00	23.30	29.22	57.27	62.19
8	7.82	15.45	22.80	49.96	56.16
9	6.60	11.99	17.79	43.56	52.03
10	5.52	9.71	12.46	42.58	46.54
15	4.12	6.60	8.58	29.36	31.94
16	3.38	3.37	6.41	23.24	26.97

MO concentration change on shape-controlled TiO_2 nanosized particles
Jan 21-25/2006

Conc. (μg/L) / Time (hr)	TiO_2 nanosized particles synthesized from $Ti(OBu)_4$ Surfactants				
	SDS	Cellulose	DBS	P-25	Neat TiO_2
0	498	498	498	498	498
0.5	226.05	303.83	364.46	404.35	398.61
1	91.88	183.72	266.08	308.97	321.44
1.5	46.12	103.36	133.69	230.26	261.96
2	26.34	52.09	69.02	128.26	170.08
2.5	18.79	44.07	49.08	51.97	89.93
3	12.00	29.26	22.62	24.18	48.67
3.5	6.89	17.66	20.47	23.62	22.12
4	6.21	14.17	17.23	22.63	10.60
Conc. (μg/L) / Time (hr)	TiO_2 nanosized particles synthesized from $TiCl_4$ Surfactants				
	SDS	Cellulose	DBS	P-25	Neat TiO_2
0	503	503	503	503	503
0.5	330.48	337.49	357.27	451.79	458.69
1	158.50	242.60	263.83	314.03	361.47
1.5	63.46	145.41	191.38	253.79	290.29
2	19.71	50.75	112.92	150.56	205.55
2.5	15.15	30.70	58.82	107.23	143.23
3	8.83	28.96	30.58	90.88	110.47
3.5	5.09	27.53	27.16	61.73	88.42
4	5.05	22.34	24.11	48.01	50.13

Appendix IV Kinetical studies of photocatalytic reactions

Concentration change of phenol on different shape- and size-controlled TiO_2 nanosized particles
July 11-30/2006

Conc. (mg/L) / Time (hr)	DBS/Ti(OBu)$_4$=0.25:1 Spherical, D=800nm					DBS/Ti(OBu)$_4$=0.5:1 Spherical, D=500nm				
0	12.42	28.87	52.96	94.65	95.05	12.42	27.91	51.87	94.65	94.51
1.00	11.19	26.82	50.16	91.03	91.04	10.99	25.25	48.45	89.49	90.90
2.00	9.55	23.34	44.02	86.46	87.16	8.94	21.91	42.52	85.00	85.57
3.00	8.53	18.83	42.18	76.29	78.37	7.37	18.83	40.74	78.60	79.64
4.00	6.96	16.10	38.22	74.18	76.20	5.73	15.83	36.92	73.56	75.47
5.00	5.66	13.72	32.83	70.56	72.06	4.78	12.90	32.14	68.11	70.42
6.00	4.37	12.21	27.37	64.49	66.23	3.68	11.26	27.50	64.48	64.35
7.00	3.82	9.49	23.34	60.60	62.24	2.93	8.80	23.07	56.62	55.41
8.00	2.73	7.66	20.27	55.41	57.07	2.18	7.03	19.59	53.71	53.16
9.00	2.32	7.05	16.38	50.70	52.21	1.84	6.34	16.52	49.00	48.31
10.00	1.84	6.07	14.95	47.36	49.47	1.57	5.19	15.36	45.79	45.45
15.00			9.76	44.70	47.02			8.12	41.35	40.06
16.00			7.30	35.62	35.01			6.35	29.48	31.05

Conc. (mg/L) / Time (hr)	DBS/Ti(OBu)$_4$=2:1 Spherical, D=200nm					DBS/Ti(OBu)$_4$=5:1 Spherical, D=50nm				
0	12.63	21.61	48.58	92.59	92.59	12.63	21.61	48.47	93.93	93.93
1.00	10.55	18.08	42.89	86.16	85.09	10.06	17.51	42.87	85.19	86.96
2.00	8.61	16.44	38.97	79.46	78.59	8.19	15.94	39.63	80.14	75.95
3.00	7.08	13.42	35.25	73.70	68.54	6.25	12.79	34.50	74.97	71.87
4.00	6.52	10.02	30.99	70.35	67.00	4.51	9.83	29.30	67.70	64.10
5.00	4.58	8.31	27.87	64.32	62.51	3.33	6.93	25.59	60.44	59.09
6.00	3.54	6.93	23.95	60.16	59.69	2.78	5.61	20.52	55.88	55.46
7.00	2.29	5.61	20.70	53.60	52.26	1.80	4.79	15.93	50.65	50.25
8.00	1.73	3.97	18.81	49.58	45.42	1.39	3.40	14.18	45.16	45.87
9.00	1.39	3.04	15.22	45.22	43.95	1.04	2.08	10.53	41.51	40.56
10.00		2.65	13.73	37.92	38.59			8.57	37.18	35.78
15.00			7.04	29.34	30.21			4.39	31.29	30.55
16.00			5.89	23.78	21.51			3.78	19.23	18.02

Conc. (mg/L) / Time (hr)	Celulose/$Ti(OBu)_4$=$5x10^{-4}$:1 Nanorods, D=500nm, L=5000nm					Celulose/$Ti(OBu)_4$=$1x10^{-3}$:1 Nanorods, D=300nm, L=1000nm				
0	11.35	26.42	51.28	93.12	93.12	11.55	26.09	53.37	95.32	95.32
1.00	9.08	22.02	43.30	85.42	80.12	9.08	21.00	42.61	85.69	77.85
2.00	7.15	19.45	40.80	79.16	73.66	6.88	14.97	32.41	72.28	65.68
3.00	5.36	15.99	34.37	72.97	67.88	4.61	10.64	23.94	58.66	53.23
4.00	4.26	12.67	28.96	67.20	63.18	2.34	7.86	18.32	46.63	42.34
5.00	3.37	9.35	22.53	62.71	58.29	1.72	5.35	12.35	37.32	33.90
6.00	2.68	7.45	20.57	58.56	55.00	1.24	3.25	10.83	29.61	26.87
7.00	2.06	5.89	15.36	54.80	51.99	0.96	2.37	8.54	24.39	22.18
8.00	1.58	4.54	13.80	49.44	46.03	0.76	1.63	5.41	18.89	17.15
9.00	1.17	2.33	11.91	45.32	42.49			3.54	14.67	13.33
10.00	0.83	1.42	9.74	41.00	38.12				11.19	10.18
15.00			5.34	26.93	24.92				4.22	4.67
16.00			3.75	21.43	19.32				3.89	3.48

Conc. (mg/L) / Time (hr)	Celulose/$Ti(OBu)_4$=0.01:1 Cubic, D=200nm					Celulose/$Ti(OBu)_4$=0.04:1 Cubic, D=100nm				
0	11.35	26.42	51.28	94.08	94.08	11.55	26.09	53.37	94.22	94.22
1.00	9.63	23.85	47.49	89.41	90.09	8.87	19.31	42.96	77.51	83.29
2.00	7.84	20.53	41.41	86.38	87.76	6.95	17.34	37.89	74.13	72.42
3.00	6.74	15.92	38.43	81.29	80.40	4.95	14.43	30.88	57.75	56.81
4.00	4.54	13.14	33.63	74.37	74.77	3.58	9.76	23.73	47.04	45.56
5.00	3.78	10.16	29.43	68.40	67.73	2.61	6.84	18.60	40.68	39.06
6.00	2.68	7.99	25.30	66.19	65.32	1.93	5.89	13.95	34.83	33.36
7.00	2.20	6.98	20.03	61.50	61.84	1.10	4.40	10.13	26.70	26.60
8.00	1.93	6.03	17.52	54.54	53.93	0.83	2.98	7.77	21.80	20.43
9.00	1.72	4.54	15.83	51.92	51.25		2.10	6.80	17.56	16.55
10.00	1.17	2.24	14.00	47.23	47.77			4.93	14.63	13.67
15.00			8.12	36.58	35.64				5.71	4.89
16.00			5.07	30.55	28.94				4.15	3.89

1

Conc. (mg/L) / Time (hr)	$SDS/Ti(OBu)_4$=0.01:1 Nanorods, D=100nm, L=800nm					$SDS/Ti(OBu)_4$=0.02:1 Nanorods, D=50nm, L=500nm				
0	9.59	23.68	66.89	103.78	103.78	9.81	24.03	60.03	102.74	102.74
1.00	7.43	17.32	49.38	85.11	84.23	6.43	16.61	41.15	80.25	83.90
2.00	5.47	12.91	36.71	75.64	74.90	3.65	11.14	26.86	68.98	72.07
3.00	3.04	9.01	29.87	69.96	69.21	1.83	5.33	17.63	46.49	48.89
4.00	2.03	6.68	19.66	60.96	63.06	1.08	3.17	13.95	35.21	37.34
5.00	1.35	4.66	15.05	54.67	53.18		1.69	7.84	23.86	24.34
6.00	1.03	2.46	13.67	45.74	46.48		0.95	5.97	21.32	21.87
7.00		1.89	10.68	38.36	37.48			2.98	14.58	15.13
8.00			6.68	32.41	31.46			1.80	10.87	11.14
9.00			4.15	27.54	26.18				8.84	9.58
10.00				22.46	21.65					
15.00				18.81	17.46					
16.00				13.73	12.79					

2
3

Conc. (mg/L) / Time (hr)	$SDS/Ti(OBu)_4$=0.5:1 Cubic, D=500nm					$SDS/Ti(OBu)_4$=2.5:1 Cubic, D=200nm				
0	9.59	23.68	60.45	94.76	94.76	9.81	24.03	60.03	97.57	97.57
1.00	7.83	19.21	53.09	86.99	86.24	7.17	15.87	43.86	82.54	83.97
2.00	5.88	13.04	45.39	77.98	77.85	4.19	12.49	28.87	69.56	70.31
3.00	3.65	10.39	34.49	69.11	69.59	2.37	7.43	24.15	52.29	53.44
4.00	2.30	7.37	26.23	62.85	63.47	1.49	5.27	14.78	39.16	39.84
5.00	1.69	5.42	23.73	55.29	55.15	0.81	2.90	9.30	32.36	31.62
6.00	1.22	4.09	17.77	48.00	48.48		2.16	7.29	21.83	22.10
7.00		2.83	14.71	41.33	42.09		1.01	3.89	17.41	18.15
8.00		1.64	12.35	36.79	37.48			3.12	11.35	11.90
9.00			8.81	30.55	31.82				8.36	8.98
10.00			6.18	26.66	27.80					
15.00				20.84	22.44					
16.00				15.34	15.68					

4

Concentration change of MO on different shape- and size-controlled TiO_2 nanosized particles
Jun 10-29/2006

Conc.(μg/L) / Time (hr)	DBS/$Ti(OBu)_4$=0.25:1 Spherical, D=800nm				DBS/$Ti(OBu)_4$=0.5:1 Spherical, D=500nm			
0	1555.09	2542.45	3073.16	3603.86	1542.75	2591.82	3122.53	3751.97
0.50	1160.15	2061.11	2616.50	3036.13	1098.44	1727.88	2431.37	2591.82
1.00	691.15	1481.04	1888.33	2382.01	654.13	1320.59	1789.59	2159.85
1.50	444.31	1123.12	1382.30	1875.98	382.60	888.62	1406.99	1629.14
2.00	370.26	691.15	1036.73	1382.30	283.87	715.84	1110.78	1419.33
2.50	209.81	530.71	826.91	1061.41	148.10	506.02	691.15	851.60
3.00	160.45	431.97	654.13	950.33	98.74	370.26	555.39	765.20
3.50	98.74	283.87	543.05	641.78	86.39	234.50	419.63	592.42
4.00		222.16	394.94	518.36		135.76	271.52	456.65

Conc.(μg/L) / Time (hr)	DBS/$Ti(OBu)_4$=2:1 Spherical, D=200nm				DBS/$Ti(OBu)_4$=5:1 Spherical, D=50nm			
0	1579.78	2468.40	3110.18	3640.89	1616.80	2505.43	3060.82	3653.23
0.50	1049.07	1653.83	2542.45	2616.50	987.36	1678.51	2221.56	2813.98
1.00	654.13	1246.54	1653.83	2159.85	617.10	1184.83	1579.78	1999.40
1.50	370.26	962.68	1110.78	1431.67	357.92	752.86	987.36	1431.67
2.00	246.84	691.15	987.36	1221.86	259.18	580.07	863.94	1073.75
2.50	148.10	543.05	678.81	1036.73	123.42	370.26	580.07	789.89
3.00	86.39	296.21	506.02	777.55	74.05	296.21	407.29	543.05
3.50	74.05	172.79	320.89	444.31	49.37	172.79	246.84	370.26
4.00		123.42	209.81	320.89		86.39	172.79	271.52

Conc.(μg/L) / Time (hr)	Celulose/Ti(OBu)$_4$=5x10^{-4}:1 Nanorods, D=500nm, L=5000nm				Celulose/Ti(OBu)$_4$=1x10^{-3}:1 Nanorods, D=300nm, L=1000nm			
0	1530.41	2493.08	2999.11	3529.81	1555.09	2468.40	3036.13	3579.18
0.50	1135.46	1740.22	2246.24	2727.58	888.25	1764.91	1752.56	2542.45
1.00	863.94	1481.04	1764.91	2172.19	530.71	1110.78	1357.62	1764.91
1.50	407.29	1012.04	1357.62	1764.91	345.58	641.78	678.81	1209.52
2.00	308.55	666.47	1160.15	1419.33	123.42	382.60	394.94	913.31
2.50	197.47	431.97	654.13	1135.46		209.81	308.55	641.78
3.00		370.26	580.07	802.23		123.42	246.84	407.29
3.50		308.55	481.34	493.68			160.45	197.47
4.00		172.79	357.92	370.26			98.74	123.42

Conc.(μg/L) / Time (hr)	Celulose/Ti(OBu)$_4$=0.01:1 Cubic, D=200nm				Celulose/Ti(OBu)$_4$=0.04:1 Cubic, D=100nm			
0	1579.78	2530.11	2974.42	3628.55	1542.75	2567.14	3048.47	3529.81
0.50	999.70	1789.59	2172.19	2419.03	1024.39	1740.22	2061.11	2628.85
1.00	715.84	1258.88	1764.91	2061.11	567.73	1160.15	1382.30	1703.20
1.50	481.34	876.28	1073.75	1357.62	308.55	728.18	937.99	1592.12
2.00	259.18	530.71	765.20	1160.15	234.50	431.97	728.18	1061.41
2.50	148.10	394.94	715.84	950.33		296.21	456.65	728.18
3.00		296.21	518.36	678.81		246.84	370.26	506.02
3.50		222.16	407.29	518.36			271.52	333.23
4.00		86.39	259.18	333.23			148.10	234.50

Conc.(μg/L) / Time (hr)	$SDS/Ti(OBu)_4$=0.01:1 Nanorods, D=100nm, L=800nm				$SDS/Ti(OBu)_4$=0.02:1 Nanorods, D=50nm, L=500nm			
0	1555.09	2542.45	3073.16	3480.44	1530.41	2542.45	3073.16	3480.44
0.50	802.23	1789.59	2196.88	2616.50	678.81	1481.04	2073.46	2246.24
1.00	641.78	1098.44	1431.67	1641.49	419.63	925.65	1308.25	1518.07
1.50	370.26	715.84	1098.44	1295.91	259.18	617.10	666.47	1123.12
2.00	222.16	530.71	629.44	962.68	123.42	283.87	469.00	592.42
2.50	111.08	345.58	555.39	641.78	74.05	185.13	296.21	382.60
3.00		197.47	370.26	506.02		98.74	160.45	296.21
3.50		148.10	259.18	333.23		86.39	123.42	222.16
4.00		111.08	135.76	209.81		49.37	61.71	148.10

Conc.(μg/L) / Time (hr)	$SDS/Ti(OBu)_4$=0.5:1 Cubic, D=500nm				$SDS/Ti(OBu)_4$=2.5:1 Cubic, D=200nm			
0	1555.09	2604.16	3073.16	3529.81	1530.41	2591.82	3073.16	3603.86
0.50	1086.10	1974.72	2196.88	3048.47	962.68	1542.75	2406.69	2480.74
1.00	666.47	1271.23	1493.38	1653.83	543.05	1110.78	1419.33	1826.62
1.50	431.97	925.65	962.68	1592.12	283.87	641.78	975.02	1357.62
2.00	209.81	530.71	703.49	1061.41	148.10	419.63	691.15	740.52
2.50	123.42	345.58	555.39	728.18	98.74	296.21	444.31	629.44
3.00	74.05	234.50	382.60	506.02		185.13	296.21	419.63
3.50		148.10	271.52	370.26		123.42	172.79	246.84
4.00		123.42	197.47	259.18		61.71	123.42	172.79

Appendix V Effect of light intensity on the photocatalytic reactions

Concentration change of phenol on different TiO_2 nanosized particles under different light intensity.

Aug 10-18/2006

DBS/$Ti(OBu)_4$=5:1

Spherical, D=50nm Conc. (mg/L) / Time (hr)	Light intensity (W/cm^2)				
	1.3	1.9	2.5	3.0	3.4
0	97.03	96.69	96.41	97.79	98.34
1.00	90.22	87.75	86.44	86.37	85.62
2.00	87.27	84.24	80.11	76.33	68.91
3.00	82.59	78.67	75.37	64.09	57.97
4.00	79.50	72.62	67.65	46.35	47.31
5.00	73.24	67.05	61.34	38.99	40.99
6.00	68.63	59.42	57.14	33.35	29.98
7.00	64.09	52.68	51.78	30.19	22.28
8.00	58.11	48.89	46.72	22.28	17.60

Celulose/$Ti(OBu)_4$=$1x10^{-3}$:1

Nanorods, D=300nm, L=1000nm

Conc. (mg/L) / Time (hr)	Light intensity (W/cm^2)				
	1.3	1.9	2.5	3.0	3.4
0	99.03	98.48	95.31	99.99	100.68
1.00	87.13	84.24	78.74	81.01	79.36
2.00	81.01	77.36	67.87	69.59	61.69
3.00	76.33	71.11	55.01	55.84	48.41
4.00	69.04	68.36	44.97	42.84	34.59
5.00	63.47	60.24	35.97	27.85	26.41
6.00	58.11	54.53	28.54	24.89	20.29
7.00	51.99	48.96	23.52	17.47	12.24
8.00	48.89	42.02	18.22	13.07	9.83

SDS/$Ti(OBu)_4$=0.02:1

Nanorods, D=50nm, L=500nm

Conc. (mg/L) / Time (hr)	Light intensity (W/cm^2)				
	1.3	1.9	2.5	3.0	3.4
0	103.98	101.64	102.74	103.02	103.57
1.00	88.23	82.32	81.01	76.88	76.13
2.00	79.50	71.86	70.52	67.67	62.72
3.00	63.34	58.11	47.69	43.39	34.80
4.00	49.72	42.71	36.28	34.52	30.40
5.00	38.24	37.34	24.10	22.35	21.32
6.00	32.94	29.09	21.59	15.47	16.71
7.00	25.10	20.49	14.85	13.62	9.97
8.00	17.60	14.44	9.63	8.25	4.61

Concentration change of MO on different TiO_2 nanosized particles under different light intensity.
Aug 21-30/2006

DBS/$Ti(OBu)_4$=5:1
Spherical, D=50nm

Conc. (μg/L) / Time (hr)	Light intensity (W/cm^2)					
	1.3	1.9	2.5	Time (hr)	3.0	3.4
0	1641.49	1703.20	1604.46	0	1764.91	1727.88
0.50	1357.62	1246.54	888.62	0.25	1518.07	1357.62
1.00	962.68	876.28	518.36	0.50	1073.75	925.65
1.50	826.91	580.07	444.31	0.75	876.28	691.15
2.00	666.47	493.68	222.16	1.00	641.78	543.05
2.50	530.71	407.29	135.76	1.25	394.94	407.29
3.00	431.97	234.50	86.39	1.50	308.55	320.89
3.50	296.21	209.81	74.05	1.75	246.84	197.47
4.00	209.81	160.45	53.78	2.00	197.47	160.45

Celulose/$Ti(OBu)_4$=$1x10^{-3}$:1
Nanorods, D=300nm, L=1000nm

Conc. (μg/L) / Time (hr)	Light intensity (W/cm^2)					
	1.3	1.9	2.5	Time (hr)	3.0	3.4
0	1641.49	1703.20	1604.46	0	1764.91	1727.88
0.50	1271.23	1332.94	888.25	0.25	1308.25	1184.83
1.00	900.97	839.26	444.31	0.50	1098.44	863.94
1.50	629.44	641.78	345.58	0.75	851.60	666.47
2.00	518.36	481.34	160.45	1.00	543.05	481.34
2.50	444.31	333.23	123.42	1.25	394.94	345.58
3.00	345.58	209.81		1.50	308.55	185.13
3.50	234.50	123.42		1.75	209.81	135.76
4.00	160.45	86.39		2.00	135.76	111.08

SDS/$Ti(OBu)_4$=0.02:1
Nanorods, D=50nm, L=500nm

Conc. (μg/L) / Time (hr)	Light intensity (W/cm^2)					
	1.3	1.9	2.5	Time (hr)	3.0	3.4
0	1641.49	1703.20	1604.46	0	1764.91	1727.88
0.50	1061.41	950.33	678.81	0.25	1184.83	1110.78
1.00	814.57	666.47	370.26	0.50	826.91	740.52
1.50	481.34	345.58	283.87	0.75	617.10	506.02
2.00	382.60	296.21	160.45	1.00	419.63	320.89
2.50	333.23	123.42	74.05	1.25	271.52	271.52
3.00	234.50	74.05		1.50	209.81	160.45
3.50	172.79	61.71		1.75	160.45	98.74
4.00	123.42	49.37		2.00	98.74	61.71